

THE IMPACT OF EXTREME GREENLAND BLOCKING EPISODES AND
NORTH ATLANTIC PRECURSOR CYCLONES ON THE ACCELERATION OF
SUMMER MELTING ACROSS THE GREENLAND ICE SHEET

by

JORDAN TAYLOR MCLEOD

(Under the Direction of Thomas L. Mote)

ABSTRACT

Rapid changes in atmospheric circulation variability over the North Atlantic region and the extent of surface melting across the Greenland ice sheet (GrIS) have been observed during recent decades. In this thesis, a historical climatology of extreme Greenland blocking episodes, associated with unusually strong and persistent synoptic-scale ridges, from 1958–2013 is examined within the context of anomalous anticyclonic circulation patterns over Greenland during recent years. The role of other atmospheric and oceanic features within the North Atlantic climate system, including extratropical cyclone activity and sea surface temperatures, on the evolution of extreme Greenland blocking episodes and GrIS melting is also examined.

Contributions from adiabatic and diabatic sources of heating are quantified in order to determine processes associated with blocking anticyclones and precursor cyclones that can enhance GrIS melting. The long-term increase in Greenland blocking, coupled with additional factors, suggests that GrIS melting may continue to accelerate into the future.

INDEX WORDS: Greenland blocking, North Atlantic cyclones, Greenland ice sheet, Arctic amplification

THE IMPACT OF EXTREME GREENLAND BLOCKING EPISODES AND
NORTH ATLANTIC PRECURSOR CYCLONES ON THE ACCELERATION OF
SUMMER MELTING ACROSS THE GREENLAND ICE SHEET

by

JORDAN TAYLOR MCLEOD

B.A., The University of North Carolina at Chapel Hill, 2011

A Thesis Submitted to the Graduate Faculty of The University of Georgia in Partial Fulfillment
of the Requirements for the Degree

MASTER OF SCIENCE

ATHENS, GEORGIA

2014

© 2014

Jordan Taylor McLeod

All Rights Reserved

THE IMPACT OF EXTREME GREENLAND BLOCKING EPISODES AND
NORTH ATLANTIC PRECURSOR CYCLONES ON THE ACCELERATION OF
SUMMER MELTING ACROSS THE GREENLAND ICE SHEET

by

JORDAN TAYLOR MCLEOD

Major Professor: Thomas L. Mote

Committee: J. Marshall Shepherd
Andrew J. Grundstein

Electronic Version Approved:

Julie Coffield
Interim Dean of the Graduate School
The University of Georgia
December 2014

ACKNOWLEDGEMENTS

First and foremost, I would like to recognize my Lord and Savior, Jesus Christ, for providing me with the daily strength and motivation needed to successfully complete this Master's thesis. I would also like to thank my major professor, Dr. Tom Mote, and my committee members, Dr. Marshall Shepherd and Dr. Andy Grundstein, for their helpful assistance and feedback in the construction of this thesis. It has been a privilege to continue my academic education in atmospheric science under your guidance and instruction. Finally, I would like to thank all of the family members and friends who have encouraged me along this journey and contributed to my professional development.

TABLE OF CONTENTS

	Page
ACKNOWLEDGEMENTS	iv
LIST OF TABLES	vii
LIST OF FIGURES	viii
CHAPTER	
1 INTRODUCTION AND LITERATURE REVIEW	1
Overview	1
Project Motivation	3
Background	6
2 LINKING SEASONAL CHANGES IN EXTREME GREENLAND BLOCKING EPISODES TO THE RECENT INCREASE IN SUMMER MELTING ACROSS THE GREENLAND ICE SHEET	19
Introduction	21
Data and Methods	24
Results	31
Discussion and Conclusion	40
References	45
Figures and Tables	52

3	ASSESSING THE ROLE OF PRECURSOR CYCLONES ON THE FORMATION OF EXTREME GREENLAND BLOCKING EPISODES AND THEIR IMPACT ON SUMMER MELTING ACROSS THE GREENLAND ICE SHEET	63
	Introduction	65
	Data and Methods	71
	Results	75
	Discussion and Conclusion	86
	References	90
	Figures and Tables	97
4	CONCLUSION.....	109
	REFERENCES	117

LIST OF TABLES

	Page
Table 2.1: Percentage of extreme GBEs by season occurring within 14-year periods from 1958–2013	52
Table 2.2: OLS multiple regression model for western Greenland meltwater production (1979–2008)	53
Table 2.3: OLS multiple regression model for eastern Greenland meltwater production (1979–2008)	54
Table 3.1: Geographic coordinates of the nine selected Greenland locations	97
Table 3.2: Comparison of precursor and non- precursor cyclone attributes by season (1979–2008)	98
Table 3.3: Seasonal distribution of extreme GBEs categorized by the number of precursor cyclones (1979–2008)	99
Table 3.4: Comparison of HYSPLIT backward trajectories for extreme GBEs during the extended summer season	100
Table 3.5: Comparison of surface energy budget fields for the nine selected Greenland locations (1979–2008)	101

LIST OF FIGURES

	Page
Figure 2.1: Spatial domain for the Greenland Blocking Index based on <i>Hanna et al.</i> [2013a].....	55
Figure 2.2: Composite maps of 500 hPa geopotential heights over the North Atlantic for all days from 1958–2013 in which the GBI ranked within the 90th–100th percentiles based on the entire 56-year climatological distribution	56
Figure 2.3: Time series of the annual frequency of extreme blocking days (daily mean GBI is ranked at or above the 97th percentile of the climatological distribution) from 1958–2013	57
Figure 2.4: 7-year frequency (a), daily count (b), departure of strength from average (c), and departure of duration from average (d) of extreme GBEs from 1958–2013	58
Figure 2.5: Composite maps of 500 hPa geopotential height (left) and 2-meter air temperature (right) for all extreme GBEs grouped by season from 1958–2013	59
Figure 2.6: Frequency, strength, and duration of extreme GBEs by season from 1958–2013 (n = 94)	60
Figure 2.7: Geographic distributions of North Atlantic cyclones during the top 10 summer melting seasons from 1979–2008 over eastern Greenland (a) and western Greenland (b).....	61
Figure 2.8: Composite anomalies of 10-meter vector winds for high melt days compared to low melt days during the top 10 summer melting seasons from 1979–2008 over eastern Greenland (a) and western Greenland (b)	62

Figure 3.1: Geographic origin of all precursor cyclones associated with extreme GBEs from 1979–2008.....	102
Figure 3.2: Geographic distribution of precursor (a) and non- precursor (b) cyclones from 1979–2008	103
Figure 3.3: Composite maps of 500 hPa geopotential heights associated with extreme GBEs that were (a) and were not (b) accompanied by a precursor cyclone(s)	104
Figure 3.4: Geographic distribution of HYSPLIT backward trajectories for all extreme GBEs with a precursor cyclone(s) from 1979–2008	105
Figure 3.5: Geographic distribution of HYSPLIT backward trajectories for all extreme GBEs with a precursor cyclone(s) compared to all extreme GBEs without a precursor cyclone from 1979–2008.....	106
Figure 3.6: Composite time series of the air parcel elevation along backward trajectories during extreme GBEs with a precursor cyclone(s) (red lines) compared to extreme GBEs lacking a precursor cyclone (blue lines)	107
Figure 3.7: Composite maps of North Atlantic SST anomalies associated with extreme GBEs that were (a) and were not (b) accompanied by a precursor cyclone(s)	108

CHAPTER 1

INTRODUCTION AND LITERATURE REVIEW

1.1 Overview

Across the Northern Hemisphere, synoptic-scale ridges of high pressure extending poleward from the mid-latitudes to the Arctic region are observed frequently throughout the year. If they are sufficiently strong and persistent, these anticyclonic systems, known as atmospheric blocks, can divert migratory shortwave disturbances toward higher latitudes by displacing the predominant steering flow of the polar jet stream equatorward. Atmospheric blocks, particularly those over the North Atlantic region, are usually generated by cyclonic wave breaking of synoptic-scale eddies that advects relatively warm and moist air masses toward the polar latitudes [Benedict *et al.*, 2004; Woollings *et al.*, 2008]. These modified air masses often cut off from the polar jet stream and may persist over high-latitude regions for up to several weeks [Barriopedro *et al.*, 2006]. While blocking anticyclones can develop over many areas of the Northern Hemisphere, the focus of this study pertains to blocks that are located over the northwestern region of the Atlantic Ocean, commonly referred to as Greenland blocks.

Previous studies have examined climatological characteristics of atmospheric blocks across the Northern Hemisphere [Lupo and Smith, 1995; Barriopedro *et al.*, 2006; Tyrlis and Hoskins, 2008], while other research has been focused on the development of improved blocking detection techniques [Pelly and Hoskins, 2003; Barnes *et al.*, 2012]. In addition, the long-term variability of atmospheric circulation patterns over the North Atlantic region has been linked to an increased rate of surface melting and runoff across the Greenland ice sheet (GrIS) during recent decades [Mote, 1998a, 1998b; Fettweis *et al.*, 2011; Hanna *et al.*, 2013a; Rajewicz and

Marshall, 2014]. However, a climatological investigation of extreme Greenland blocks and their impact on the extent of GrIS surface melting has remained largely unexplored. This relationship is particularly significant given that the quantity of freshwater stored in the GrIS would correspond to 6–7 meters of global sea level rise if it were all to be released [*Cuffey and Marshall*, 2000; *Nghiem et al.*, 2012].

Other features of the North Atlantic climate system, such as extratropical cyclone activity and sea surface temperatures, may play a significant role in the evolution of extreme Greenland blocks and, in turn, GrIS melting. *Hanna et al.* [2013a] revealed that the North Atlantic Oscillation (NAO), the dominant mode of atmospheric variability over the Atlantic Ocean, alone could not sufficiently explain the exceptional Greenland blocking patterns during the summers of 2007–2010, which suggests that a complex interaction of atmospheric and oceanic processes may be responsible. Previous research, including both case studies [*Colucci*, 1985, 1987; *Tsou and Smith*, 1990] and climatological analyses [*Konrad and Colucci*, 1988; *Dole*, 1989; *Nakamura and Wallace*, 1990, 1993; *Lupo and Smith*, 1995] has identified a link between surface cyclogenesis and downstream block development across the Northern Hemisphere. For example, *Konrad and Colucci* [1988] examined 500 hPa circulation changes associated with 141 explosive cyclones (“bombs”) over the western half of the Northern Hemisphere from September 1980 through May 1987 (excluding the summer months of June–August). Based on their findings, explosive cyclogenesis does appear to contribute to the development of North Atlantic blocks, but the period of greatest upper-level wave amplification typically occurs after the most rapid phase of surface cyclogenesis, possibly in connection with enhanced air mass advection.

The structure of this thesis is outlined as follows. In the second chapter, various aspects (frequency, strength, and duration) of extreme Greenland blocking episodes during 1958–2013

will be examined in order to assess the future potential for significant changes in the North Atlantic atmospheric circulation. A seasonal analysis of these extreme Greenland blocking episodes will also be presented to evaluate their role in summer melting trends across the GrIS, and an OLS multiple regression approach will be used to determine any statistically significant predictors of GrIS melting since the beginning of the satellite observational period in 1979. In the third chapter, the contribution of North Atlantic cyclones and sea surface temperatures to the development and maintenance of extreme Greenland blocking episodes from 1979–2008 will be assessed. In addition, air mass advection associated with both the blocking anticyclones and the extratropical cyclones are linked to surface melting conditions across the western and eastern sectors of the GrIS. Finally, a concluding discussion of the results of these studies in the context of global climate change and some suggestions for future research are provided in the fourth chapter.

1.2 Project Motivation

The frequency and intensity of Greenland blocking, particularly during the summer, strongly influences the interannual variability in the extent of GrIS melting. With the exception of 2009, unprecedented rates of melting and runoff have been recorded across the GrIS during six recent years (2007–2012), which can at least partially be attributed to persistent negative NAO anomalies and an associated increase in the frequency of Greenland blocking patterns [Fettweis *et al.*, 2011]. The summer of 2012 was characterized by exceptional rates of GrIS melting and runoff as approximately 86% (79 of 92) of all days from June through August experienced above-normal melt extents compared to the 30-year (1981–2010) climatological mean [Tedesco *et al.*, 2013]. From 11–12 July 2012, observations from three satellite-based instruments, including MODIS and SSMIS, indicated that melting had occurred across

approximately 98.6% of the GrIS, which represents the daily record for maximum melt extent during the satellite era [Nghiem *et al.*, 2012; Tedesco *et al.*, 2013]. According to multiple ice core records from Summit Station, an extreme melting event of this magnitude had not occurred since 1889 [Clausen *et al.*, 1988; Nghiem *et al.*, 2012]. Two major factors that contributed to such extreme melting across the GrIS during the summer of 2012 were the anomalous frequency of days characterized by anticyclonic circulation over Greenland (55% compared to the 1958–2011 climatological mean of $20\% \pm 10\%$), the highest in over 50 years, and the occurrence of the most negative NAO episode from June through August since 1950 [Hanna *et al.*, 2013b; Tedesco *et al.*, 2013].

Greenland blocks have also been directly and indirectly linked to recent extreme weather events across the North Atlantic region, most notably the landfall of Hurricane Sandy in 2012. From 22–29 October 2012, an unusually strong Greenland block persisted over the North Atlantic and prevented the northward-tracking Hurricane Sandy from recurving northeastward similarly to most tropical cyclones along the East Coast of the United States [Greene *et al.*, 2013; Mattingly *et al.*, 2014]. Quantified by the Greenland Blocking Index [Fang, 2004; Hanna *et al.*, 2013a], the strength of the block prior to Sandy’s landfall on 29 October 2012 remained above the 97th percentile of mean climatological values for four consecutive days from 24–27 October, which likely diverted Sandy into the New Jersey coastline after an unprecedented westward turn [Mattingly *et al.*, 2014].

Historical trends in Greenland blocking are also important within the context of recent climate change across the broader Arctic region. Over the past few decades, the Arctic has been warming at a much faster rate than both the mid-latitudes and the tropics, a phenomenon known as Arctic amplification [Serreze and Francis, 2006]. While Arctic amplification has likely

contributed to unprecedented tropospheric warming and melt/runoff rates over the GrIS, there is only limited evidence that atmospheric circulation patterns from the mid- to high latitudes have also been affected. A recent study by *Francis and Vavrus* [2012] has suggested that the frequency of blocking across the North Atlantic region will increase in the future due to a reduction in the poleward thickness gradient, resulting in a weakening of the upper-level zonal flow, and a meridional elongation of planetary waves. However, subsequent research has questioned this assertion because the most reliable global circulation models generally project a decreasing frequency of blocking conditions across the North Atlantic region [*Barnes et al.*, 2012; *Belleflamme et al.*, 2013; *Masato et al.*, 2013].

Though an assessment of future trends in Greenland blocking remains inconclusive, the impact of these amplified atmospheric planetary waves on the frequency of mid-latitude weather extremes is more clearly established. *Screen and Simmonds* [2014] investigate the relationship between normalized wave amplitude anomalies for wave numbers 3–8 and monthly mean land-based temperature and precipitation extremes across various regions of the Northern Hemisphere mid-latitudes (35°–60°N) from 1979–2012. While months characterized by extreme weather conditions across the mid-latitudes were often linked to significantly amplified quasi-stationary planetary waves, months associated with near-average weather conditions were usually accompanied by significantly attenuated planetary wave patterns [*Screen and Simmonds*, 2014]. However, the strength of these relationships and the type of extreme weather produced were not consistent across all regions of the Northern Hemisphere mid-latitudes. For example, amplified planetary waves increased the probability of heat waves in western North America, cold outbreaks in eastern North America, and droughts in central North America. Thus, these results highlight the widespread geographic impacts, ranging from anomalous GrIS melting at the local

scale to cold outbreaks across the eastern United States at the regional scale, that can potentially be attributed to Greenland blocks as persistent episodes of amplified mid-tropospheric wave patterns over the North Atlantic.

1.3 Background

To this point, there have been no studies published regarding an assessment of characteristics associated with Greenland blocks over a long-term climatological period. Numerous climatologies of blocking anticyclones across the Northern Hemisphere, including the North Atlantic region, have been developed and extended since the mid-20th century [Rex, 1950; Sumner, 1954, 1959; Treidl *et al.*, 1981; Knox and Hay, 1985]. However, the first and seminal study of atmospheric blocks in the Northern Hemisphere, published by Daniel F. Rex (for whom the split-flow blocking pattern is named) in 1950, provides a climatological perspective on North Atlantic blocks that remains generally consistent with more recent research. Based on a manual inspection of 82 North Atlantic split-flow blocks spanning the 13-year period of record from 1933–1940 and 1945–1949, the frequency of blocks was highest during the spring season from March through May (~40% of total blocked days) and lowest during the summer months from July through September (~15% of total blocked days) [Rex, 1950]. The temporal duration of these blocks ranged from a minimum of 10 days to a maximum of 41 days, with a median duration of 14 days and a mean duration of approximately 16.6 days [Rex, 1950].

Recent climatological analyses of Northern Hemisphere blocking have largely supported the original findings of Rex [1950], and any discrepancies can likely be attributed to differences in the selected geographic domain or blocking definition. North Atlantic blocks can occur at any time throughout the year, but their frequency is largely determined by a distinct seasonal cycle [Barriopedro *et al.*, 2006]. Over a 3-year period from July 1985 through June 1988, the

frequency of North Atlantic blocks (80°W–40°E) is fairly consistent during the fall, winter, and spring (~2–4 blocks per year on average), but there is a distinct summer minimum in blocking activity over this region (~1 block per year on average) [Lupo and Smith, 1995]. According to Lupo and Smith [1995], 23.7% of all days during the period of record were characterized by blocking conditions over the North Atlantic region. Blocking anticyclones were largest and strongest during the winter compared to the other seasons, and winter blocks persisted four days longer on average than summer blocks (11 days versus 7 days) [Lupo and Smith, 1995]. Finally, Barriopedro et al. [2006] have shown that North Atlantic (100°W–0°) blocking days, events, intensity, and size have significantly ($p \leq 0.1$) declined over the 55-year period from 1948–2002.

Greenland blocking is directly related to a low-frequency teleconnection pattern known as the North Atlantic Oscillation (NAO), the dominant mode of atmospheric variability over the Atlantic Ocean [Shabbar et al., 2001; Benedict et al., 2004; Woollings et al., 2008; Davini et al., 2012]. Greenland blocks, particularly the stronger and more persistent events, develop most frequently during negative phases of the NAO, which are characterized by a weak, high-amplitude polar jet stream over the North Atlantic [Woollings et al., 2008]. Indeed, the annual number of Greenland blocking days is highly anticorrelated ($r = -0.81$) with the yearly-averaged NAO index [Davini et al., 2012]. Despite this strong relationship, it is important to note that the dipole pattern in mean sea-level pressure characterizing NAO variability evolves both seasonally and geographically [Portis et al., 2001; Folland et al., 2009]. A distinct mode of atmospheric variability known as the summer NAO, with centers of actions located to the northwest of those established for the traditional wintertime NAO, more closely reflects variations in North Atlantic atmospheric circulation during the warm season [Portis et al., 2001; Folland et al., 2009]. The Arctic Oscillation (AO), a hemispheric mode of atmospheric variability capturing pressure

differences between the Arctic region and the mid-latitudes, is also strongly correlated with the NAO and further modulates the potential for Greenland block development.

Several recent studies have suggested that Greenland blocking actually represents the primary physical mechanism leading to variability in the NAO [Woollings *et al.*, 2008; Davini *et al.*, 2012]. This assertion challenges the traditional theory that negative phases of the NAO precondition the upper-level flow over the North Atlantic such that cyclonic Rossby wave-breaking events are more likely to occur; instead, negative NAO anomalies simply reflect the development of Greenland blocks [Woollings *et al.*, 2008]. Davini *et al.* [2012] found that the NAO centers of action were strengthened and displaced westward during years associated with a relatively high frequency of Greenland blocks (i.e. negative NAO phase). Conversely, the NAO did not reflect a zonal mode of variability and its centers of action were shifted eastward during years with a relatively low frequency of Greenland blocks. Thus, the recent positive trend in the NAO coupled with an eastward displacement in its dipole pressure pattern is directly linked to a decreasing frequency of Greenland blocks [Davini *et al.*, 2012].

Shabbar *et al.* [2001] provide some climatological characteristics of North Atlantic (defined as the region bounded by the 60°W and 10°E meridians) blocking events based on the phase of the NAO. Wintertime blocking days from 1958–1996 were 67% more frequent during negative phases of the NAO compared to positive phases. The duration of North Atlantic blocking events is also correlated with the NAO phase as blocking events during negative phases, with an average length of approximately 11 days, are almost twice as long as blocking events during positive phases, with an average length of only 6 days. Based on a linear regression analysis, the NAO explained only 30% of the variance in wintertime North Atlantic blocking during this 39-year period.

A robust linkage has been established between the anomalous frequency of mid-tropospheric anticyclonic circulation patterns and the recent acceleration of GrIS surface melting during the past few decades. *Fettweis et al.* [2011] employ an automatic Circulation Type Classification (CTC) scheme based on 500 hPa geopotential heights to create groups of analogous synoptic patterns over the GrIS and to link them directly with corresponding surface melting and runoff conditions simulated by the MAR regional climate model. Warm synoptic patterns, particularly types 3 and 7 characterized by a strong ridge centered over Greenland, have become much more prevalent since 1998, while cold synoptic patterns, especially types 2, 5, and 8 characterized by a strong trough centered over Greenland, have been declining significantly since the late 1990s [*Fettweis et al.*, 2011]. From 1958–2009, the summer seasons with the greatest number of days classified in the warm synoptic types occurred during 2007 and 2008, which at least partially explains the extreme GrIS surface melting and runoff observed during these two years [*Fettweis et al.*, 2011]. In a subsequent study, *Fettweis et al.* [2013] found that the frequency of anticyclonic circulation days over the GrIS has increased significantly (from ~15% to ~40% of all days from June through August) over the past two decades, and this frequency increase was independent of the background signal corresponding to global warming.

Several additional studies have reported similar findings with regards to the frequency of anomalous anticyclonic circulation during recent summers. Using self-organizing maps based on 500 hPa height anomaly fields from the NCEP/NCAR Reanalysis, *Bezeau et al.* [2014] found that strong anticyclonic circulations over the Canadian Arctic Archipelago and western Greenland were 2.7 times more frequent between 2007 and 2012 than from 1948–2006. Indeed, the frequency of anticyclonic circulation patterns from 2007–2012 was significantly higher than any other period during the 65-year climatological period of record, and none of the five CMIP5

models selected in this study were able to reproduce the magnitude of the anomalously high frequency of 500 hPa height anomalies from 2007–2012 [Bezeau *et al.*, 2014]. Moreover, the frequency of these strong positive anomalies in 500 hPa heights was greater than two standard deviations above the long-term (1951–2010) mean during four individual years from 2007–2012 [Bezeau *et al.*, 2014].

The recent increase in anticyclonic circulation patterns over Greenland has contributed to enhanced GrIS surface melting during the spring and summer months, especially since the early 2000s. Based on an analysis of the Greenland Blocking Index (GBI) during the NCEP/NCAR Reanalysis period of record (1948–2010) and GrIS surface melt extent data derived from SnowModel simulations driven by MicroMet observations, Hanna *et al.* [2013a] detected a close relationship between unprecedented high pressure patterns over Greenland and highly anomalous surface melting and runoff across the ice sheet during the summers of 2007–2010. A noticeable shift toward strong melt anomalies associated with an increase in anticyclonic circulation over Greenland occurred in 2001, which partially explains the exceptional summer meltwater production in seven individual years from 1998–2012 [Fettweis *et al.*, 2013; Rajewicz and Marshall, 2014]. Overland *et al.* [2012] attribute increases in Greenland blocking from 2007–2012 to the persistence of an Arctic Dipole pattern over the high latitudes of the Northern Hemisphere, which is linked to enhanced GrIS melting due to a greater frequency of meridional wind flow patterns. Despite the close relationship between Greenland blocking and GrIS surface melting, an anomalous frequency of Greenland blocking days during a summer season does not necessarily correspond to exceptionally high melt extents across the GrIS [Häkkinen *et al.*, 2014]. Though June–July 2007 had the greatest number blocking days for any two-month period during 2000–2013, the summer 2007 melt season was not extreme because near-surface

temperature anomalies over the GrIS were insufficient in magnitude, barely reaching 1.5 standard deviations above the summer mean for a few days [Häkkinen *et al.*, 2014].

During episodes of Greenland blocking, the magnitude of surface melt across the GrIS is not spatially homogeneous due to the complex topography of the ice sheet, leading to the formation of numerous regional microclimates within Greenland [Mote 1998a, b]. This is especially true for the eastern and western sectors of Greenland, which are divided by the North Dome (~3,200 meters in elevation) near the center of the ice sheet and the South Dome (~2,900 meters in elevation) in southern Greenland. According to Mote [1998a], variations in surface melt extent, largely dependent on lower-tropospheric temperatures, are more closely linked to the mid-tropospheric circulation early in the melt season (~May), while late-season (~August) circulation patterns predominately govern melt variations in the northern sector of the ice sheet. Many regions of the GrIS, particularly the northern and eastern coasts, require onshore flow throughout the lower troposphere for the development of significant melt events [Mote, 1998b]. Onshore flow is especially critical for much of the eastern half of the GrIS because it can effectively inhibit the downslope drainage of cold katabatic winds from the elevated interior region [Mote, 1998b; Noel *et al.*, 2014]. Blocking highs typically result in a southwesterly onshore flow across western Greenland, producing warmer-than-average surface temperatures and increased melting [Mote, 1998b; Fettweis *et al.*, 2011]. However, subsidence is prevalent over much of eastern Greenland, allowing cold air originating over the North Dome of the ice sheet to drain eastward via katabatic winds and suppress melting over the region [Fettweis *et al.*, 2011]. Using a system of synoptic classification types, Mote (1998b) revealed that higher-than-normal melting was observed over the southwestern, western, and northern sectors of the ice sheet when a 700 hPa ridge axis was centered over eastern Greenland, while above-average

melting over the northeastern, eastern, and southeastern portions of the ice sheet typically occurs when anomalous 700 hPa heights are centered over western Greenland and Baffin Bay.

In addition to these atmospheric processes, GrIS surface melting can also be affected by other important factors, including cloud cover, aerosols, and Arctic sea ice. In an analysis of the exceptional melt event during July 2012, *Bennartz et al.* [2013] revealed that surface melting over broad areas of the GrIS, most notably around Summit Station, was likely amplified by low-level liquid clouds within a narrow range of optical thickness. These clouds were thin enough to allow the penetration of incoming solar radiation but thick enough to prevent an excessive amount of longwave radiation from escaping the lower troposphere. The deposition of atmospheric aerosols, especially black carbon and mineral dust, onto the surface of the GrIS has also been linked to enhanced melting during recent years. A substantial decline in the springtime albedo of the GrIS since 2009 has been linked to an increase in the quantity of light-absorbing impurities, particularly mineral dust, that are advected from Arctic regions affected by earlier snow melt due to global warming [*Dumont et al.*, 2014]. Likewise, the combination of exceptionally warm temperatures and black carbon sediments deposited by Northern Hemisphere forest fires, which significantly lowers the albedo of the dry snow region, likely caused the extreme GrIS melt events of 1889 and 2012 [*Keegan et al.*, 2014].

The rapid decline of Arctic sea ice coverage during the past few decades has also been linked to the recent acceleration of GrIS summer melting [*Liu et al.*, in review]. As the coverage of sea ice decreases in the oceanic waters surrounding Greenland, the vertically integrated (surface to 300 hPa) heat flux that is transported over the ice sheet increases, leading to enhanced surface melting through the formation of a heat dome. In agreement with the results of *Bennartz et al.* [2013], reduced Arctic sea ice coverage also promotes a significant increase in atmospheric

water vapor content over the GrIS due to a greater quantity of ocean water available for evaporation by southerly winds. Increased atmospheric water vapor allows for a higher frequency of low-level liquid cloud formation over the ice sheet, which contributes to additional surface heating through the downward radiation of longwave energy. While low-level clouds reduce incoming solar radiation over the region extending from west-central to northeastern Greenland, increases in surface downwelling longwave radiation over the entire GrIS are much greater in magnitude.

A recent study by *Neff et al.* [2014] identified several factors that likely contributed to the exceptional GrIS surface melting during July 2012. First, anomalously warm air originating within the boundary layer over the central United States, which was experiencing a record heat wave and drought, was transported northeastward to Greenland. Second, unusually moist air, characterized by 4–5 cm of integrated water vapor, was advected northward within an atmospheric river that transected the west coast of Greenland. Finally, the transition to a wave-one pattern in the polar jet stream, represented by low pressure over the central Arctic Ocean and high pressure over Greenland, during a moderately positive AO phase created favorable mid-tropospheric flow conditions for the northward transport of warm humid air to western Greenland. *Neff et al.* [2014] suggest that extreme warming events over Greenland, such as the one that occurred from 11–12 July 2012, coincide with transient patterns in the large-scale polar circulation rather than persistent episodes of high pressure (i.e. Greenland blocks). Slower climatic processes operating on the time scale of months to seasons, such as the development of regional heat waves over North America and anomalously warm SSTs over the North Atlantic, increase the probability of GrIS melt events, but the faster meteorological processes that evolve

over days to weeks, including atmospheric circulation patterns, are required to generate the more extreme melting episodes [Neff *et al.*, 2014].

While the relationship between Greenland blocking and the recent increase in summer melting across the GrIS has been established, the role of other atmospheric and oceanic processes, such as North Atlantic cyclone activity and sea surface temperatures, on the evolution of Greenland blocks remains relatively unexplored. Previous research, including both case studies [Colucci, 1985, 1987; Tsou and Smith, 1990] and climatological analyses [Konrad and Colucci, 1988; Dole, 1989; Nakamura and Wallace, 1990, 1993; Lupo and Smith, 1995] has identified a link between surface cyclogenesis and downstream block development across the Northern Hemisphere. For example, Konrad and Colucci [1988] examined 500 hPa circulation changes associated with 141 explosive cyclones (“bombs”) over the western half of the Northern Hemisphere from September 1980 through May 1987 (excluding the summer months of June–August). Explosive cyclones associated with downstream ridge-building tended to be relatively weaker compared to the remaining sample of bombs. Konrad and Colucci [1988] hypothesize that the shallow, intense circulations of the stronger explosive cyclones are unable to penetrate the middle troposphere, prohibiting any significant meridional advection of air masses. Based on their findings, explosive cyclogenesis does appear to contribute to the development of North Atlantic blocks, but the period of greatest upper-level wave amplification typically occurs after the most rapid phase of surface cyclogenesis, possibly in connection with enhanced air mass advection.

Lupo and Smith [1995] provide an updated climatological analysis regarding the role of extratropical cyclones on downstream block development, but this study only covers a short 3-year period from July 1985 through June 1988. Known as precursor cyclones, a distinct class of

extratropical cyclones originating upstream, or to the west, of blocking anticyclones was examined. All 29 blocking events that occurred in the North Atlantic region (80°W – 40°E) were accompanied by a precursor cyclone, and approximately 72% of these precursor cyclones were characterized by explosive development [Lupo and Smith, 1995]. During the seven winter seasons from December 1980 through February 1987, only 46% (6 of 13) of blocking events over the western half of the Northern Hemisphere (90°W – 90°E) were accompanied by a rapidly intensifying precursor cyclone [Colucci and Alberta, 1996]. The majority (78%) of precursor cyclones during autumn through spring underwent rapid intensification, while none of the precursor cyclones during summer achieved explosive development [Lupo and Smith, 1995]. Finally, the deepening rate of the precursor cyclones was not significantly correlated with the duration or size of the blocking anticyclones [Lupo and Smith, 1995].

An alternative approach is adopted by Gómará *et al.* [2014], in which Rossby wave-breaking (RWB) events are considered to act as precursors, temporally rather than geographically, to explosive cyclone development over the Euro-Atlantic region. Cyclonic RWB is a close corollary to atmospheric blocking, but not all atmospheric blocks over the North Atlantic are generated by cyclonic RWB of synoptic-scale eddies [Benedict *et al.*, 2004; Woollings *et al.*, 2008]. Based on an investigation of 44 winter seasons from October 1957 through March 2001, enhanced cyclonic RWB over the western subpolar North Atlantic region served as a significant precursor of explosive cyclogenesis over the western North Atlantic [Gómará *et al.*, 2014]. In fact, the probability of an explosive cyclone developing in the western North Atlantic is increased by a factor of 1.5 when cyclonic RWB is present over Greenland [Gómará *et al.*, 2014]. In addition, cyclones with greater intensities are more closely associated with cyclonic RWB over Greenland. While 70% of the top 50 most intense cyclones are

preceded by cyclonic RWB over Greenland, only about 37% of all non-explosive cyclones are linked to cyclonic RWB over Greenland [Gómara *et al.*, 2014]. These results are not consistent with the findings of *Konrad and Colucci* [1988], who noted that downstream ridge-building was produced more frequently by relatively weaker explosive cyclones. Moreover, the percentage (46%) of wintertime blocking events accompanied by an explosive precursor cyclone, as determined by *Colucci and Alberta* [1996], is somewhat greater than the percentage (33%) of cyclonic RWB events leading to explosive cyclogenesis over the western North Atlantic. However, these discrepancies could be attributed to observational differences in the related processes of blocking, downstream ridge-building, and cyclonic RWB over different time periods. Also, the theoretical framework for each study was fundamentally different: *Konrad and Colucci* [1988] and *Colucci and Alberta* [1996] viewed explosive cyclones as precursors to upper-level wave amplification while *Gómara et al.* [2014] regarded cyclonic RWB as a precursor to explosive cyclogenesis.

Interannual variability in North Atlantic sea surface temperatures (SSTs) can modulate the intensity of GrIS summer melting and may also govern the frequency of Greenland block development. The Atlantic Multidecadal Oscillation (AMO), the dominant low-frequency mode of SST variability across the North Atlantic, has remained in a persistent positive phase, which is associated with warmer-than-normal SSTs over the North Atlantic Ocean, since the mid-1990s [*Hanna et al.*, 2013a]. More frequent blocking over the subpolar North Atlantic (defined as the region extending from south of Greenland to western Europe) coincided with unusually warm SSTs during the early 2000s [*Häkkinen et al.*, 2011]. Both Greenland coastal station temperatures and GrIS runoff are significantly correlated with the AMO during the past 30–40 years, and the ongoing AMO warm phase likely amplified GrIS melting and runoff over the past

few decades [*Hanna et al.*, 2013a]. However, *Noel et al.* [2014] conclude that oceanic forcing did not have a significant effect on the exceptional surface melting of the GrIS since 2007 because katabatic winds are usually strong enough to prevent an inland incursion of maritime air masses.

Despite the anomalously high frequency of Greenland blocks since the early 2000s, it is difficult to conclude whether this trend will persist into the future. As previously stated, the Arctic region has been warming at an accelerated rate compared to both the mid-latitudes and the tropics over the past few decades, a phenomenon known as Arctic amplification [*Serreze and Francis*, 2006]. While Arctic sea ice loss has been shown to be the primary driver of Arctic amplification during autumn and winter, the increasing tendency for earlier snow melt and a corresponding dry-out of high-latitude land surfaces is largely responsible for anomalous upper-level wave patterns during the summer [*Francis and Vavrus*, 2012]. *Francis and Vavrus* [2012] detected a statistically significant northward stretching of 500 hPa ridge peaks and a weakened polar jet stream over the North American / North Atlantic region from 1979–2010, which suggests an increasingly favorable environment for block formation during more recent years. Recent summer heat waves across the mid-latitudes tend to be associated with persistent, high-amplitude Rossby wave patterns that are characterized by a high zonal wavenumber, which affirms the dynamical process of “ridge stretching” as suggested by *Francis and Vavrus* [2012] [*Petoukhov et al.*, 2013].

Subsequent studies, however, have challenged the linkage between Arctic amplification and high-latitude atmospheric circulation variability by demonstrating that this relationship is statistically sensitive to methodological choices [*Screen and Simmonds*, 2013; *Barnes*, 2013]. According to *Screen and Simmonds* [2013], the impact of Arctic amplification is tenuous

because the interannual variability of planetary wave patterns is substantially greater than recent changes in their meridional amplitude. *Barnes et al.* [2014] remark that blocking frequencies over the North Atlantic region during the past few years are unexceptional when compared to the large amount of interannual blocking variability since 1948. Though very few significant trends in Northern Hemisphere blocking frequency were identified in their study, an increase in summer (JJA) blocking frequency based on the *Masato et al.* [2013] index was detected over the North Atlantic region near Greenland (300°–0°E) for three out of four reanalysis products [*Barnes et al.*, 2014].

Most global circulation models (GCMs), even the most advanced versions such as CMIP5, have also struggled to simulate atmospheric blocking reliably with respect to reanalysis-based verification. Both CMIP3 and CMIP5 model projections indicate a significantly large decrease in summertime blocking frequency (~40% fewer blocked days) over the North Atlantic region by the end of the century [*Barnes et al.*, 2012; *Masato et al.*, 2013]. However, these results must be interpreted with caution given the large amount of model bias and inter-model variability [*Masato et al.*, 2013]. *Belleflamme et al.* [2013] used the circulation type classification developed by *Fettweis et al.* [2011] to compare daily 500 hPa heights simulated by CMIP5 GCMs with three reanalysis products for the current (1961–1990) climate. The GCMs cannot effectively simulate the historical anomalies of 500 hPa heights over Greenland, and they do not project any significant changes in atmospheric circulation frequency into the future [*Belleflamme et al.*, 2013]. Thus, future changes in blocking frequency over the North Atlantic region remain highly uncertain.

CHAPTER 2

LINKING SEASONAL CHANGES IN EXTREME GREENLAND BLOCKING EPISODES TO THE RECENT INCREASE IN SUMMER MELTING ACROSS THE GREENLAND ICE SHEET ¹

¹ McLeod, J.T. and T.L. Mote. To be submitted to *Journal of Geophysical Research: Atmospheres*

Abstract

Atmospheric blocks commonly form over the high latitudes as persistent areas of high pressure that lead to warmer-than-average surface temperatures. In this study, a historical climatology of extreme Greenland blocking episodes from 1958–2013 is examined within the context of anomalous anticyclonic circulation patterns over the North Atlantic region during recent years. The Greenland Blocking Index is used to quantify 500 hPa geopotential height anomalies for the identification of extreme “Greenland blocking episodes”. The annual rate of extreme blocking days has doubled since 1958, reaching an average of approximately 20 days per year by 2013. The frequency and, to some extent, duration of extreme Greenland blocking episodes were unprecedentedly high from 2007–2013 compared to the 56-year period of record, with a majority of the increase occurring during the spring (MAM) and summer (JJA). A multiple linear regression analysis reveals that Greenland blocking and the AMO are significant drivers of surface meltwater production across the entire GrIS, while North Atlantic cyclone activity is an important factor for summer melting primarily over eastern Greenland.

Key words: Greenland blocking, North Atlantic cyclones, Greenland ice sheet, Arctic amplification

2.1 Introduction

Across the Northern Hemisphere, synoptic-scale ridges of high pressure extending poleward from the mid-latitudes to the Arctic region are observed frequently throughout the year. If they are sufficiently strong and persistent, these anticyclonic systems, known as atmospheric blocks, can divert migratory shortwave disturbances toward higher latitudes by displacing the predominant steering flow of the polar jet stream equatorward. Atmospheric blocks, particularly those over the North Atlantic region, are usually generated by cyclonic wave breaking of synoptic-scale eddies that advects relatively warm and moist air masses toward the polar latitudes [Benedict *et al.*, 2004; Woollings *et al.*, 2008]. These modified air masses often cut off from the polar jet stream and may persist over high-latitude regions for up to several weeks [Barriopedro *et al.*, 2006]. While blocking anticyclones can develop over many areas of the Northern Hemisphere, the focus of this study pertains to blocks that are located over the northwestern Atlantic Ocean, commonly referred to as Greenland blocks.

Greenland blocking is directly related to a low-frequency teleconnection pattern known as the North Atlantic Oscillation (NAO), the dominant mode of atmospheric variability over the Atlantic Ocean [Shabbar *et al.*, 2001; Benedict *et al.*, 2004; Woollings *et al.*, 2008; Davini *et al.*, 2012]. Greenland blocks, particularly the stronger and more persistent events, develop most frequently during negative phases of the NAO, which are characterized by a weak, high-amplitude polar jet stream over the North Atlantic [Woollings *et al.*, 2008]. Indeed, the annual number of Greenland blocking days is highly anticorrelated ($r = -0.81$) with the yearly-averaged NAO index [Davini *et al.*, 2012]. Despite this strong relationship, Hanna *et al.* [2013a] revealed that the NAO alone could not sufficiently explain the exceptional Greenland blocking patterns during the summers of 2007–2010, which suggests that a complex interaction of atmospheric and

oceanic processes may be responsible. For example, the Arctic Oscillation (AO), a hemispheric mode of atmospheric variability capturing pressure differences between the Arctic region and the mid-latitudes, is strongly correlated with the NAO and further modulates the potential for Greenland block development.

Previous studies have examined climatological characteristics of atmospheric blocks across the Northern Hemisphere [*Lupo and Smith, 1995; Barriopedro et al., 2006; Tyrlis and Hoskins, 2008*], while other research has been focused on the development of improved blocking detection techniques [*Pelly and Hoskins, 2003; Barnes et al., 2012*]. In addition, the long-term variability of atmospheric circulation patterns over the North Atlantic region has been linked to an increased rate of surface melting and runoff across the Greenland ice sheet (GrIS) during recent decades [*Mote, 1998a, 1998b; Fettweis et al., 2011; Hanna et al., 2013a; Rajewicz and Marshall, 2014*]. However, a climatological investigation of extreme Greenland blocking episodes and their impact on the extent of GrIS surface melting has remained largely unexplored. This relationship is particularly significant given that the quantity of freshwater stored in the GrIS would correspond to 6–7 meters of global sea level rise if it were all to be released [*Cuffey and Marshall, 2000; Nghiem et al., 2012*].

Within the past few years, Greenland blocks have been both directly and indirectly linked to two major climatic events in the North Atlantic, namely Hurricane Sandy (2012) and the record-breaking melt episode across the GrIS during July 2012. From 22–29 October 2012, an unusually strong Greenland block persisted over the North Atlantic and prevented the northward-tracking Hurricane Sandy from recurving northeastward similarly to most tropical cyclones along the East Coast of the United States [*Greene et al., 2013; Mattingly et al., 2014*]. Quantified by the Greenland Blocking Index [*Fang, 2004; Hanna et al., 2013a*], the strength of the block

prior to Sandy's landfall on 29 October 2012 remained above the 97th percentile of mean climatological values for four consecutive days from 24–27 October, which likely diverted Sandy into the New Jersey coastline after an unprecedented westward turn [Mattingly *et al.*, 2014]. From 11–12 July 2012, observations from three satellite-based instruments, including MODIS and SSMIS, indicated that melting was detected across approximately 98.6% of the GrIS [Nghiem *et al.*, 2012]. According to multiple ice core records from Summit Station, an extreme melting event of this magnitude had not occurred since 1889 [Clausen *et al.*, 1988; Nghiem *et al.*, 2012]. A series of exceptionally anomalous Greenland blocks developed from the end of May until mid-July during the summer of 2012, which was characterized by the most negative NAO index since 1950 [Hanna *et al.*, 2013b; Tedesco *et al.*, 2013].

Historical trends in Greenland blocking are also important within the context of recent climate change across the broader Arctic region. Over the past few decades, the Arctic has been warming at a much faster rate than both the mid-latitudes and the tropics, a phenomenon known as Arctic amplification [Serreze and Francis, 2006]. While Arctic amplification has likely contributed to unprecedented tropospheric warming and melt/runoff rates over the GrIS, there is only limited evidence that atmospheric circulation patterns from the mid- to high latitudes have also been affected. A recent study by Francis and Vavrus [2012] has suggested that the frequency of blocking across the North Atlantic region will increase in the future due to a reduction in the poleward thickness gradient, resulting in a weakening of the upper-level zonal flow, and a meridional elongation of planetary waves. However, subsequent research has questioned this assertion because the most reliable global circulation models generally project a decreasing frequency of blocking conditions across the North Atlantic region [Barnes *et al.*, 2012; Belleflamme *et al.*, 2013; Masato *et al.*, 2013].

The purpose of this study is to examine various aspects (frequency, strength, and duration) of extreme “Greenland blocking episodes” (GBEs) during 1958–2013 in order to assess the future potential for significant changes in the North Atlantic atmospheric circulation. While recent work [e.g. *Fettweis et al.*, 2011; *Hanna et al.*, 2013a; *Rajewicz and Marshall*, 2014] has focused primarily on the variability of anticyclonic circulation patterns over Greenland, only the most extreme GBEs in the historical record will be examined in this study. A seasonal analysis of these extreme GBEs will also be presented to evaluate their role in summer melting trends across the GrIS. Finally, an OLS multiple regression approach will be used to determine any statistically significant predictors of GrIS melt since the beginning of the satellite observational period in 1979. Section 2 provides an explanation of the data sources and methods employed in this study, including the construction of the extreme GBE climatology and the development of the multivariate regression models. Some key results and associated discussion are provided in Section 3. Finally, a brief description of the results within the context of Arctic amplification and a concluding summary are offered in Section 4.

2.2 Data and Methods

In order to generate a database of extreme GBEs, daily mean fields of 500 hPa geopotential heights were created from six-hourly output provided by a combination of the ERA-40 and ERA-Interim reanalysis datasets [*Uppala et al.*, 2005; *Dee et al.*, 2011]. ERA-40 reanalysis data spanning the period from 1958–1978 were used to augment the ERA-Interim dataset, which covers the satellite observational era from 1979 to present. Because these reanalysis products are characterized by different spatial resolutions and data assimilation schemes, the raw data were interpolated onto a $0.5^\circ \times 0.5^\circ$ gridded domain for the entire period of record. Though ERA-40 temperature departures from radiosonde observations near the 500

hPa level (strongly correlated to 500 hPa geopotential heights) are characterized by a slightly higher RMSE than those assimilated in ERA-Interim, the interannual variability in 500 hPa heights should be sufficiently preserved across the two reanalysis products (Figure 18 in *Dee et al.* [2011]). In addition, the suite of observations assimilated into ERA-40 and ERA-Interim are very similar, so any biases between the reanalyses can be traced exclusively to improvements in modeling rather than background atmospheric trends [*Dee and Uppala, 2009*].

The Greenland Blocking Index was selected to quantify episodes of extreme blocking over Greenland during a 56-year period of record from 1958–2013. Based on *Hanna et al.* [2013a], the Greenland Blocking Index (GBI) is defined as the mean 500 hPa geopotential height over the Greenland region spanning from 60°–80°N latitude and 20°–80°W longitude (Figure 2.1). Rather than detecting Greenland blocks based on a set of strict objective criteria, this approach is used to identify 500 hPa circulation patterns characterized by extreme positive values of the GBI, which indicates highly anomalous ridging over the GrIS. Thus, the extreme GBEs analyzed in this study may not satisfy all of the established criteria for atmospheric blocks as discussed in previous research [*Pelly and Hoskins, 2003; Barnes et al., 2012; Masato et al., 2013*]. Recent studies [*Barnes et al., 2014; Rajewicz and Marshall, 2014*] have raised concerns over the use of a metric based on mid-tropospheric height anomalies to assess changes in atmospheric circulation variability. Though 500 hPa geopotential heights are a good indicator of synoptic-scale circulation patterns, they are also affected by surface-based temperature changes due to global warming and Arctic amplification [*Rajewicz and Marshall, 2014*].

Nevertheless, *Bezeau et al.* [2014] stated that this methodological approach was appropriate because the daily climatological variability in 500 hPa height anomalies over the Northern Hemisphere is significantly greater than the long-term increase in these heights due to

Arctic amplification. Based on a linear regression of 500 hPa height anomalies computed at each 2.5° by 2.5° grid cell within the daily NCEP/NCAR Reanalysis fields, the increase in these height anomalies during 1948–2012 was 17 meters on average across the Northern Hemisphere, and the standard deviation of these anomalies was 61 meters [Bezeau *et al.*, 2014]. Despite this finding, it is necessary to preserve the long-term increase in mid-tropospheric heights within the GBI time series in order to capture the combined effects of natural variability in atmospheric circulation and Arctic amplification on extreme Greenland blocking. Though the GBI and NAO are strongly and significantly correlated ($r = -0.75$, $p < 0.001$), the GBI was preferable to the NAO index because it reflects atmospheric circulation patterns that are specific to Greenland rather than the broader North Atlantic region. In addition, variations in these circulation patterns will be linked to surface melting across the GrIS in this study, and *Hanna et al.* [2013a] showed that Greenland coastal summer temperatures and ice melt runoff have been more strongly correlated with the GBI than the NAO since the 1970s.

An objective approach for identifying extreme GBEs based on the GBI was developed. Specifically, a mean GBI value was computed for each day during the period of record by averaging the index across the four observations gathered at standard 6-hourly intervals (0000 UTC, 0600 UTC, 1200 UTC, 1800 UTC). A low-pass filter based on *Blackmon* [1976] was applied to these daily GBI values in order to minimize the high frequency variability and preserve the more relevant features (e.g. blocks) within the 500 hPa height field. In addition, the seasonal cycle in 500 hPa heights over Greenland was removed by standardizing the GBI time series. Specifically, the GBI value for each day during the 56-year period of record was quantitatively compared to all other daily GBI values from 1958–2013 that occurred within a 7-day period centered on the day in question. The 7-day moving periods were selected as the

climatological baseline for this analysis in order to capture sampling distributions of GBI values that are sufficiently representative of each day's potential range of observations. Thus, the GBI value for each day from 1958-2013 was assigned a Z-score and associated percentile rank with respect to its unique 7-day climatological distribution.

Due to the lack of an established definition for extreme GBEs, it was necessary to develop a set of objective criteria by which these events could be consistently identified. Therefore, composite maps of 500 hPa heights over the North Atlantic region were generated for sets of days in which the GBI ranked within a unit percentile range (e.g. 99.0th– 99.9th percentile) from the 90th–100th percentiles when compared to the 56-year climatological distribution (Figure 2.2). Based on this approach, an extreme GBE is defined as a sequence of at least five consecutive days in which the GBI equals or exceeds the 97th percentile (or a Z-score of +1.88 standard deviations) of all daily GBI values from 1958–2013 that occurred within a 7-day window centered on the day(s) in question. While the duration criterion is somewhat subjective, it has become the accepted threshold for blocking events in many prior climatological studies, beginning with *Treidl et al.* [1981]. The intensity threshold for extreme blocking conditions was set at the 97th percentile because the composite maps, displayed with a standard contour interval of 60 meters, reveal that extreme GBEs lose their distinguishing signature of at least one closed 500 hPa isoheight below this percentile rank.

It is hypothesized that interannual variability in summer melting across the GrIS can be explained effectively by certain aspects of the North Atlantic atmospheric and oceanic circulations. However, the magnitude of surface melt is not spatially homogeneous due to the complex topography of the ice sheet, leading to the formation of numerous regional microclimates within Greenland [*Mote* 1998a, b]. This is especially true for the eastern and

western sectors of Greenland, which are divided by the North Dome (~3,200 meters in elevation) near the center of the ice sheet and the South Dome (~2,900 meters in elevation) in southern Greenland. Therefore, standard OLS multiple regression models are used to quantify the relative impact of six predictors on the average daily meltwater production over eastern and western Greenland for each summer (June–August) season from 1979–2008. The following seven independent variables were also constructed for each summer season from 1979–2008: (1) the mean GBI value, (2) the mean value of the summer NAO index, (3) the mean value of the AO index, (4) the frequency of North Atlantic cyclones, (5) the average intensity of these cyclones, (6) the maximum deepening rate of these cyclones, and (7) the mean value of the AMO index. The period of record for the regression models is constrained to the satellite observational era beginning in 1979 to ensure the most reliable estimates of surface meltwater production over a relatively data-sparse region of the high latitudes. In addition, the period of record is terminated in 2008 due to a lack of North Atlantic cyclone data from 2009–2013.

Meltwater production data were obtained from the MAR Greenland Explorer, which provides daily gridded output at a 25km spatial resolution [*Fettweis, 2007; Tedesco et al., 2013; Tedesco et al., 2014*]. MAR is a three-dimensional atmosphere-land surface regional climate model coupled to the SISVAT vegetation scheme, which includes a version of the CROCUS snow model [*Brun et al., 1992*]. CROCUS is more sophisticated than most snow models used in regional climate models because it is capable of more fully simulating the evolution of snow properties and refreezing of meltwater. The ERA-Interim reanalysis is used as the atmospheric forcing at the MAR lateral boundaries every six hours [*Tedesco et al., 2013*]. The meltwater data was divided into a West Greenland subset, spanning the entire area of the ice sheet located westward of the 45°W meridian, and an East Greenland subset, covering the portion of the ice

sheet situated eastward of the 45°W meridian. These two regional subsets are roughly separated by the topographical divide that extends along the center of the ice sheet in a generally north-south orientation.

While it would be more precise to use the frequency of all extreme GBEs or extreme blocking days as independent variables in these models, there are many years during this relatively short period of record in which summer events were not observed. Therefore, the mean GBI value was selected as a proxy metric for Greenland blocking activity during each summer season because it is a continuous quantitative variable with unique values for each annual observation. The raw, unfiltered version of the GBI was used to preserve all modes of frequency variability when statistically compared to the regional meltwater trends. The mean AO and summer NAO indices for each summer season were calculated by averaging the daily AO and summer NAO observations provided by the Climate Prediction Center [CPC, 2014] and KNMI Climate Explorer [KNMI, 2014], respectively. The mean summer AMO index was computed by averaging the daily AMO observations generated by the *van Oldenborgh et al.* [2009] method, which only captures sea surface temperature (SST) changes northward of 25°N in order to minimize the influence of ENSO [KNMI, 2014].

North Atlantic cyclone data was obtained from the “Northern Hemisphere Cyclone Locations and Characteristics from NCEP/NCAR Reanalysis Data” record compiled by *Serreze* [2009] at the National Snow and Ice Data Center (NSIDC). A spatial criterion capturing only those cyclones located between 45°–60°N latitude and 75°–25°W longitude was implemented in order to ensure that the GrIS could have been affected by all cyclones in the sample. A cyclone must persist for at least 24 hours within this geographic domain in order to be included in the analysis, but cyclones that remained stationary throughout their entire life cycles were discarded

[*Serreze and Barrett, 2008*]. The frequency of North Atlantic cyclones for each summer season was acquired by summing the total number of storms from June through August that satisfied all of these criteria, and the mean intensity of these cyclones was based on the average minimum central pressure (measured at 6-hourly intervals) across the entire life cycle of each storm. Finally, the maximum 6-hourly deepening rate was acquired for each cyclone, and these values were averaged across all cyclones during each summer season in order to produce a measure of mean cyclone intensification.

A standard OLS linear regression approach was used to estimate the model parameters, but a diagnostic inspection was also needed to verify the robustness of the statistically modeled relationships. First, this investigation revealed excessive multicollinearity between the GBI and summer NAO variables for both model configurations because they are strongly correlated metrics of atmospheric pressure patterns over the North Atlantic region. The variance inflation factors (VIFs) for the GBI variable and, to some extent, the summer NAO variable were excessively high due to this strong positive correlation. Therefore, it was necessary to remove the summer NAO variable (in favor of preserving the proxy variable for Greenland blocking activity) and re-estimate the regression model in order to account for this excessive amount of multicollinearity between independent variables. The VIFs for each of the six remaining predictors decreased to more satisfactory values after removing the summer NAO variable from the estimated model, with the greatest reduction associated with the GBI variable. The model was also analyzed for highly influential observations and heteroscedasticity, and the results were satisfactory.

2.3 Results

A time series of the annual frequency of days characterized by extreme positive anomalies of the GBI, referred to as “extreme blocking days”, from 1958–2013 is presented in Figure 2.3. This graph reflects the frequency of all extreme blocking days regardless of whether or not each day was associated with an extreme GBE as previously defined. However, it is worth noting that approximately 93% of all extreme blocking days during the period of record were linked to extreme GBEs, which require sequences of at least 5 consecutive days characterized by extreme positive anomalies of the GBI. While there is considerable interannual variability from 1958–2013, the frequency of extreme blocking days has been steadily increasing since the early 1990s, reaching a maximum in the late 2000s and early 2010s. Based on a linear regression of this time series, the annual rate of extreme blocking days has doubled since 1958, reaching an average of approximately 20 days per year by 2013. Approximately 24% of all extreme blocking days from 1958–2013 occurred during the 7-year period from 2007–2013, which is nearly twice the expected 7-year frequency (i.e. 12.5%) based on a 56-year period of record. Using a circulation type classification scheme based on 500 hPa heights from two reanalysis products, *Fettweis et al.* [2011] showed that warm synoptic patterns associated with mid-tropospheric ridging have become much more prevalent since the late 1990s. While *Fettweis et al.* [2011] focused exclusively on summer conditions, the trends in anticyclonic circulation variability presented in their study largely support those shown in Figure 2.3.

The primary focus of this paper is to examine climatological characteristics of extreme GBEs rather than extreme blocking days, which may not be linked to significant events of interest (Figure 2.4). The frequency (events or daily counts) of extreme GBEs was exceptionally high, nearly two standard deviations greater than the long-term average, from 2007–2013 with

respect to the 56-year period of record (Figure 2.4a, b). While the mean duration of extreme GBEs was noticeably high from 2007–2013, approaching two days greater than the climatological mean, the range of uncertainty in this estimated value is not statistically distinct from the climatological distribution (Figure 2.4d). The mean strength of extreme GBEs has exhibited very little variability from 1958–2013 (Figure 2.4c). These results differ significantly from *Barnes et al.* [2014], who remark that blocking frequencies over the North Atlantic region during the past few years are unexceptional when compared to the large amount of interannual blocking variability since 1948. Though very few significant trends in Northern Hemisphere blocking frequency were identified in their study, an increase in summer (JJA) blocking frequency based on the *Masato et al.* [2013] index was detected over the North Atlantic region near Greenland (300°-0°E) for three out of four reanalysis products [*Barnes et al.*, 2014].

With the frequency and, to some extent, duration of extreme GBEs increasing over the past few decades, it is important to determine whether extreme blocking has become more prevalent during a particular season(s). This is especially significant in the context of highly anomalous melting across the GrIS, which has occurred during several summer seasons since 2002. For the following seasonal analyses, extreme GBEs were grouped according to the standard meteorological seasons: winter (December–February), spring (March–May), summer (June–August), and autumn (September–November). If an extreme GBE overlapped multiple seasons, it was assigned to the season containing the greatest number of blocking days in the sequence. Figure 2.5 provides composite anomaly maps of 500 hPa geopotential heights and 2-meter air temperatures for all extreme GBEs grouped according to season. As expected, the magnitudes of both 500 hPa height and 2-meter air temperature anomalies are greatest during winter and least during summer over the Greenland region. The greatest positive anomalies in

500 hPa heights migrate northward from southwestern Greenland during winter to west-central Greenland in spring and autumn. This pattern is accompanied by a generally northward displacement of 2-meter air temperature anomalies from western Greenland during winter and spring to northern Greenland in summer and autumn. According to *Mote* [1998a], variations in surface melt extent, largely dependent on lower-tropospheric temperatures, are more closely linked to the mid-tropospheric circulation early in the melt season (~May), while late-season (~August) circulation patterns predominately govern melt variations in the northern sector of the ice sheet. Though atmospheric blocks have the greatest direct impact on GrIS surface melting conditions throughout the summer melt season, blocking events that occur during the other three seasons can pre-condition the ice sheet for anomalous summer melting. For example, persistent blocking episodes often reduce snowfall accumulation over the GrIS due to prevailing clear sky conditions, which significantly lowers the albedo of the ice sheet as the impurity-rich multiyear ice cover is exposed with the onset of surface melting [*Box et al.*, 2012].

Both 500 hPa height and 2-meter air temperature anomalies are considerably greater across the western half rather than the eastern half of the GrIS during all seasons, which is consistent with a higher rate of surface melting typically observed across the western coast of Greenland [*Mote*, 1998b]. Blocking highs typically result in a southwesterly onshore flow across western Greenland, producing warmer-than-average surface temperatures and increased melting [*Mote*, 1998b; *Fettweis et al.*, 2011]. However, subsidence is prevalent over much of eastern Greenland, allowing cold air originating over the North Dome of the ice sheet to drain eastward via katabatic winds and suppress melting over the region [*Fettweis et al.*, 2011]. The area of maximum 500 hPa height anomalies also corresponds well with the westward shift in the NAO center of action that occurs during years with a high frequency of Greenland blocks [*Davini et*

al., 2012]. Years characterized by negative NAO conditions and relatively high Greenland blocking activity are associated with an NAO center of action that is located over the Labrador Sea off the southwestern coast of Greenland [*Davini et al.*, 2012].

The frequency, strength, and duration of extreme GBEs from 1958–2013 are plotted by season in Figure 2.6. The frequency of extreme GBEs is consistent across all seasons with the exception of spring, which features a relatively fewer number of blocking episodes (Figure 2.6a). Based on a limited 3-year study, *Lupo and Smith* [1995] reported that blocking frequency over the North Atlantic region, bounded by the 80°W and 40°E meridians, was roughly equivalent from fall through spring (October–June) with a distinct summer (July–September) minimum. Extreme GBEs during the summer tend to have a weak-to-moderate intensity, while extreme GBEs during the winter often have a moderate-to-strong intensity (Figure 2.6b). Indeed, 75% of extreme summer GBEs are ranked within the weak or moderate category of blocking intensity, while approximately 77% of all extreme winter GBEs are ranked within the moderate or strong category of blocking intensity. Extreme winter GBEs are also characterized by a considerably longer duration on average than extreme summer GBEs (Figure 2.6c). Seventy-five percent of extreme summer GBEs are ranked within the short-to-moderate category of blocking duration, while approximately 77% of extreme winter GBEs are ranked within the moderate-to-long category of blocking duration. *Lupo and Smith* [1995] also show that winter blocks are considerably stronger than summer blocks, and they indicate that winter blocks are more persistent on average than summer blocks. The strength of both extreme spring and autumn GBEs can be quite variable, but the duration of extreme spring GBEs is significantly greater ($p < 0.05$) than all other seasons (Figure 2.6b, c). These patterns are consistent with the seasonal cycle of the polar jet stream's strength and position across the North Atlantic region. A strong but

southward-displaced jet stream during the winter favors relatively intense, long-lasting GBEs, while a much weaker but northward-displaced jet stream during the summer coincides with relatively weak, transient GBEs. Extreme spring and autumn GBEs display much more diverse ranges of strength and duration due to the transitional nature of the polar jet stream during these seasons.

The percentages of extreme GBEs occurring within 14-year periods from 1958–2013 are computed for each season (Table 2.1). A bin size of fourteen years was selected instead of the 7-year periods used in Figure 2.4 to maintain appropriate sample sizes of extreme events across all four seasons. Fifty percent of all extreme summer GBEs were observed during the most recent 14-year period from 2000–2013, which is double the expected frequency of 25% for each 14-year period within a 56-year climatological record. In addition, approximately 43% of all extreme spring GBEs occurred from 2000–2013, a disproportionately greater percentage than the previous three 14-year periods. Several studies have reported similar findings with regards to the frequency of anomalous anticyclonic circulation during recent summers. Using self-organizing maps based on 500 hPa height anomaly fields from the NCEP/NCAR Reanalysis, *Bezeau et al.* [2014] found that strong anticyclonic circulations over the Canadian Arctic Archipelago and western Greenland were 2.7 times more frequent between 2007 and 2012 than from 1948–2006. In addition, the frequency of these strong positive anomalies in 500 hPa heights was greater than two standard deviations above the long-term (1951–2010) mean during four individual years from 2007–2012 [*Bezeau et al.*, 2014].

Taken together, these results suggest the potential for a robust linkage between extreme blocking activity and observed surface melting across the GrIS during the spring and summer months, especially since the early 2000s. Based on an analysis of the GBI during the

NCEP/NCAR Reanalysis period of record (1948–2010) and GrIS surface melt extent data derived from SnowModel simulations driven by MicroMet observations, *Hanna et al.* [2013a] detected a close relationship between unprecedented high pressure patterns over Greenland and highly anomalous melt/runoff across the ice sheet during the summers of 2007–2010. A noticeable shift toward strong melt anomalies associated with an increase in anticyclonic circulation over Greenland occurred in 2001, which partially explains the exceptional summer meltwater production in seven individual years from 1998–2012 [*Fettweis et al.*, 2013; *Rajewicz and Marshall*, 2014].

While previous studies have identified various atmospheric and oceanic processes that are strongly linked to GrIS surface melting, the relative contribution of each factor to the variability in summer melt extents has not been quantified. Two OLS multiple regression models are developed in order to reveal any statistically significant predictors of GrIS surface meltwater production during the summer (JJA). As previously mentioned, the first model is designed to capture variables that explain average summer melting conditions across western Greenland most effectively, and the second model is used to identify significant predictors of summer melting over eastern Greenland. Different aspects of the climate system within the North Atlantic region, such as cyclone activity and SST anomalies, may be relatively more important for surface melting over these two distinct regions of the GrIS.

The results for each multiple regression model are presented in Tables 2.2 and 2.3, respectively. For the first model, the mean summer GBI and AMO indices are the only statistically significant predictors (at the 95% confidence level) of mean daily meltwater production across western Greenland for each summer season from 1979–2008. A positive GBI, signifying greater-than-normal 500 hPa heights over the GrIS, and a positive AMO index, which

represents warmer-than-normal North Atlantic SSTs, are associated with a high summer meltwater production over western Greenland. Though only two of the six variables are statistically significant predictors, the model explains approximately 82% of the variance in mean daily meltwater production across western Greenland.

All six independent variables for the second model are statistically significant predictors of mean daily meltwater production across eastern Greenland for summer seasons between 1979 and 2008. While the GBI and AMO indices remain the strongest predictors, North Atlantic cyclone activity and the AO also play a significant role in modulating eastern Greenland meltwater production during the summer. According to the partial slope coefficients, high summer meltwater production over eastern Greenland is associated with a low frequency and weak intensity of North Atlantic cyclones that occur during the positive phase of the AO. The North Atlantic cyclone track is typically active during positive phases of the AO, but this relationship is much stronger in winter rather than summer [*Thompson and Wallace, 1998*]. Though relatively weak, cyclones that occur during summers characterized by high meltwater production over eastern Greenland generally exhibit rapid rates of intensification (Table 2.2). This is consistent with previous research by *Konrad and Colucci [1988]*, who found that blocking ridges of high pressure are often preceded geographically by a rapidly intensifying surface cyclone. Indeed, 72% of blocking events in the North Atlantic region from July 1985 to June 1988 were preceded by an explosive cyclone, and the more rapidly deepening cyclones were generally associated with the development of stronger blocks [*Lupo and Smith, 1995*].

Though cyclone activity over the broader North Atlantic region is likely reduced during periods of high meltwater production across eastern Greenland, the frequency of cyclones along the eastern coast of Greenland may be unusually high, leading to an enhanced poleward transport

of relatively warm, moist air over the ice sheet. In order to test this hypothesis, the spatial frequency of cyclones that occurred during the top tercile (i.e. top 10 years) of summer meltwater production seasons for eastern Greenland were compared to the geographic distribution of cyclones within the remaining 20 summer melting seasons (Figure 2.7a). For these 10 summer seasons, the frequency of North Atlantic cyclones was anomalously high off the southeastern coast of Greenland extending eastward toward the British Isles, possibly connected with a strong Icelandic low. As indicated by *Barry and Kiladis* [1982], cyclones affecting eastern Greenland during summer generally originate from the North American continent and track toward the vicinity of the Icelandic low [*Mote*, 1998b].

Many regions of the GrIS, particularly the northern and eastern coasts, require onshore flow throughout the lower troposphere for the development of significant melt events [*Mote*, 1998b]. Onshore flow is especially critical for much of the eastern half of the GrIS because it can effectively inhibit the downslope drainage of cold katabatic winds from the elevated interior region [*Mote*, 1998b; *Noel et al.*, 2014]. Figure 2.8 displays the near-surface vector wind anomalies for high melt days, defined by daily meltwater production values at least 1 standard deviation greater than the respective long-term (1979–2008) monthly mean, compared to low melt days, characterized by daily meltwater production values at least 1 standard deviation lower than the respective long-term (1979–2008) monthly mean, during the aforementioned top 10 summer melting seasons. During high melt days over eastern Greenland (Figure 2.8a), katabatic winds were slightly weaker across much of the eastern half of the ice sheet, particularly the southeastern and northeastern sectors. This diminished katabatic wind flow may be connected with enhanced onshore winds associated with persistent cyclonic activity centered to the west of Iceland, consistent with the pattern depicted in Figure 2.7a. While the frequency of cyclones

during the top 10 summer melting seasons for western Greenland was anomalously high over Quebec, some of these cyclones did not continue to track northward into the Baffin Bay region (Figure 2.7b). Nevertheless, near-surface winds during high melt days were considerably stronger along the entire western coast of Greenland, which suggests that southerly winds within the warm sectors of northward-tracking cyclones can contribute to melting across the western GrIS (Figure 2.8b).

Despite the importance of North Atlantic cyclones, the regression models indicate that the interannual variability in average summer melting conditions across the GrIS can largely be attributed to a dynamic linkage between the AMO and Greenland blocking activity during the last 30 years. Persistent above-average SSTs over the North Atlantic associated with the warm phase of the AMO likely amplified GrIS melt and runoff, particularly since the mid-1990s [Hanna *et al.*, 2013a]. Hakkinen *et al.* [2011] found that wintertime atmospheric blocking was more frequent over the North Atlantic region extending from southern Greenland to western Europe during the recent AMO warm phase since 1996. Noel *et al.* [2014] suggested that the role of oceanic forcing on surface meltwater production might be restricted to the coastal regions of Greenland because katabatic winds originating from the center of the ice sheet are usually strong enough to prevent a substantial inland incursion of marine air masses. However, the AMO is a statistically significant predictor of surface meltwater production over the entire western and eastern sectors of the GrIS, not just the coastal regions.

It is worth mentioning that the summer NAO variable is a statistically significant (at the 95% confidence level) predictor of surface meltwater production for both the western and eastern regions of the GrIS. If the summer NAO variable is substituted into the western Greenland model for the GBI variable, the multiple R^2 value decreases substantially from 0.824 to 0.583,

indicating that approximately 42% rather than 18% of the sample variance in the dependent variable remains unexplained. A similar pattern exists for the eastern Greenland model, but there is a less significant decline in the multiple R^2 value from 0.807 to 0.656. Though the summer NAO is a statistically significant predictor in these regression models, the GBI can explain a greater proportion of the variance in summer melting conditions across the GrIS because it is a more precise measure of atmospheric circulation variability over Greenland.

2.4 Discussion and Conclusion

The frequency and, to some extent, duration of extreme GBEs has been increasing during the past few decades, with the greatest increase observed during the summer months. Though extreme GBEs during the summer are relatively weak and short-lived, a continued increase in their frequency or duration could have significant ramifications for the intensity of future GrIS melt seasons. The regression analysis confirms that summer melting conditions are more sensitive to local atmospheric anomalies, such as mid-tropospheric blocking or extratropical cyclone activity, than broader-scale teleconnection patterns like the AO and NAO. Indeed, GrIS melt and the NAO were weakly anticorrelated from 2000–2013, with the daily NAO index explaining only 15% of GrIS melt variability [Hakkinen *et al.*, 2014]. Based on MODIS-derived daily melt areas calculated from clear-sky ice surface temperature data, it has been shown that relatively inactive melting seasons during the past decade (2000, 2001, 2003, 2008, 2010) occurred when the summer NAO regime was either neutral or negative [Hakkinen *et al.*, 2014]. In addition, prolific melting during the summer of 2002 was associated with a positive NAO phase, which is contrary to the traditionally established relationship between these two processes [Hakkinen *et al.*, 2014].

In addition to the atmospheric and oceanic processes discussed in this study, surface melting across the GrIS is also influenced by other important factors, including cloud cover and aerosols. In an examination of the widespread melt event during July 2012, *Bennartz et al.* [2013] revealed that low-level liquid clouds within a narrow range of optical thickness likely enhanced the surface melting over broad areas of the GrIS, most notably around Summit Station. These clouds were thin enough to allow the penetration of incoming solar radiation but thick enough to prevent an excessive amount of longwave radiation from escaping the lower troposphere. The deposition of atmospheric aerosols, especially black carbon and mineral dust, onto the surface of the GrIS has also been linked to enhanced melting during recent years. *Keegan et al.* [2014] state that the extreme melt events of 1889 and 2012 were similarly caused by the combination of exceptionally warm temperatures and black carbon sediments deposited by Northern Hemisphere forest fires, which significantly lowers the albedo of the dry snow region. Likewise, a substantial decline in the springtime albedo of the GrIS since 2009 has been connected to an increase in the quantity of light-absorbing impurities, particularly mineral dust, that are advected from Arctic regions affected by earlier snow melt due to global warming [*Dumont et al.*, 2014].

Despite the exceptionally high frequency of extreme GBEs during the summers from 2007–2013, it is difficult to conclude whether this trend will persist into the future. Studies based on an assessment of historical observations have generally surmised that Rossby wave amplification will become more prevalent with an increasing thermal gradient between the polar and equatorial regions leading to higher-amplitude planetary wave patterns. While Arctic sea ice loss has been shown to be the primary driver of Arctic amplification during autumn and winter, the increasing tendency for earlier snow melt and a corresponding dry-out of high-latitude land

surfaces is largely responsible for anomalous upper-level wave patterns during the summer [Francis and Vavrus, 2012]. Francis and Vavrus [2012] detected a statistically significant northward stretching of 500 hPa ridge peaks and a weakened polar jet stream over the North American / North Atlantic region from 1979–2010, which suggests an increasingly favorable environment for block formation during more recent years. In addition, Fettweis *et al.* [2013] found that the frequency of anticyclonic circulation days over the GrIS has increased significantly (from ~15% to ~40% of all June-August days) during the past two decades, and this variability was shown to be independent of the background Arctic amplification signal. Recent summer heat waves across the mid-latitudes tend to be associated with persistent, high-amplitude Rossby wave patterns that are characterized by a high zonal wavenumber, which affirms the dynamical process of “ridge stretching” as suggested by Francis and Vavrus [2012] [Petoukhov *et al.*, 2013]. Increases in Greenland blocking from 2007–2012 have also been linked to the persistence of an Arctic Dipole pattern over the high latitudes of the Northern Hemisphere, which is associated with enhanced cryospheric melting due to more meridional wind flow patterns [Overland *et al.*, 2012].

Subsequent studies, however, have challenged the linkage between Arctic amplification and high-latitude atmospheric circulation variability by demonstrating that this relationship is statistically sensitive to methodological choices (Screen and Simmonds, 2013; Barnes, 2013). According to Screen and Simmonds [2013], the impact of Arctic amplification is tenuous because the interannual variability of planetary wave patterns is substantially greater than recent changes in their meridional amplitude. The frequency, strength, and duration of extreme GBEs as discussed in this paper are also characterized by considerable temporal variability, which makes it problematic to distinguish natural fluctuations from changes due to global warming. To

address this issue, global circulation models (GCMs) have been utilized to project the future North Atlantic atmospheric circulation under different warming scenarios.

Most GCMs, even the most advanced versions such as CMIP5, have struggled to simulate atmospheric blocking reliably with respect to reanalysis-based verification. Both CMIP3 and CMIP5 model projections indicate a significantly large decrease in summertime blocking frequency (~40% fewer blocked days) over the North Atlantic region by the end of the century [Barnes *et al.*, 2012; Masato *et al.*, 2013]. However, these results must be interpreted with caution given the large amount of model bias and inter-model variability [Masato *et al.*, 2013]. Belleflamme *et al.* [2013] used the circulation type classification developed by Fettweis *et al.* [2011] to compare daily 500 hPa heights simulated by CMIP5 GCMs with three reanalysis products for the current (1961–1990) climate. The GCMs cannot effectively simulate the historical anomalies of 500 hPa heights over Greenland, and they do not project any significant changes in atmospheric circulation frequency into the future [Belleflamme *et al.*, 2013]. Thus, future changes in blocking frequency over the North Atlantic region remain highly uncertain.

Based on the Greenland Blocking Index, climatological characteristics of extreme Greenland blocking episodes have been examined from 1958–2013. With the frequency and, to some extent, duration of extreme GBEs increasing since the early 1990s, a seasonal analysis of these trends revealed that extreme summer GBEs were responsible for a large proportion of this signal. In order to quantify the effects of numerous atmospheric and oceanic processes on GrIS melting during the summer, a multiple regression analysis was employed. These statistical results suggest that variations in Greenland blocking and North Atlantic SSTs predominately control summer meltwater production across the entire GrIS, with North Atlantic cyclone activity playing an important role for melting primarily over eastern Greenland. Regardless of whether or

not recent trends in the frequency of extreme Greenland blocking persist into the future, GrIS melting will likely continue to accelerate as Arctic amplification reshapes the Earth's cryosphere.

2.5 References

- Barnes, E. A., J. Slingo, and T. Woollings (2012), A methodology for the comparison of blocking climatologies across indices, models and climate scenarios, *Climate Dynamics*, 38(11–12), 2467–2481.
- Barnes, E. A. (2013), Revisiting the evidence linking Arctic amplification to extreme weather in midlatitudes, *Geophysical Research Letters*, 40(17), 4734–4739.
- Barnes, E. A., E. Dunn-Sigouin, G. Masato, and T. Woollings (2014), Exploring recent trends in Northern Hemisphere blocking, *Geophysical Research Letters*.
- Barriopedro, D., R. García-Herrera, A. R. Lupo, and E. Hernández (2006), A climatology of Northern Hemisphere blocking, *Journal of Climate*, 19(6), 1042–1063.
- Barry, R. G., and G. N. Kiladis (1982), Climatic characteristics of Greenland, *Climatic and Physical Characteristics of the Greenland Ice Sheet*, Cooperative Institute for Research in Environmental Science, University of Colorado, Boulder, CO, 7–34.
- Belleflamme, A., X. Fettweis, C. Lang, and M. Erpicum (2013), Current and future atmospheric circulation at 500 hPa over Greenland simulated by the CMIP3 and CMIP5 global models, *Climate Dynamics*, 41(7–8), 2061–2080.
- Benedict, J. J., S. Lee, and S. B. Feldstein (2004), Synoptic view of the North Atlantic Oscillation, *Journal of the Atmospheric Sciences*, 61(2), 121–144.
- Bennartz, R., M. Shupe, D. Turner, V. Walden, K. Steffen, C. Cox, M. Kulie, N. Miller, and C. Pettersen (2013), July 2012 Greenland melt extent enhanced by low-level liquid clouds, *Nature*, 496(7443), 83–86.

- Bezeau, P., M. Sharp, and G. Gascon (2014), Variability in summer anticyclonic circulation over the Canadian Arctic Archipelago and west Greenland in the late 20th/early 21st centuries and its effect on glacier mass balance, *International Journal of Climatology*.
- Blackmon, M. L. (1976), A climatological spectral study of the 500 mb geopotential height of the Northern Hemisphere, *Journal of the Atmospheric Sciences*, 33(8), 1607–1623.
- Box, J., X. Fettweis, J. Stroeve, M. Tedesco, D. Hall, and K. Steffen (2012), Greenland ice sheet albedo feedback: thermodynamics and atmospheric drivers, *The Cryosphere*, 6(4), 821–839.
- Brun, E., P. David, M. Sudul, and G. Brunot (1992), A numerical model to simulate snow-cover stratigraphy for operational avalanche forecasting, *Journal of Glaciology*, 38(1), 13–22.
- Clausen, H. B., N. S. Gundestrup, S. J. Johnsen, R. Bindshadler, and J. Zwally (1988), Glaciological investigations in the Crête area, central Greenland: A search for a new deep-drilling site, *Annals of Glaciology*, 10, 10–15.
- CPC (2014), Arctic Oscillation, *Climate Prediction Center WWW page*,
[ftp://ftp.cpc.ncep.noaa.gov/cwlinks/norm.daily.ao.index.b500101.current.ascii].
- Cuffey, K. M., and S. J. Marshall (2000), Substantial contribution to sea-level rise during the last interglacial from the Greenland ice sheet, *Nature*, 404(6778), 591–594.
- Davini, P., C. Cagnazzo, R. Neale, and J. Tribbia (2012), Coupling between Greenland blocking and the North Atlantic Oscillation pattern, *Geophysical Research Letters*, 39(14).
- Dee, D., S. Uppala, A. Simmons, P. Berrisford, P. Poli, S. Kobayashi, U. Andrae, M. Balmaseda, G. Balsamo, and P. Bauer (2011), The ERA-Interim reanalysis: Configuration and performance of the data assimilation system, *Quarterly Journal of the Royal Meteorological Society*, 137(656), 553–597.

- Dumont, M., E. Brun, G. Picard, M. Michou, Q. Libois, J. Petit, M. Geyer, S. Morin, and B. Josse (2014), Contribution of light-absorbing impurities in snow to Greenland's darkening since 2009, *Nature Geoscience*.
- Fang, Z. (2004), Statistical relationship between the northern hemisphere sea ice and atmospheric circulation during wintertime, *Observation, Theory and Modeling of Atmospheric Variability*. Zhu X (ed.). *World Scientific Series on Meteorology of East Asia*. World Scientific Publishing Company: Singapore, 131–141.
- Fettweis, X. (2007), Reconstruction of the 1979–2006 Greenland ice sheet surface mass balance using the regional climate model MAR, *The Cryosphere Discussions*, 1, 123–168.
- Fettweis, X., G. Mabilhe, M. Erpicum, S. Nicolay, and M. Van den Broeke (2011), The 1958–2009 Greenland ice sheet surface melt and the mid-tropospheric atmospheric circulation, *Climate Dynamics*, 36(1–2), 139–159.
- Fettweis, X., E. Hanna, C. Lang, A. Belleflamme, M. Erpicum, and H. Gallée (2013), Important role of the mid-tropospheric atmospheric circulation in the recent surface melt increase over the Greenland ice sheet, *The Cryosphere*, 7(1), 241–248.
- Francis, J. A., and S. J. Vavrus (2012), Evidence linking Arctic amplification to extreme weather in mid-latitudes, *Geophysical Research Letters*, 39(6).
- Greene, C., J. Francis, and B. Monger (2013), Superstorm Sandy: A series of unfortunate events, *Oceanography*, 26(1), 8–9.
- Häkkinen, S., P. B. Rhines, and D. L. Worthen (2011), Atmospheric blocking and Atlantic multidecadal ocean variability, *Science*, 334(6056), 655–659.

- Häkkinen, S., D. K. Hall, C. A. Shuman, D. L. Worthen, and N. E. DiGirolamo (2014), Greenland ice sheet melt from MODIS and associated atmospheric variability, *Geophysical Research Letters*, *41*(5), 1600–1607.
- Hanna, E., J. M. Jones, J. Cappelen, S. H. Mernild, L. Wood, K. Steffen, and P. Huybrechts (2013a), The influence of North Atlantic atmospheric and oceanic forcing effects on 1900–2010 Greenland summer climate and ice melt/runoff, *International Journal of Climatology*, *33*, 862–880.
- Hanna, E., X. Fettweis, S. H. Mernild, J. Cappelen, M. H. Ribergaard, C. A. Shuman, K. Steffen, L. Wood, and T. L. Mote (2013b), Atmospheric and oceanic climate forcing of the exceptional Greenland ice sheet surface melt in summer 2012, *International Journal of Climatology*.
- Keegan, K. M., M. R. Albert, J. R. McConnell, and I. Baker (2014), Climate change and forest fires synergistically drive widespread melt events of the Greenland Ice Sheet, *Proceedings of the National Academy of Sciences*, *111*(22), 7964–7967.
- KNMI (2014), Monthly climate indices, *KNMI Climate Explorer WWW page*, [<http://climexp.knmi.nl/selectindex.cgi>].
- Konrad, C. E., and S. J. Colucci (1988), Synoptic climatology of 500 mb circulation changes during explosive cyclogenesis, *Monthly Weather Review*, *116*(7), 1431–1443.
- Lupo, A. R., and P. J. Smith (1995), Climatological features of blocking anticyclones in the Northern Hemisphere, *Tellus A*, *47*(4), 439–456.
- Masato, G., B. J. Hoskins, and T. Woollings (2013), Winter and summer Northern Hemisphere blocking in CMIP5 models, *Journal of Climate*, *26*(18), 7044–7059.

- Mattingly, K. S., J. T. McLeod, J. A. Knox, J. M. Shepherd, and T. L. Mote (2014), A climatological assessment of Greenland blocking conditions associated with the track of Hurricane Sandy and historical North Atlantic hurricanes, *International Journal of Climatology*.
- Mote, T. L. (1998a), Mid-tropospheric circulation and surface melt on the Greenland ice sheet. Part I: Atmospheric teleconnections, *International Journal of Climatology*, 18(2), 111–129.
- Mote, T. L. (1998b), Mid-tropospheric circulation and surface melt on the Greenland ice sheet. Part II: Synoptic climatology, *International Journal of Climatology*, 18(2), 131–145.
- Nghiem, S., D. Hall, T. Mote, M. Tedesco, M. Albert, K. Keegan, C. Shuman, N. DiGirolamo, and G. Neumann (2012), The extreme melt across the Greenland ice sheet in 2012, *Geophysical Research Letters*, 39(20).
- Noel, B., X. Fettweis, W. van de Berg, M. van den Broeke, and M. Erpicum (2014), Small impact of surrounding oceanic conditions on 2007–2012 Greenland Ice Sheet surface mass balance, *The Cryosphere Discussions*, 8(2), 1453–1477.
- Overland, J. E., J. A. Francis, E. Hanna, and M. Wang (2012), The recent shift in early summer Arctic atmospheric circulation, *Geophysical Research Letters*, 39(19).
- Pelly, J., and B. Hoskins (2003), A new perspective on blocking, *Journal of the Atmospheric Sciences*, 60(5), 743–755.
- Petoukhov, V., S. Rahmstorf, S. Petri, and H. J. Schellnhuber (2013), Quasiresonant amplification of planetary waves and recent Northern Hemisphere weather extremes, *Proceedings of the National Academy of Sciences*, 110(14), 5336–5341.

- Rajewicz, J., and S. J. Marshall (2014), Variability and trends in anticyclonic circulation over the Greenland ice sheet, 1948–2013, *Geophysical Research Letters*.
- Screen, J. A., and I. Simmonds (2013), Exploring links between Arctic amplification and mid-latitude weather, *Geophysical Research Letters*, *40*, 959–964.
- Serreze, M. C., and J. A. Francis (2006), The Arctic amplification debate, *Climatic Change*, *76*(3–4), 241–264.
- Serreze, M. C., and A. P. Barrett (2008), The summer cyclone maximum over the central Arctic Ocean, *Journal of Climate*, *21*(5), 1048–1065.
- Serreze, M. C. (2009), *Northern Hemisphere Cyclone Locations and Characteristics from NCEP/NCAR Reanalysis Data*, Boulder, Colorado USA: National Snow and Ice Data Center. Digital media.
- Shabbar, A., J. Huang, and K. Higuchi (2001), The relationship between the wintertime North Atlantic Oscillation and blocking episodes in the North Atlantic, *International Journal of Climatology*, *21*(3), 355–369.
- Tedesco, M., X. Fettweis, T. Mote, J. Wahr, P. Alexander, J. Box, and B. Wouters (2013), Evidence and analysis of 2012 Greenland records from spaceborne observations, a regional climate model and reanalysis data, *The Cryosphere*, *7*(2), 615–630.
- Tedesco, M., X. Fettweis, P. Alexander, G. Green, and T. Datta (2014), MAR Greenland Outputs 1979–2008 ver. 3.2, CCNY Digital Archive.
- Thompson, D. W., and J. M. Wallace (1998), The Arctic Oscillation signature in the wintertime geopotential height and temperature fields, *Geophysical Research Letters*, *25*(9), 1297–1300.

- Treidl, R., E. Birch, and P. Sajecki (1981), Blocking action in the Northern Hemisphere: A climatological study, *Atmosphere-Ocean*, 19(1), 1–23.
- Tyrlis, E., and B. Hoskins (2008), Aspects of a Northern Hemisphere atmospheric blocking climatology, *Journal of the Atmospheric Sciences*, 65(5), 1638–1652.
- Uppala, S. M., P. Kållberg, A. Simmons, U. Andrae, V. Bechtold, M. Fiorino, J. Gibson, J. Haseler, A. Hernandez, and G. Kelly (2005), The ERA-40 re-analysis, *Quarterly Journal of the Royal Meteorological Society*, 131(612), 2961–3012.
- van Oldenborgh, G., L. Te Raa, H. Dijkstra, and S. Philip (2009), Frequency-or amplitude-dependent effects of the Atlantic meridional overturning on the tropical Pacific Ocean, *Ocean Science Discussions*, 6(3).
- Woollings, T., B. Hoskins, M. Blackburn, and P. Berrisford (2008), A new Rossby wave-breaking interpretation of the North Atlantic Oscillation, *Journal of the Atmospheric Sciences*, 65(2), 609–626.

2.6 Figures and Tables

Table 2.1. Percentage of extreme GBEs by season occurring within 14-year periods from 1958–2013

Season	1958–1971	1972–1985	1986–1999	2000–2013
Winter (DJF)	34.6%	23.1%	11.5%	30.8%
Spring (MAM)	14.3%	21.4%	21.4%	42.9%
Summer (JJA)	25%	10%	15%	50%
Autumn (SON)	27.3%	18.2%	22.7%	31.8%

Table 2.2. OLS multiple regression model for western Greenland meltwater production (1979–2008)^a

Predictors	Slope Coefficient	Standard Error	Standardized Slope Coefficient	t-statistic	p-value
GBI	84.85	13.24	0.839	6.408	<0.001
AO	1638.41	1040.25	0.201	1.575	0.129
NAC frequency	-177.69	93.21	-0.208	-1.906	0.069
NAC strength	-7.08	216.60	-0.004	-0.033	0.974
NAC intensification	-490.29	734.08	-0.074	-0.668	0.511
AMO	3886.77	1103.0	0.348	3.524	0.002
Number of obs	30				
F-statistic	17.9				
p-value for F	<0.001				
R ²	0.824				
Adjusted R ²	0.778				
Mean Squared Error	1230.5				

^aPredictor variables that are statistically significant at or above the 95% confidence level are bolded. "North Atlantic cyclone" is abbreviated "NAC" above.

Table 2.3. OLS multiple regression model for eastern Greenland meltwater production (1979–2008)^b

Predictors	Slope Coefficient	Standard Error	Standardized Slope Coefficient	t-statistic	p-value
GBI	88.95	14.63	0.833	6.08	<0.001
AO	2935.75	1149.29	0.342	2.554	0.018
NAC frequency	-341.50	102.98	-0.379	-3.316	0.003
NAC strength	565.75	239.31	0.280	2.364	0.027
NAC intensification	-1830.04	811.03	-0.260	-2.256	0.034
AMO	4357.06	1218.62	0.370	3.575	0.002
Number of obs	30				
F-statistic	16.02				
p-value for F	<0.001				
R ²	0.807				
Adjusted R ²	0.757				
Mean Squared Error	1359.5				

^bPredictor variables that are statistically significant at or above the 95% confidence level are bolded. "North Atlantic cyclone" is abbreviated "NAC" above.

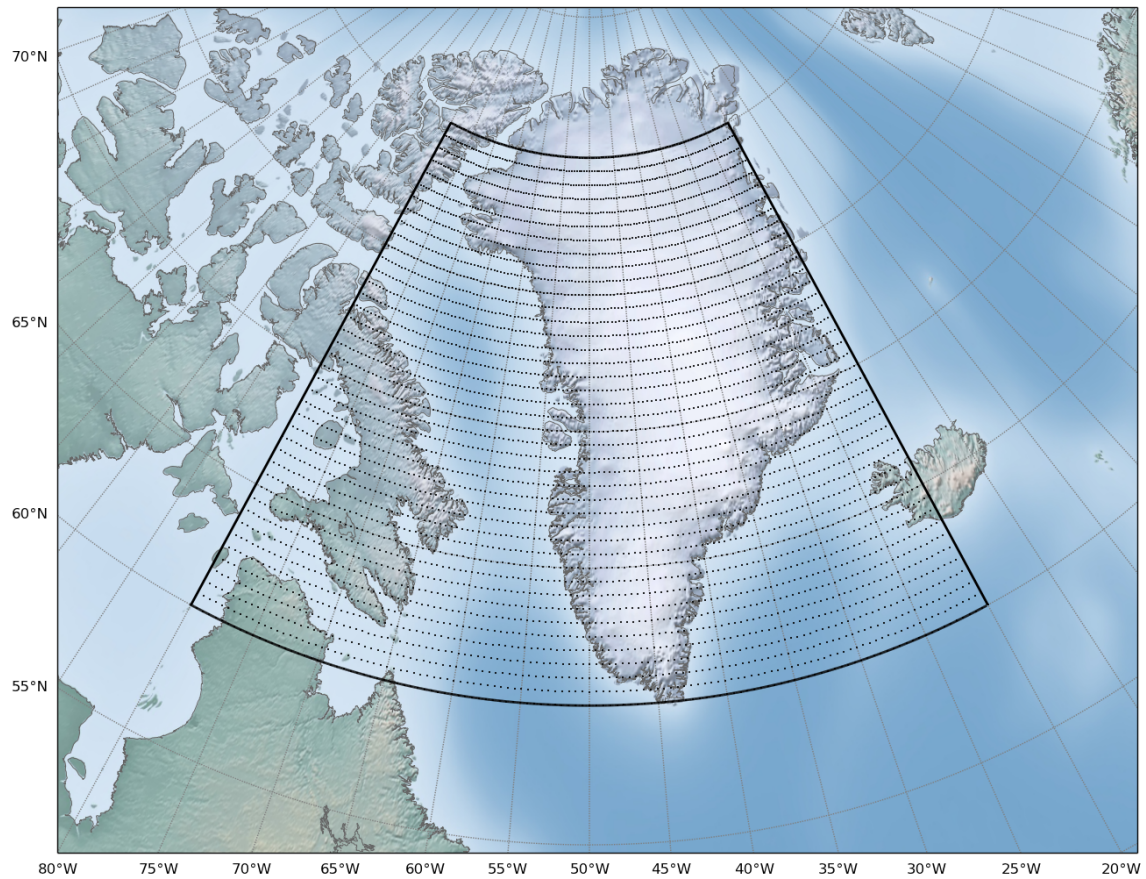


Figure 2.1. Spatial domain for the Greenland Blocking Index based on *Hanna et al.* [2013a]. Gridded observations of 500 hPa geopotential heights were obtained from the ERA-40 and ERA-Interim reanalyses at a $0.5^\circ \times 0.5^\circ$ spatial resolution.

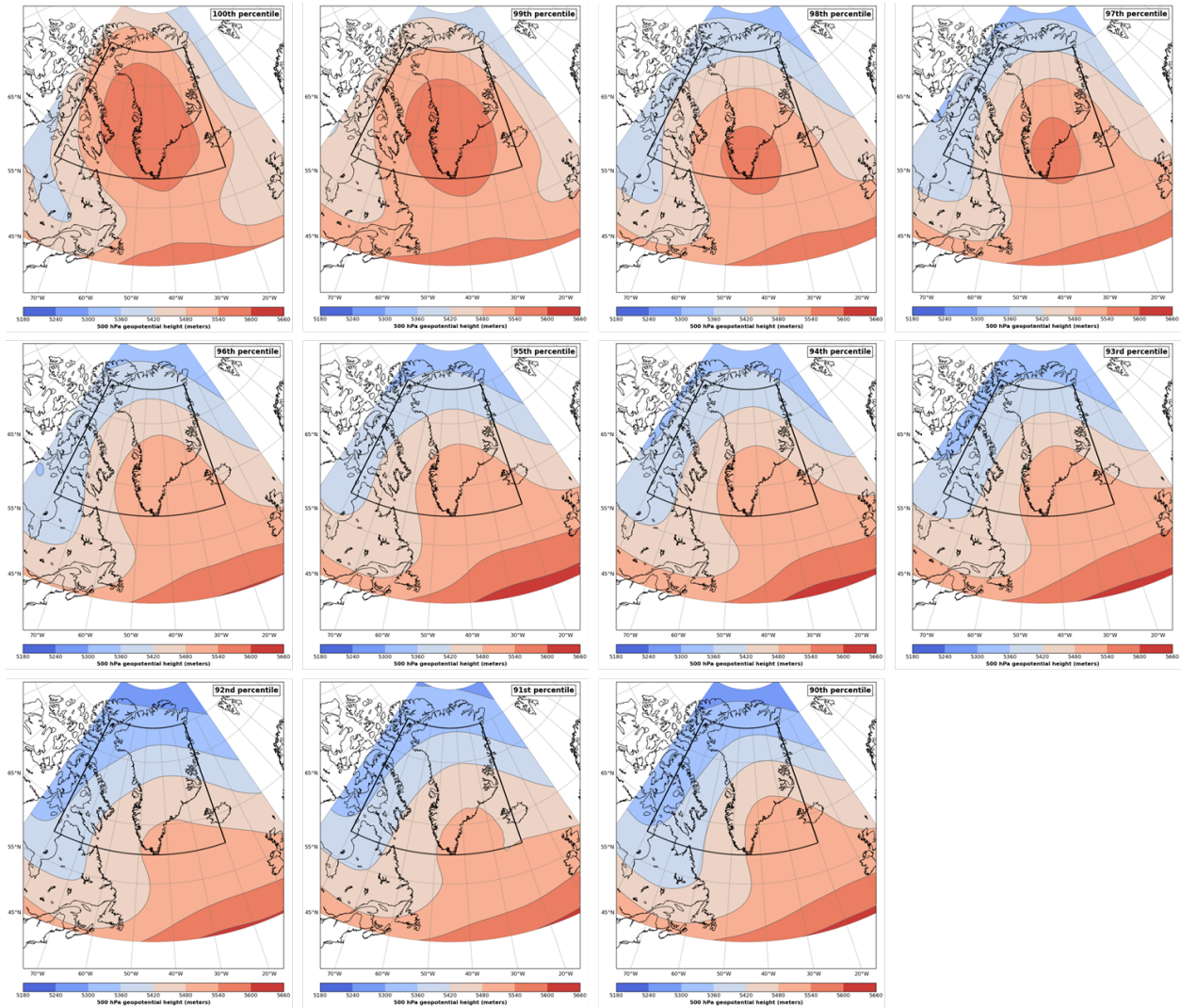


Figure 2.2. Composite maps of 500 hPa geopotential heights over the North Atlantic for all days from 1958–2013 in which the GBI ranked within the 90th–100th percentiles based on the entire 56-year climatological distribution. Maps are shown in a row-wise descending order. The domain used to calculate the GBI is indicated by the black polygon [Hanna *et al.*, 2013a].

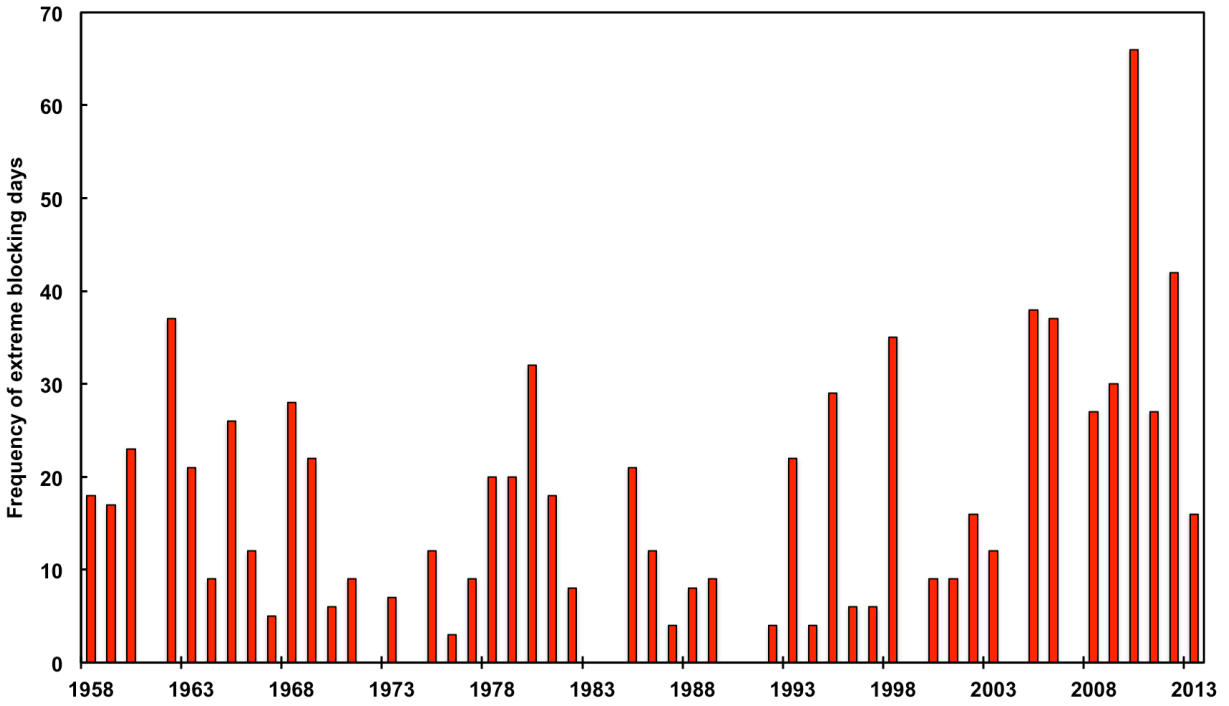


Figure 2.3. Time series of the annual frequency of extreme blocking days (daily mean GBI is ranked at or above the 97th percentile of the climatological distribution) from 1958–2013.

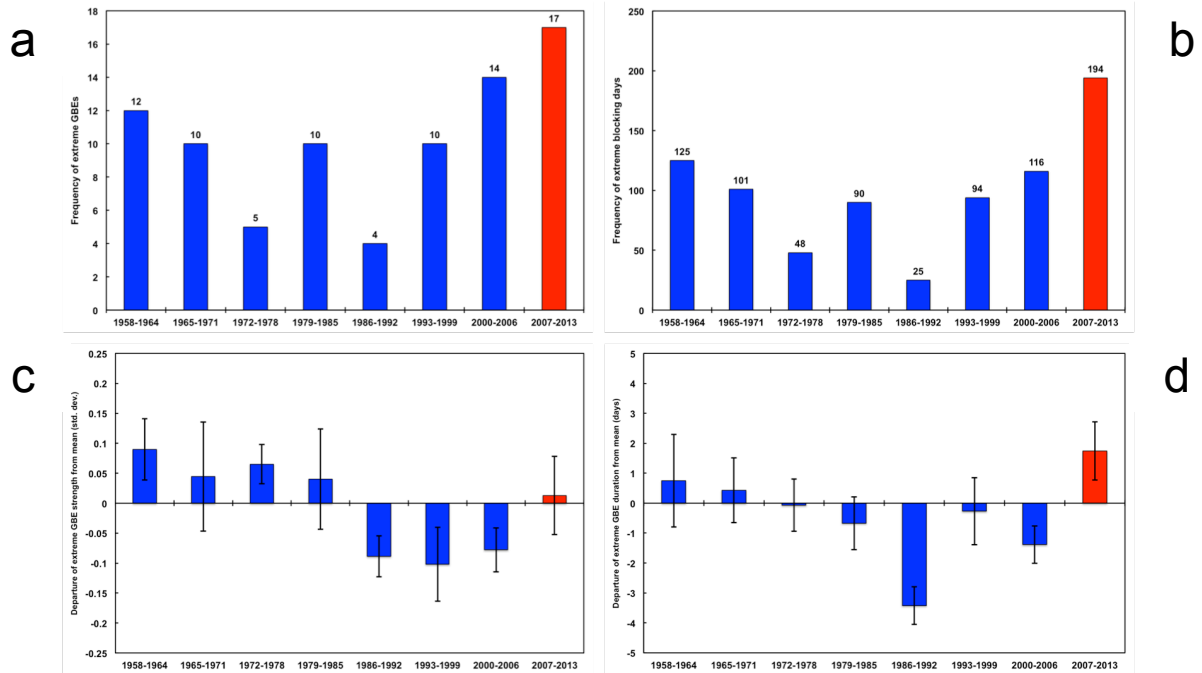


Figure 2.4. 7-year frequency (a), daily count (b), departure of strength from average (c), and departure of duration from average (d) of extreme GBEs from 1958–2013. The standard error for each 7-year mean value of extreme GBE strength and duration is indicated by black whiskers. The most recent 7-year period from 2007–2013 is highlighted in red.

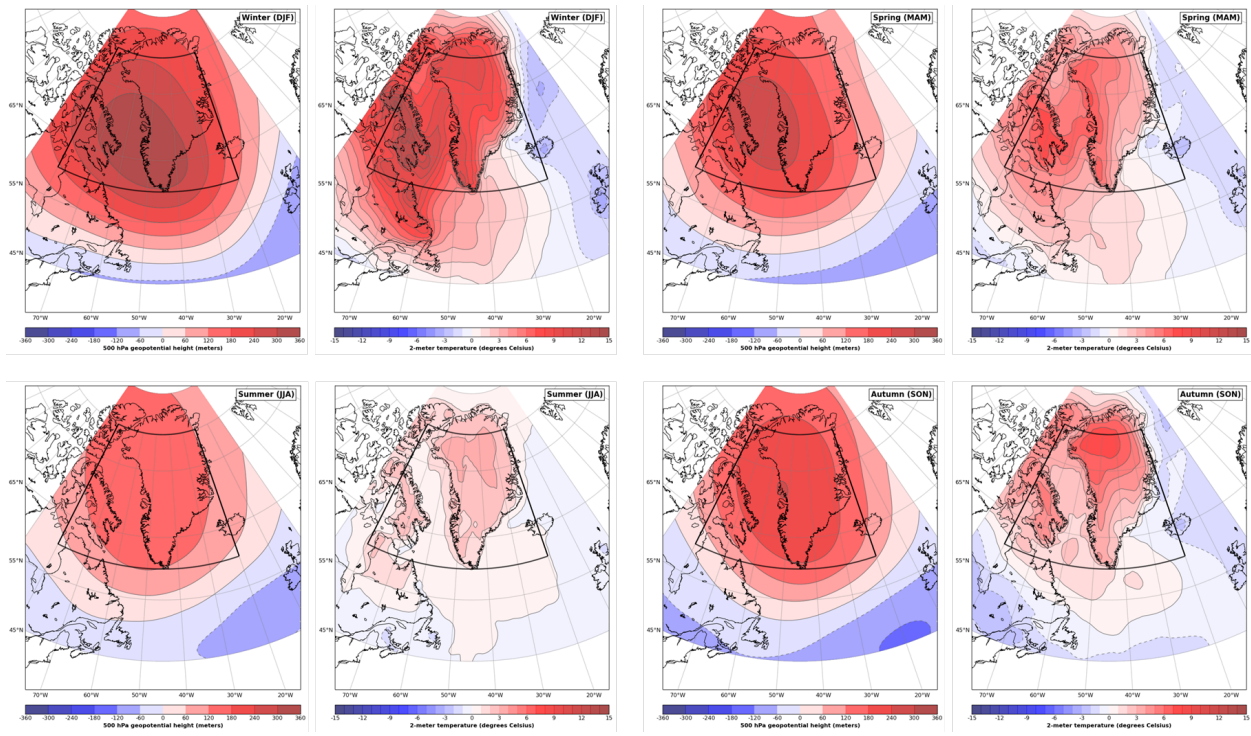


Figure 2.5. Composite anomaly maps of 500 hPa geopotential height (left) and 2-meter air temperature (right) for all extreme GBEs grouped by season from 1958–2013. Seasonal maps are displayed as follows: winter (top left), spring (top right), summer (bottom left), and autumn (bottom right).

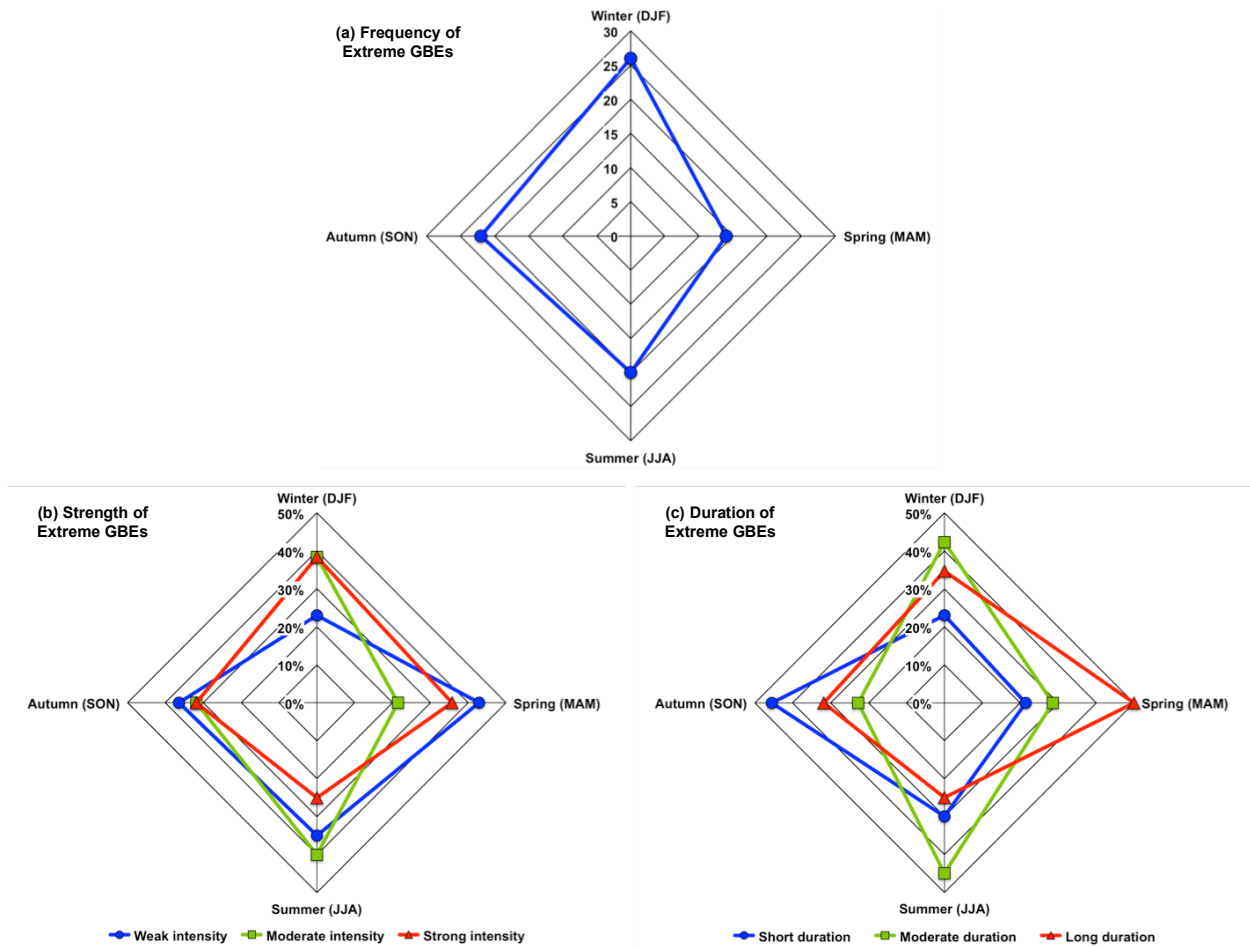


Figure 2.6. Frequency (a), strength (b), and duration (c) of extreme GBEs by season from 1958–2013 ($n = 94$). For plot (b), GBEs are grouped into nearly equally-sized terciles based on the standardized magnitude of the GBI as follows: weak intensity ($n = 27$), moderate intensity ($n = 28$), and strong intensity ($n = 27$). For plot (c), the quasi-normal distribution of GBE duration necessitated the use of unequally-sized terciles as follows: short duration ($n = 25$), moderate duration ($n = 29$), and long duration ($n = 28$).

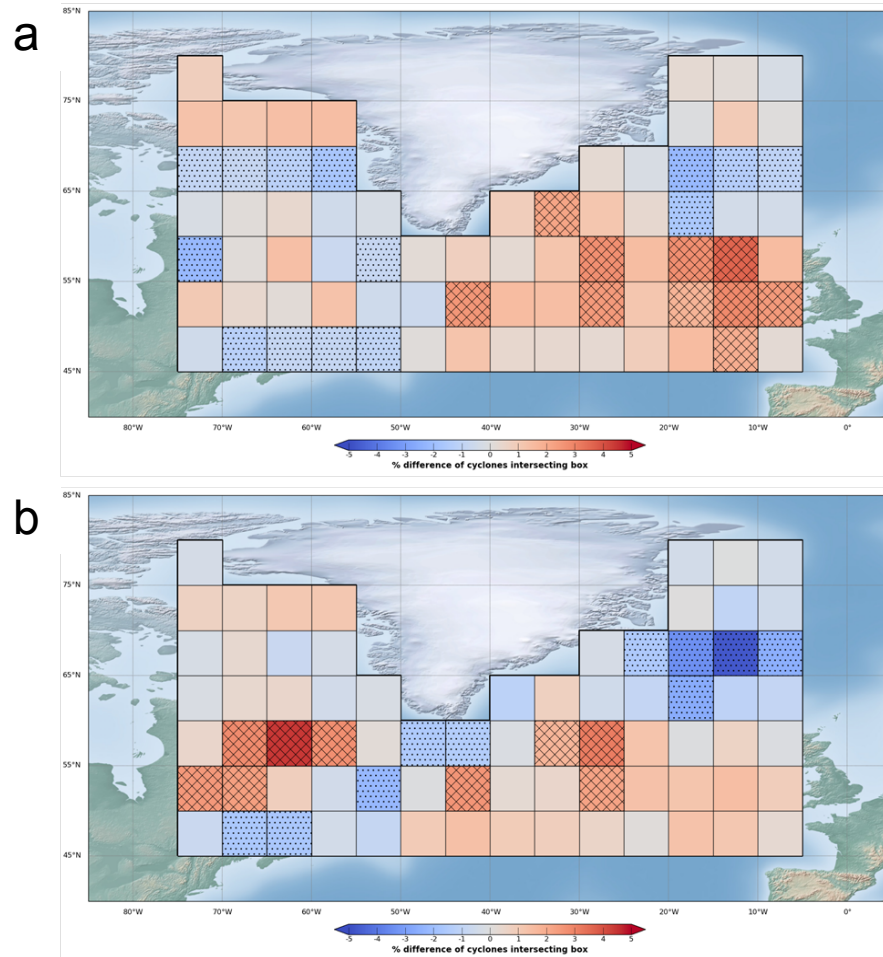


Figure 2.7. Geographic distribution of North Atlantic cyclones during the top 10 summer melting seasons from 1979–2008 over eastern Greenland (a) and western Greenland (b). The value in each 5° x 5° grid box represents the percentage difference in the frequency of cyclones that intersect the box during the top 10 summer melting seasons compared to those during the remaining 20 melting seasons. Cross hatching (dot hatching) indicates percentage values that are at least 1 standard deviation greater (lower) than the sample mean. Plots are generated using the Northern Hemisphere cyclone dataset provided by *Serreze* [2009].

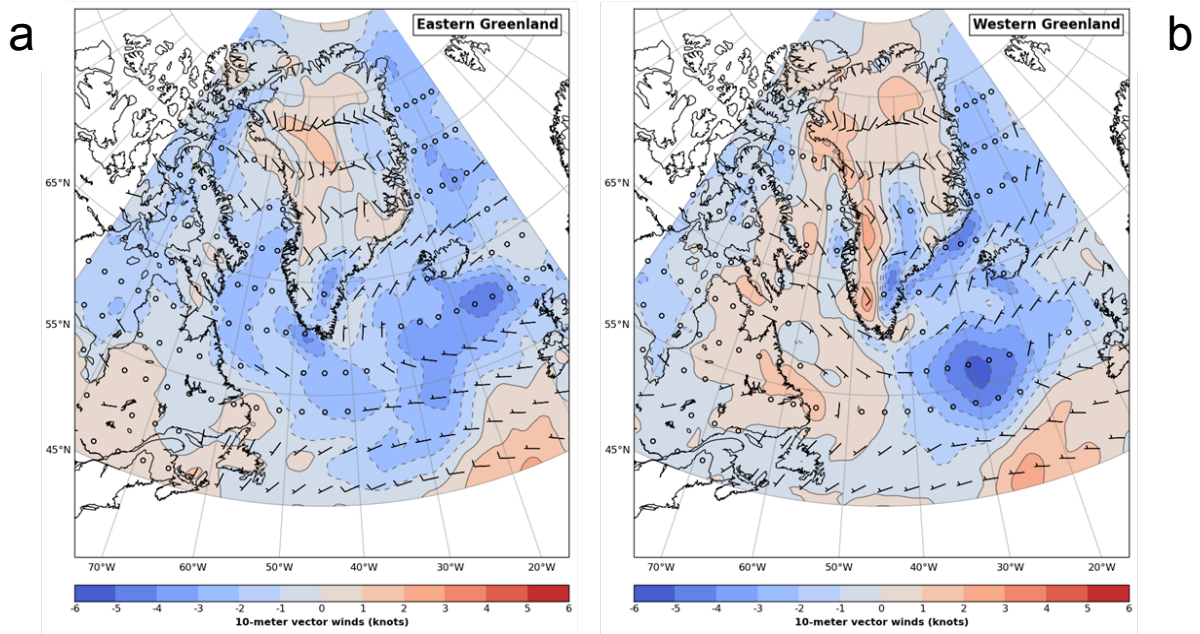


Figure 2.8. Composite anomalies of 10-meter vector winds for high melt days compared to low melt days during the top 10 summer melting seasons from 1979–2008 over eastern Greenland (a) and western Greenland (b). The color-shaded contours indicate vector wind speed anomalies, but the wind barbs represent the composite mean flow during high melt days for each region of the GrIS. Plots are generated using the ERA-Interim dataset [Dee *et al.*, 2011].

CHAPTER 3

ASSESSING THE ROLE OF PRECURSOR CYCLONES ON THE FORMATION OF EXTREME GREENLAND BLOCKING EPISODES AND THEIR IMPACT ON SUMMER MELTING ACROSS THE GREENLAND ICE SHEET ²

² McLeod, J.T. and T.L. Mote. To be submitted to *Journal of Geophysical Research: Atmospheres*

Abstract

A 30-year climatology of North Atlantic cyclones from 1979–2008 is examined within the context of extreme Greenland blocking and accelerating GrIS surface melting. A distinct class of extratropical cyclones, known as precursor cyclones, contributed to a significant strengthening of extreme Greenland blocking episodes through the process of upper-level wave amplification. Across all seasons, most extreme blocking episodes are associated with multiple precursor cyclones prior to peaking in intensity, and a majority of these cyclones have continental rather than oceanic origins. Over the western and eastern sectors of Greenland, daily meltwater production simulated by the MAR regional climate model is greater during extreme blocking episodes accompanied by precursor cyclones compared to blocking events lacking a precursor cyclone. Based on an analysis of HYSPLIT backward trajectories and North Atlantic SST anomalies, enhanced surface melting during the summer, particularly over southern and western Greenland, is strongly linked to the combination of vigorous tropospheric warming generated by the blocking anticyclones and anomalous warm air advection supplied by the precursor cyclones. Long-term increases in GrIS surface melting can be partially attributed to the interaction of these atmospheric and oceanic processes.

Key words: Greenland blocking, North Atlantic cyclones, Greenland ice sheet, Arctic amplification

3.1 Introduction

Over the northwestern region of the Atlantic Ocean, strong and persistent synoptic-scale ridges, known as atmospheric blocks, develop frequently throughout the year. Commonly referred to as Greenland blocks, these anticyclonic systems can divert migratory shortwave disturbances toward higher latitudes by displacing the predominant steering flow of the polar jet stream equatorward. Greenland blocks are usually generated by cyclonic wave breaking of synoptic-scale eddies that advects relatively warm and moist air masses toward the polar latitudes [Benedict *et al.*, 2004; Woollings *et al.*, 2008]. These modified air masses often cut off from the polar jet stream and may persist over high-latitude regions for up to several weeks [Barriopedro *et al.*, 2006]. Greenland blocking is related to a low-frequency teleconnection pattern known as the North Atlantic Oscillation (NAO), the dominant mode of atmospheric variability over the Atlantic Ocean [Shabbar *et al.*, 2001; Benedict *et al.*, 2004; Woollings *et al.*, 2008; Davini *et al.*, 2012]. Blocks occur most frequently during negative phases of the NAO, which are characterized by a weak, high-amplitude polar jet stream over the North Atlantic [Woollings *et al.*, 2008].

Greenland blocks play a significant role in the global climate system with a variety of direct and indirect impacts. During 22–29 October 2012, an unusually strong Greenland block persisted over the North Atlantic and prevented the northward-tracking Hurricane Sandy from recurving northeastward similarly to most tropical cyclones along the eastern coast of the United States [Greene *et al.*, 2013; Mattingly *et al.*, 2014]. In addition, the frequency and intensity of blocking anticyclones can strongly influence the extent of surface melting across the Greenland ice sheet (GrIS) during the summer. For example, a series of exceptionally anomalous Greenland blocks that developed from the end of May until mid-July throughout the summer of 2012

contributed to an extreme melt event during 11–12 July in which surface melting was detected across approximately 98.6% of the GrIS [*Hanna et al.*, 2013b; *Nghiem et al.*, 2012; *Tedesco et al.*, 2013]. According to multiple ice core records from Summit Station, an extreme melting event of this magnitude had not occurred since 1889 [*Clausen et al.*, 1988; *Nghiem et al.*, 2012].

Previous research has identified a robust linkage between Greenland blocking activity and observed surface melting across the GrIS, especially since the early 2000s. Based on an analysis of the Greenland Blocking Index during the NCEP/NCAR Reanalysis period of record (1948–2010) and GrIS surface melt extents derived from SnowModel simulations driven by MicroMet observations, *Hanna et al.* [2013a] detected a close relationship between unprecedented high pressure patterns over Greenland and highly anomalous melt/runoff across the ice sheet during the summers of 2007–2010. A noticeable shift toward strong melt anomalies associated with an increase in anticyclonic circulation over Greenland occurred in 2001, which partially explains the exceptional summer meltwater production in seven individual years from 1998–2012 [*Fettweis et al.*, 2013; *Rajewicz and Marshall*, 2014]. However, the recent acceleration in surface melting is not homogeneous across the GrIS due to its complex topography, with the greatest increases broadly observed over the southern and western sectors of the ice sheet [*Mote*, 2007; *Mernild et al.*, 2011]. The effect of atmospheric circulation variability on GrIS melting is particularly significant given that the quantity of freshwater stored in the ice sheet would correspond to 6–7 meters of global sea level rise if it were all to be released [*Cuffey and Marshall*, 2000; *Nghiem et al.*, 2012].

While the relationship between Greenland blocking and the recent increase in summer melting across the GrIS has been established, the role of other atmospheric and oceanic processes, such as North Atlantic cyclone activity and sea surface temperatures, on the evolution

of Greenland blocks remains relatively unexplored. *Hanna et al.* [2013a] revealed that the NAO alone could not sufficiently explain the exceptional Greenland blocking patterns during the summers of 2007–2010, which suggests that a complex interaction of atmospheric and oceanic processes may be responsible. Previous research, including both case studies [*Colucci*, 1985, 1987; *Tsou and Smith*, 1990] and climatological analyses [*Konrad and Colucci*, 1988; *Dole*, 1989; *Nakamura and Wallace*, 1990, 1993; *Lupo and Smith*, 1995] has identified a link between surface cyclogenesis and downstream block development across the Northern Hemisphere. *Konrad and Colucci* [1988] examined 500 hPa circulation changes associated with 141 explosive cyclones (“bombs”) over the western half of the Northern Hemisphere from September 1980 through May 1987 (excluding the summer months of June–August). Based on their findings, explosive cyclogenesis does appear to contribute to the development of North Atlantic blocks, but the period of greatest upper-level wave amplification typically occurs after the most rapid phase of surface cyclogenesis, possibly in connection with enhanced air mass advection.

Lupo and Smith [1995] provide an updated climatological analysis regarding the role of extratropical cyclones on downstream block development, but this study only covers a short 3-year period from July 1985 through June 1988. Known as precursor cyclones, a distinct class of extratropical cyclones originating upstream, or to the west, of blocking anticyclones was examined. All 29 blocking events that occurred in the North Atlantic region (80°W–40°E) were accompanied by a precursor cyclone, and approximately 72% of these precursor cyclones were characterized by explosive development [*Lupo and Smith*, 1995]. During the seven winter seasons from December 1980 through February 1987, only 46% (6 of 13) of blocking events over the western half of the Northern Hemisphere (90°W–90°E) were accompanied by a rapidly intensifying precursor cyclone [*Colucci and Alberta*, 1996]. The majority (78%) of precursor

cyclones during autumn through spring underwent rapid intensification, while none of the precursor cyclones during summer achieved explosive development [*Lupo and Smith, 1995*]. Finally, the deepening rate of the precursor cyclones was not significantly correlated with the duration or size of the blocking anticyclones [*Lupo and Smith, 1995*].

An alternative approach is adopted by *Gómara et al. [2014]*, in which Rossby wave-breaking (RWB) events are considered to act as precursors (temporally rather than geographically) to explosive cyclone development over the Euro-Atlantic region. Cyclonic RWB is a close corollary to atmospheric blocking, but not all atmospheric blocks over the North Atlantic are generated by cyclonic RWB of synoptic-scale eddies [*Benedict et al., 2004; Woollings et al., 2008*]. Based on an investigation of 44 winter seasons from October 1957 through March 2001, enhanced cyclonic RWB over the western subpolar North Atlantic region was a significant precursor of explosive cyclogenesis over the western North Atlantic [*Gómara et al., 2014*]. In fact, the probability of an explosive cyclone developing in the western North Atlantic is increased by a factor of 1.5 when cyclonic RWB is present over Greenland [*Gómara et al., 2014*]. In addition, cyclones with greater intensities are more closely associated with cyclonic RWB over Greenland. For example, while 70% of the top 50 most intense cyclones are preceded by cyclonic RWB over Greenland, only about 37% of all non-explosive cyclones are linked to cyclonic RWB over Greenland [*Gómara et al., 2014*]. These results are not consistent with the findings of *Konrad and Colucci [1988]*, who noted that downstream ridge-building was produced more frequently by relatively weaker explosive cyclones. Moreover, the percentage (46%) of wintertime blocking events accompanied by an explosive precursor cyclone, as determined by *Colucci and Alberta [1996]*, is somewhat greater than the percentage (33%) of cyclonic RWB events leading to explosive cyclogenesis over the western North Atlantic.

However, these discrepancies could be attributed to observational differences in the related processes of blocking, downstream ridge-building, and cyclonic RWB over different time periods. Also, the theoretical framework for each study was fundamentally different: *Konrad and Colucci* [1988] and *Colucci and Alberta* [1996] viewed explosive cyclones as precursors to upper-level wave amplification while *Gómara et al.* [2014] regarded cyclonic RWB as a precursor to explosive cyclogenesis.

Interannual variability in North Atlantic sea surface temperatures (SSTs) can modulate the intensity of GrIS summer melting and may also govern the frequency of Greenland block development. The Atlantic Multidecadal Oscillation (AMO), the dominant low-frequency mode of SST variability across the North Atlantic, has remained in a persistent positive phase, which is associated with warmer-than-normal SSTs over the North Atlantic Ocean, since the mid-1990s [*Hanna et al.*, 2013a]. Both Greenland coastal station temperatures and GrIS runoff are significantly correlated with the AMO during the past 30–40 years, and the ongoing AMO warm phase likely amplified GrIS melting and runoff over the past few decades [*Hanna et al.*, 2013a]. However, *Noel et al.* [2014] conclude that oceanic forcing did not have a significant effect on the exceptional surface melting of the GrIS since 2007 because katabatic winds are usually strong enough to prevent an inland incursion of maritime air masses.

Several additional atmospheric and oceanic factors, including cloud cover, aerosols, and Arctic sea ice, can play a significant role in controlling the variability of surface melting across the GrIS. The presence of thin, liquid clouds was pivotal in the development of super-freezing temperatures across broad areas of the GrIS during the extreme melt event of July 2012, leading to observed surface melting at the highest elevations of the ice sheet near Summit Station [*Bennartz et al.*, 2013]. *Keegan et al.* [2014] noted that exceptionally warm temperatures during

the extreme GrIS melt events of 1889 and 2012 were also driven by the deposition of black carbon sediments originating from Northern Hemisphere forest fires, which significantly lowers the albedo of the dry snow region. The rapid decline of Arctic sea ice coverage during the past few decades has promoted an enhanced flux of heat and water vapor from the exposed ocean to the GrIS, resulting in greater surface warming due to increases in sensible heating and downwelling longwave radiation [*Liu et al.*, in review].

The frequency of Greenland blocking and the associated impact on GrIS surface melting is also important within the context of global climate change, particularly Arctic amplification. Over the past few decades, the Arctic has been warming at an accelerated rate compared to both the mid-latitudes and the tropics, a phenomenon known as Arctic amplification [*Serreze and Francis*, 2006]. There is considerable uncertainty in the projection of future trends in Greenland blocking from both an observational [*Francis and Vavrus*, 2012; *Screen and Simmonds*, 2013; *Barnes et al.*, 2014; *Rajewicz and Marshall*, 2014] and modeling [*Barnes et al.*, 2012; *Belleflamme et al.*, 2013; *Masato et al.*, 2013] approach. For example, *Barnes et al.* [2014] remark that blocking frequencies over the North Atlantic region during the past few years are unexceptional when compared to the large amount of interannual blocking variability since 1948. Though very few significant trends in Northern Hemisphere blocking frequency were identified in their study, an increase in summer (JJA) blocking frequency based on the *Masato et al.* [2013] index was detected over the North Atlantic region near Greenland (300°–0°E) for three out of four reanalysis products [*Barnes et al.*, 2014]. In contrast, *Rajewicz and Marshall* [2014] detected a noticeable shift toward strong melt anomalies associated with an increase in anticyclonic circulation over Greenland in 2001, which partially explains the exceptional summer meltwater production in seven individual years from 1998–2012. Thus, an

understanding of the atmospheric and oceanic processes that can influence the development of Greenland blocks is critical for a more robust assessment of potential changes in their frequency and intensity.

In this study, the contribution of all North Atlantic cyclones, not just explosive cyclones, to the development and maintenance of extreme “Greenland blocking episodes” (GBEs) will be assessed. According to Sutcliffe-Petterssen self-development theory, warm air advection associated with a mature midlatitude cyclone can lead to downstream ridge-building, or upper-level wave amplification, due to a thermodynamic expansion of the tropospheric column [Lackmann, 2011]. Therefore, it is hypothesized that extreme GBEs preceded geographically by a midlatitude cyclone, known as precursor cyclones, are more intense than those lacking a precursor cyclone. In addition, extreme GBEs accompanied by a precursor cyclone(s) may lead to greater surface melting over the GrIS in comparison to blocking episodes lacking a precursor cyclone, particularly if warmer-than-normal SSTs are present. Southerly warm air advection accompanying the precursor cyclone combined with adiabatic heating under the dome of blocking high pressure could produce enhanced melting over the GrIS. Section 2 provides an explanation of the data sources and methods employed in this study. Some key results and associated discussion are provided in Section 3. Finally, a brief description of the results within the context of Arctic amplification and a concluding summary are offered in Section 4.

3.2 Data and Methods

In order to generate a database of extreme GBEs from 1979–2008, daily mean fields of 500 hPa geopotential heights were created from six-hourly output provided by the ERA-Interim reanalysis dataset [Dee *et al.*, 2011]. This 30-year period of record was selected to correspond with the satellite observational period beginning in 1979, and North Atlantic cyclone data is

currently unavailable after 2008. The raw data were interpolated onto a $0.5^\circ \times 0.5^\circ$ gridded domain and daily mean fields were computed for the entire period of record. The Greenland Blocking Index (GBI) was selected to quantify episodes of extreme Greenland blocking. Based on *Hanna et al.* [2013a], the GBI is defined as the mean 500 hPa geopotential height over the Greenland region spanning from 60° – 80° N latitude and 20° – 80° W longitude. Rather than detecting Greenland blocks based on a set of strict objective criteria, this approach is used to identify 500 hPa circulation patterns characterized by extreme positive values of the GBI, which indicates highly anomalous ridging over the GrIS. Thus, the extreme GBEs analyzed in this study may not satisfy all of the established criteria for atmospheric blocks as discussed in previous research [*Pelly and Hoskins, 2003; Barnes et al., 2012; Masato et al., 2013*]. An extreme GBE is defined as a sequence of at least five consecutive days in which the GBI equals or exceeds the 97th percentile (or a *Z*-score of +1.88 standard deviations) of all daily GBI values that occurred within a 7-day window centered on the day(s) in question. More details regarding the development of the GBI and the construction of the extreme GBE database can be found in *McLeod and Mote* [in review].

North Atlantic cyclone data from 1979–2008 was obtained from the “Northern Hemisphere Cyclone Locations and Characteristics from NCEP/NCAR Reanalysis Data” record compiled by *Serreze* [2009] at the National Snow and Ice Data Center (NSIDC). Only cyclones located between 45° – 60° N latitude and 75° – 25° W longitude were selected for analysis in order to ensure that all cyclones in the sample were within reasonably close proximity to the GrIS. A cyclone must persist for at least 24 hours within this geographic domain in order to be included in the analysis, and cyclones that remained stationary throughout their entire life cycles were discarded [*Serreze and Barrett, 2008*]. In order to compare extreme GBEs that were and were

not preceded by extratropical cyclones, it was necessary to develop an objective definition by which “precursor cyclones” could be consistently identified. Thus, a precursor cyclone was defined as any extratropical cyclone that originated upstream, or to the west, of a blocking ridge’s central meridional axis at or prior to the peak of the ridge’s intensity (quantified by daily GBI Z-scores). All remaining cyclones that did not satisfy these criteria were considered to be non-precursor cyclones. Each extreme GBE from 1979–2008 was manually inspected using daily 500 hPa geopotential height and MSLP fields from the NCEP/NCAR Reanalysis for the detection of precursor cyclones.

The NOAA Hybrid Single-Particle Lagrangian Integrated Trajectory (HYSPLIT) model was employed to compare air parcel trajectories associated with extreme GBEs that were and were not accompanied by at least one precursor cyclone [*Draxler and Hess, 1998; Draxler and Rolph, 2014*]. For this analysis, backward trajectories were simulated for nine locations across the GrIS using gridded NCEP/NCAR Reanalysis data (Table 3.1) [*Kalnay et al., 1996*]. In addition to the elevated inland sites at South Dome and Summit Station, the coastal locations were selected at 5° intervals of latitude extending northward from the tip of southern Greenland. The model was initialized at the 700 hPa pressure level for each location with the exception of Summit Station (500 hPa) due to its elevation. The 700 hPa pressure level represents the standard isobaric height for diagnosing mid-tropospheric circulation patterns, so the synoptic-scale flow associated with GBEs and their precursor cyclones should be sufficiently captured. Each trajectory was simulated for 120 hours backward in time beginning at 1200 UTC on the day of interest, and the vertical motion of the trajectory was modeled according to the omega field supplied by the reanalysis dataset.

Because the focus of this study is to examine the relationship between extreme Greenland blocking and surface melting across the GrIS, only extreme GBEs that occurred during an extended summer season defined from May through September were considered. For each of these GBEs, backward trajectories were simulated for all days prior to and including the peak intensity of the blocking episode (i.e. peak GBI value) in order to exclusively capture any potential effects from the precursor cyclones. Modeled potential temperature and ambient air temperature are also calculated to assess the thermodynamic evolution of each trajectory.

Meltwater production data were obtained from the MAR Greenland Explorer, which provides daily gridded output at a 25km spatial resolution [Fettweis, 2007; Tedesco *et al.*, 2013; Tedesco *et al.*, 2014]. MAR is a three-dimensional atmosphere-land surface regional climate model coupled to the SISVAT vegetation scheme, which includes a version of the CROCUS snow model [Brun *et al.*, 1992]. CROCUS is more sophisticated than most snow models used in regional climate models because it is capable of more fully simulating the evolution of snow properties and the refreezing of meltwater. The ERA-Interim reanalysis is used as the atmospheric forcing at the MAR lateral boundaries every six hours [Tedesco *et al.*, 2013]. The meltwater data was divided into a West Greenland subset, spanning the entire area of the ice sheet located westward of the 45°W meridian, and an East Greenland subset, covering the portion of the ice sheet situated eastward of the 45°W meridian. These two regional subsets are roughly separated by the topographical divide that extends along the center of the ice sheet in a generally north-south orientation.

For the comparison of surface meltwater produced during periods of extreme Greenland blocking, it was not necessary to detrend the daily MAR time series spanning 1979–2008. The purpose of this analysis is to determine whether there is a significant difference in MAR-

simulated surface meltwater production that can be attributed to interannual variability in extreme Greenland blocking nested within the background signal of Arctic warming. Because GrIS melting is characterized by a distinct monthly cycle during the extended summer melting season, this cycle was removed by calculating standardized Z-scores for each day during the period of record. Similarly to the standardization of the GBI time series, the meltwater production value for each day during the 30-year period of record was ranked against all other daily meltwater production values from 1979–2008 that occurred within a 7-day period centered on the day in question. The 7-day moving periods were selected as the climatological baseline for this analysis in order to capture sampling distributions of meltwater production values that are sufficiently representative of each day's potential range of observations.

3.3 Results

Previous climatological studies [*Konrad and Colucci, 1988; Lupo and Smith, 1995; Colucci and Alberta, 1996*] have focused primarily on a relatively small sample of explosive precursor cyclones during the meteorological cool season, but a more comprehensive analysis of North Atlantic cyclones that potentially contributed to extreme GBE development during all seasons is presented here. Using Student's *t*-tests, various attributes of precursor cyclones are compared to those of non- precursor cyclones in order to reveal any unique characteristics of cyclones that precede extreme GBEs. First, precursor cyclones across all seasons are not significantly stronger (based on either the average or minimum central pressure) and do not intensify more rapidly than non- precursor cyclones (Table 3.2). Though not significant, with the exception of spring, the maximum deepening rates of precursor cyclones across all seasons are less than those of non- precursor cyclones, which suggests that explosive cyclogenesis may not be favorable for the downstream formation of GBEs. This is consistent with the results of

Konrad and Colucci [1988], who found that explosive cyclones associated with downstream ridge-building tended to be relatively weak compared to the remaining sample of explosive cyclones. They hypothesize that the shallow, intense circulations of the stronger explosive cyclones are unable to penetrate the middle troposphere, prohibiting any significant meridional advection of air masses [*Konrad and Colucci*, 1988]. During the seven winter seasons from December 1980 through February 1987, only 46% (6 of 13) of blocking events over the western half of the Northern Hemisphere (90°W – 90°E) were accompanied by a rapidly intensifying precursor cyclone [*Colucci and Alberta*, 1996]. However, *Lupo and Smith* [1995] report that 72% of blocking events in the North Atlantic region (80°W – 40°E) were preceded by an explosive cyclone. This discrepancy may be due to the short 3-year period of record from July 1985 through June 1988 in the *Lupo and Smith* [1995] analysis.

Table 3.2 also indicates that precursor cyclones across all seasons, particularly summer, are slower moving and more persistent within the pre-defined geographic domain than non-precursor cyclones. The average speed of movement is expressed as the mean 6-hourly distance traveled by cyclones while located within the geographic domain, and the average duration is defined as the mean frequency of 6-hourly time steps recorded for each cyclone within the geographic domain. From a synoptic perspective, these results likely reflect a reduced westerly steering flow across the North Atlantic connected with a polar jet stream that is displaced equatorward during periods of Greenland blocking. Taken together, the evidence presented in Table 3.2 suggests that the slow movement and persistent duration, rather than the strength and rate of intensification, of North Atlantic precursor cyclones, attributes possibly linked with enhanced air mass advection and upper-level wave enhancement, may be more important for the formation and maintenance of GBEs.

A seasonal distribution of extreme GBEs categorized by the number of precursor cyclones reveals that a majority of these events are preceded by multiple cyclones before attaining peak intensity (Table 3.3). The two transitional seasons, spring and autumn, are characterized by the greatest percentages of extreme GBEs with at least two precursor cyclones (80% and 69.2% respectively). Forty percent of all extreme spring GBEs from 1979–2008, which significantly exceeds all other seasons, were associated with either three or four precursor cyclones. Summer is characterized by the greatest percentage of extreme GBEs lacking a precursor cyclone (37.5%), and there were no extreme summer GBEs with only one precursor cyclone during the period of record.

Figure 3.1 displays the geographic origin of all precursor cyclones associated with extreme GBEs from 1979–2008. Approximately 57% of all precursor cyclones formed over the North American continent, while about 43% developed over the North Atlantic Ocean. Only the winter season was characterized by a greater percentage of precursor cyclones with an oceanic (60%, 9 of 15) rather than a continental (40%, 6 of 15) origin. Approximately 64% (14 of 22) of precursor cyclones during spring, 64% (7 of 11) of precursor cyclones during summer, and 59% (13 of 22) of precursor cyclones during autumn originated over the North Atlantic. The geographic centroids for precursor cyclones reveal the seasonal progression of the polar jet stream's migration. The centroids range latitudinally from about 39°N for winter cyclones, which corresponds to the maximum southward displacement of the polar jet stream, to 52.5°N for summer cyclones, reflecting a less expansive polar jet stream during the warm season. The centroids for spring and autumn cyclones are located in close proximity to each other near the 45°N parallel. One precursor cyclone during winter developed over eastern Mexico south of 25°N, while another precursor cyclone during summer formed just off the southeastern coast of

Greenland near 65°N. Thus, precursor cyclogenesis occurs most commonly within the primary cyclonic development zones of the North American mid-latitudes (e.g. leeward side of the Rocky Mountains, Mississippi Valley, Atlantic coast). Very few precursor cyclones originate poleward of the 55°N parallel in close proximity to the region of Greenland blocking.

A comparison of the geographic distribution in precursor and non- precursor cyclone tracks is presented in Figure 3.2. As expected, the frequency of precursor cyclones is much higher across the western half of the spatial domain, which partially reflects the criteria required for classification as a precursor cyclone (Figure 3.2a). The noticeably low frequency of precursor cyclone activity just south of Greenland may reflect the average position of the center of the blocking ridge (Figure 3.3a). In contrast, the distribution of non- precursor cyclones is much more homogeneous, with a slight peak in activity near the center of the domain (Figure 3.2b). Figure 3.2c provides a clearer perspective of the key differences in the spatial distribution of precursor and non- precursor cyclones. As previously stated, precursor cyclone activity is significantly reduced immediately south and southeast of Greenland because this represents the climatologically-favored location of the blocking anticyclone. Perhaps even more noteworthy is the presence of two distinct maximums in precursor cyclone frequency relative to non- precursor cyclone tracks. The first frequency maximum is located to the south of Greenland along the 50°W meridian, which likely represents the cyclonic portion of the vortex pair commonly observed in split-flow Rex blocking patterns. The second frequency maximum, situated to the southwest of Greenland near the 70°W meridian, closely resembles the upstream low typically found in omega blocking patterns.

In order to determine whether precursor cyclones can produce downstream upper-level wave amplification as suggested by Sutcliffe-Petterssen self-development theory, composite

maps of 500 hPa geopotential heights associated with extreme GBEs that are and are not accompanied by a precursor cyclone were generated (Figure 3.3). Due to a pronounced seasonal cycle in 500 hPa heights over the North Atlantic region, only extreme GBEs that occurred during the extended summer season from May through September are included. While extreme GBEs with precursor cyclones produce a composite 500 hPa height field that resembles an omega blocking pattern, the composite field for extreme GBEs lacking a precursor cyclone reflects the split-flow Rex block (Figure 3.3a, b). The difference between these two composite maps reveals that 500 hPa heights associated with extreme GBEs accompanied by precursor cyclones are significantly greater over the North Atlantic Ocean and far northern Greenland (Figure 3.3c). In addition, 500 hPa heights are significantly lower over eastern Canada and the region extending from the British Isles to Iceland. Therefore, precursor cyclones are associated with relatively stronger GBEs that resemble omega blocking patterns, potentially caused by Rossby wave amplification.

Based on these results, it is useful to test whether there are any significant differences in MAR-simulated meltwater production across the GrIS during periods of extreme blocking with and without precursor cyclone activity. Because surface melting can vary substantially over the complex terrain of Greenland, two geographic subsets of daily meltwater production were created to roughly correspond with the eastern and western topographic regions of the ice sheet. First, Student's *t*-tests confirm that simulated meltwater production for all extreme blocking days during the extended summer melting season is greater over both western ($p < 0.001$) and eastern ($p < 0.001$) Greenland in comparison to all other days during these melting seasons from 1979–2008. Moreover, simulated meltwater production over both western ($p = 0.06$) and eastern ($p < 0.01$) Greenland is greater during extreme GBEs accompanied by precursor cyclones than during

those lacking a precursor cyclone. This corroborates the previous finding that extreme GBEs connected to a precursor cyclone are stronger than those not preceded by an extratropical cyclone, leading to enhanced surface melting over the entire GrIS.

While it has been established that precursor cyclones contribute to the development of extreme GBEs during the extended summer season, any direct effect of these cyclones, such as air mass advection, on GrIS surface melting conditions remains unclear. To investigate this issue, HYSPLIT backward trajectories initialized at the 700 hPa pressure level (500 hPa for Summit Station) for nine distinct locations across Greenland (Table 3.1) were simulated for extreme GBEs accompanied by precursor cyclones during all extended summer seasons from 1979–2008 (Figure 3.4). These plots illustrate the spatial frequency of the air parcel trajectories as they are simulated backward in time from each location on the GrIS, providing an estimate of the geographic origin of the air masses observed over each location during the extreme blocking events. It is also critical to examine tropospheric flow at multiple locations across the GrIS because the flow direction can play a major role in modulating the extent of surface melting [Mote, 1998b]. For the five locations extending clockwise from southeastern to northwestern Greenland, a consistent pattern in the geographic distribution of 700 hPa trajectories is evident. Relatively high frequencies of trajectories are clustered predominately to the south and southeast of each location, which indicates a tendency for southerly air mass advection during extreme GBEs accompanied by precursor cyclones. However, 700 hPa trajectories associated with the eastern and northeastern Greenland sites are concentrated primarily over northern Greenland, suggesting a greater frequency of northwesterly air mass advection over these locations during the blocking events. Trajectories are disproportionately clustered to the south of the elevated interior locations at South Dome and Summit Station, but there is also a tendency for

northwesterly air mass advection at Summit Station. Thus, during extreme GBEs accompanied by a precursor cyclone, southerly air mass advection is prevalent across all of the selected GrIS locations with the exception of eastern and northeastern Greenland.

It is perhaps more informative to assess whether there are any significant differences in the geographic distribution of trajectories for extreme GBEs based on the presence or absence of any precursor cyclones (Figure 3.5). Each map in Figure 3.5 depicts the percentage increase or decrease in the frequency of 700 hPa trajectories corresponding to extreme GBEs accompanied by a precursor cyclone in relation to those lacking a precursor cyclone. For the five locations extending clockwise from southeastern to northwestern Greenland, the frequency of trajectories clustered over the North Atlantic Ocean between the 45°N parallel and the tip of southern Greenland is significantly greater during extreme GBEs accompanied by precursor cyclones compared to those lacking a precursor cyclone. This pattern is also evident for the elevated inland locations at South Dome and Summit Station. For the eastern and northeastern Greenland locations, the spatial distribution of 700 hPa trajectories is much less defined, though there is a tendency for northerly air mass advection originating over far northern Greenland. Taken together, the results from Figures 3.4 and 3.5 reveal that southerly air mass advection occurs much more frequently across the GrIS, except the eastern and northeastern sectors, during extreme GBEs accompanied by precursor cyclones compared to those lacking a precursor cyclone. However, this linkage does not provide a physical explanation for enhanced GrIS melting during extreme GBEs accompanied by precursor cyclones as previously identified.

Therefore, the vertical and horizontal evolution of the 700 hPa trajectories are examined in order to assess the relative contributions of diabatic and adiabatic processes on the surface energy budget across the GrIS, which strongly influences the extent of melting. The vertical

evolution of composite backward trajectories for extreme GBEs accompanied by precursor cyclones is compared to those for extreme GBEs lacking a precursor cyclone (Figure 3.6). Excluding the southwestern Greenland location, the composite trajectories associated with extreme GBEs lacking a precursor cyclone are characterized by greater vertical descent compared to extreme GBEs accompanied by precursor cyclones for all locations extending clockwise from southeastern to northwestern Greenland. This is especially true for southern Greenland, in which the difference between the vertical motion of the composite trajectories exceeds 1,000 meters. Based on the vertical motion alone, the composite temperature of the simulated air parcel associated with extreme GBEs lacking a precursor cyclone should be greater (due to enhanced adiabatic warming) than that associated with extreme GBEs accompanied by precursor cyclones. However, for all of these locations, either the potential or ambient air temperature of the simulated air parcel representing extreme GBEs lacking a precursor cyclone is significantly lower than that for extreme GBEs accompanied by precursor cyclones (Table 3.4). This suggests that additional thermal energy from diabatic processes, possibly tied to the precursor cyclones, may be contributing to the higher 700 hPa temperatures simulated over these locations. Also, this relationship is not limited to locations along the Greenland coast as the same pattern holds true for South Dome.

The role of diabatic and adiabatic processes is further investigated by quantifying various components of the surface energy budget for each of the nine selected locations across the GrIS. Surface energy budget fields are based on simulated values from the MAR regional climate model [*Fettweis, 2007; Tedesco et al., 2013; Tedesco et al., 2014*]. Due to the distinct seasonal cycle in incoming solar radiation over the high latitudes, all daily values for the surface energy budget variables were standardized by computing Z-scores with monthly averages as the

climatological baseline. Student's *t*-tests were used to compare conditions during all extreme blocking days (GBEs with and without precursor cyclones) to climatological mean conditions during all non-extreme blocking days within extended summer seasons from 1979–2008 (Table 3.5). For all locations with the exception of northwestern Greenland, northeastern Greenland, and Summit Station, both the incoming shortwave radiation and outgoing longwave radiation are significantly greater during extreme blocking days compared to non-extreme blocking days. Clear skies, which allow a large quantity of solar radiation to be absorbed during the day and emitted by the surface as longwave radiation at night, generally prevail under mid-tropospheric ridges. Incoming longwave radiation, representing the portion of terrestrial radiation re-emitted back to the Earth's surface due largely to cloud cover, is significantly greater only over northwestern Greenland, South Dome, and Summit Station. As noted by *Bennartz et al.* [2013], these are areas characterized by a relatively high frequency of thin, liquid-bearing clouds, particularly during the summer. During extreme blocking days, the net gain in radiation at the surface of the GrIS, promoting super-freezing temperatures, results in a significantly lower albedo at all locations with the exception of Summit Station because meltwater is considerably less reflective than ice/snow.

Variability in the surface radiation budget has important implications for the sensible and latent heat fluxes, two primary drivers of surface melting across the GrIS. The sensible heat flux is significantly more negative, indicating a greater transfer of heat energy from the atmosphere to the ground surface, across all locations extending clockwise from southern to northwestern Greenland, including South Dome. Sensible heat generated by the combination of maximum solar radiation under the dome of blocking high pressure and southerly air mass advection supplied by the precursor cyclones warms the surface of the ice sheet. Moreover, the latent heat

flux is significantly more negative, resulting in a net transfer of heat energy from the atmosphere to the ground surface due to condensation, over southwestern Greenland, South Dome, and Summit Station. These results support the previous finding that diabatic processes, in addition to adiabatic warming due to subsiding air motions, are critical in the enhancement of 700 hPa temperatures over southern and western Greenland during extreme GBEs accompanied by precursor cyclones relative to those lacking a precursor cyclone. The combination of diabatic sources of sensible heating, related to maximum shortwave radiation under clear-sky conditions and warm air advection contributed by the precursor cyclones, and latent heating, associated with condensational warming from moisture likely linked to precursor cyclones, can significantly enhance GrIS surface melting conditions. Likewise, *Mote* [1998b] revealed that mid-tropospheric onshore flow with a southerly directional component was generally required for high surface melting conditions across most areas of the GrIS. Precursor cyclones tracking from the southwest effectively advect warmer maritime air from the North Atlantic Ocean onto the western and southeastern coasts of Greenland, resulting in enhanced surface melting over these regions [*Barry and Kiladis*, 1982; *Mote*, 1998b].

Hanna et al. [2013a] identified a significant correlation between a persistent warm phase of the AMO, associated with higher-than-normal SSTs over the North Atlantic Ocean, and anomalous surface melting and runoff across the GrIS during the past few decades. In addition, more frequent blocking over the subpolar North Atlantic (defined as the region extending from south of Greenland to western Europe) coincided with unusually warm SSTs during the early 2000s [*Häkkinen et al.*, 2011]. However, a causal mechanism linking these atmospheric and oceanic processes has yet to be explored.

In order to address this issue, composite maps of North Atlantic SST anomalies [Dee *et al.*, 2011] associated with extreme GBEs that do and do not have a precursor cyclone were generated (Figure 3.7). As before, only extreme GBEs that occurred during the extended summer season from May through September were included. During periods of extreme Greenland blocking with precursor cyclone activity, SSTs are anomalously high by as much as 1°C over a broad area of the North Atlantic located just to the south of Greenland (Figure 3.7a). These warm anomalies extend northwestward into Baffin Bay and northeastward to Iceland. In contrast, periods of extreme Greenland blocking without precursor cyclones are characterized by anomalously cool SSTs over most of the North Atlantic region, with anomalies exceeding -3°C near the Canadian Maritimes (Figure 3.7b). When comparing the two samples of extreme GBEs, SSTs located to the south of Greenland are at least 1°C warmer during extreme GBEs accompanied by precursor cyclones, with local anomalies that are substantially greater in magnitude.

Based on these results, it is reasonable to conclude that precursor cyclones can directly enhance the extent of surface melting over western Greenland and portions of eastern Greenland by advecting unusually warm, moist air originating over anomalously high North Atlantic SSTs northward over the GrIS. As previously noted, surface meltwater production over both western and eastern Greenland is significantly greater during extreme GBEs accompanied by precursor cyclones compared to extreme GBEs lacking a precursor cyclone, and this difference in melting can be partially attributed to the poleward transport of maritime air masses by precursor cyclones that track across an anomalously warm North Atlantic Ocean. Noel *et al.* [2014] state that the direct impact of oceanic forcing on GrIS surface mass balance is restricted to the coastal periphery of Greenland, particularly along the western and southeastern coasts, because katabatic

winds are usually strong enough to prevent a substantial inland incursion of near-surface maritime air masses. However, extratropical cyclones are capable of transporting warm, moist air masses originating within the marine boundary layer over elevated topography, such as the GrIS, due to dynamic lifting. Therefore, anomalously high North Atlantic SSTs, in conjunction with precursor cyclogenesis, contributed to both the long-term melting increase and the episodic widespread melting events observed across the GrIS since 1979.

3.4 Discussion and Conclusion

In addition to the atmospheric and oceanic processes discussed in this study, GrIS surface melting can also be affected by other important factors, including cloud cover, aerosols, and Arctic sea ice. In an analysis of the exceptional melt event during July 2012, *Bennartz et al.* [2013] revealed that surface melting over broad areas of the GrIS, most notably around Summit Station, was likely amplified by low-level liquid clouds within a narrow range of optical thickness. These clouds were thin enough to allow the penetration of incoming solar radiation but thick enough to prevent an excessive amount of longwave radiation from escaping the lower troposphere. The deposition of atmospheric aerosols, especially black carbon and mineral dust, onto the surface of the GrIS has also been linked to enhanced melting during recent years. A substantial decline in the springtime albedo of the GrIS since 2009 has been linked to an increase in the quantity of light-absorbing impurities, particularly mineral dust, that are advected from Arctic regions affected by earlier snow melt due to global warming [*Dumont et al.*, 2014]. Likewise, the combination of exceptionally warm temperatures and black carbon sediments deposited by Northern Hemisphere forest fires, which significantly lowers the albedo of the dry snow region, likely caused the extreme GrIS melt events of 1889 and 2012 [*Keegan et al.*, 2014].

The rapid decline of Arctic sea ice coverage during the past few decades has also been linked to the recent acceleration of GrIS summer melting [*Liu et al.*, in review]. As the coverage of sea ice decreases in the oceanic waters surrounding Greenland, the vertically integrated (surface to 300 hPa) heat flux that is transported over the ice sheet increases, leading to enhanced surface melting through the formation of a heat dome. In agreement with the results of *Bennartz et al.* [2013], reduced Arctic sea ice coverage also promotes a significant increase in atmospheric water vapor content over the GrIS due to a greater quantity of ocean water available for evaporation by southerly winds. Increased atmospheric water vapor allows for a higher frequency of low-level liquid cloud formation over the ice sheet, which contributes to additional surface heating through the downward radiation of longwave energy. While low-level clouds reduce incoming solar radiation over the region extending from west-central to northeastern Greenland, increases in surface downwelling longwave radiation over the entire GrIS are much greater in magnitude.

Similarly to the present study, *Neff et al.* [2014] identified several key features, including the poleward transport of warm, moist air by extratropical cyclone activity and the presence of unusually high North Atlantic SSTs, that contributed to the exceptional GrIS surface melting during July 2012. First, anomalously warm air originating within the boundary layer over the central United States, which was experiencing a record heat wave and drought, was transported northeastward to Greenland. Second, unusually moist air, characterized by 4–5 cm of integrated water vapor, was advected northward within an atmospheric river that transected the west coast of Greenland. Finally, the transition to a wave-one pattern in the polar jet stream, represented by low pressure over the central Arctic Ocean and high pressure over Greenland, during a moderately positive AO phase created favorable mid-tropospheric flow conditions for the

northward transport of warm humid air to western Greenland. *Neff et al.* [2014] suggest that extreme warming events over Greenland, such as the one that occurred from 11–12 July 2012, coincide with transient patterns in the large-scale polar circulation rather than persistent episodes of high pressure (i.e. Greenland blocks). Slower climatic processes operating on the time scale of months to seasons, such as the development of regional heat waves over North America and anomalously warm SSTs over the North Atlantic, increase the probability of GrIS melt events, but the faster meteorological processes that evolve over days to weeks, including atmospheric circulation patterns, are required to generate the more extreme melting episodes [*Neff et al.*, 2014].

While Arctic amplification has likely contributed to unprecedented tropospheric warming and surface melting over the GrIS, there is only limited evidence that atmospheric circulation patterns over the North Atlantic region have also been affected. *Francis and Vavrus* [2012] suggested that the frequency of blocking across the North Atlantic region will increase in the future due to a reduction in the poleward thickness gradient, leading to a weakening of upper-tropospheric winds, and a meridional “stretching” of Rossby waves. However, there is considerable uncertainty in this hypothesis because the most reliable global circulation models generally project a decreasing frequency of blocking conditions across this region [*Barnes et al.*, 2012; *Belleflamme et al.*, 2013; *Masato et al.*, 2013]. Regardless of projected trends in Greenland blocking, the frequency and intensity of North Atlantic cyclones, some of which could act as precursor cyclones, may also undergo future changes due to shifts in the strength and orientation of the polar jet stream [*McCabe et al.*, 2001; *Yin*, 2005].

In this study, the role of North Atlantic cyclones on the evolution of extreme GBEs and surface meltwater production across the GrIS is assessed for the 30-year period from 1979–2008.

A unique subset of North Atlantic cyclones that geographically precede GBEs, known as precursor cyclones, was analyzed by season. Across all seasons, most extreme GBEs are accompanied by multiple precursor cyclones, and a majority (57%) of these cyclones originated over the North American continent rather than the North Atlantic Ocean. Extreme GBEs accompanied by precursor cyclones, resembling an omega blocking pattern, are significantly stronger than extreme GBEs lacking a precursor cyclone, which more closely reflect the split-flow Rex block. Based on MAR-simulated data, daily meltwater production over both western and eastern Greenland is statistically greater during extreme GBEs accompanied by precursor cyclones than during extreme GBEs lacking a precursor cyclone. During the extended summer season from May through September, the combination of diabatic sources of sensible heating, including maximum shortwave radiation under clear-sky conditions and warm air advection contributed by the precursor cyclones, and latent heating, notably condensational warming from moisture likely linked to precursor cyclones, can significantly enhance GrIS surface melting conditions. The interaction of these key atmospheric and oceanic processes, along with several additional factors, contributed to the long-term increase in surface melting since 1979 and may continue to impact the rate of meltwater production across the GrIS into the future.

3.5 References

- Barnes, E. A., J. Slingo, and T. Woollings (2012), A methodology for the comparison of blocking climatologies across indices, models and climate scenarios, *Climate Dynamics*, 38(11–12), 2467–2481.
- Barnes, E. A., E. Dunn-Sigouin, G. Masato, and T. Woollings (2014), Exploring recent trends in Northern Hemisphere blocking, *Geophysical Research Letters*.
- Barriopedro, D., R. García-Herrera, A. R. Lupo, and E. Hernández (2006), A climatology of Northern Hemisphere blocking, *Journal of Climate*, 19(6), 1042–1063.
- Barry, R. G., and G. N. Kiladis (1982), Climatic characteristics of Greenland, *Climatic and Physical Characteristics of the Greenland Ice Sheet*, Cooperative Institute for Research in Environmental Science, University of Colorado, Boulder, CO, 7–34.
- Belleflamme, A., X. Fettweis, C. Lang, and M. Erpicum (2013), Current and future atmospheric circulation at 500 hPa over Greenland simulated by the CMIP3 and CMIP5 global models, *Climate Dynamics*, 41(7–8), 2061–2080.
- Benedict, J. J., S. Lee, and S. B. Feldstein (2004), Synoptic view of the North Atlantic Oscillation, *Journal of the Atmospheric Sciences*, 61(2), 121–144.
- Bennartz, R., M. Shupe, D. Turner, V. Walden, K. Steffen, C. Cox, M. Kulie, N. Miller, and C. Pettersen (2013), July 2012 Greenland melt extent enhanced by low-level liquid clouds, *Nature*, 496(7443), 83–86.
- Brun, E., P. David, M. Sudul, and G. Brunot (1992), A numerical model to simulate snow-cover stratigraphy for operational avalanche forecasting, *Journal of Glaciology*, 38(1), 13–22.

- Clausen, H. B., N. S. Gundestrup, S. J. Johnsen, R. Bindshadler, and J. Zwally (1988), Glaciological investigations in the Crête area, central Greenland: A search for a new deep-drilling site, *Annals of Glaciology*, 10, 10–15.
- Colucci, S. J. (1985), Explosive cyclogenesis and large-scale circulation changes: Implications for atmospheric blocking, *Journal of the Atmospheric Sciences*, 42(24), 2701–2717.
- Colucci, S. J. (1987), Comparative diagnosis of blocking versus nonblocking planetary-scale circulation changes during synoptic-scale cyclogenesis, *Journal of the Atmospheric Sciences*, 44(1), 124–139.
- Colucci, S. J., and T. L. Alberta (1996), Planetary-scale climatology of explosive cyclogenesis and blocking, *Monthly Weather Review*, 124(11), 2509–2520.
- Cuffey, K. M., and S. J. Marshall (2000), Substantial contribution to sea-level rise during the last interglacial from the Greenland ice sheet, *Nature*, 404(6778), 591–594.
- Davini, P., C. Cagnazzo, R. Neale, and J. Tribbia (2012), Coupling between Greenland blocking and the North Atlantic Oscillation pattern, *Geophysical Research Letters*, 39(14).
- Dee, D., S. Uppala, A. Simmons, P. Berrisford, P. Poli, S. Kobayashi, U. Andrae, M. Balmaseda, G. Balsamo, and P. Bauer (2011), The ERA-Interim reanalysis: Configuration and performance of the data assimilation system, *Quarterly Journal of the Royal Meteorological Society*, 137(656), 553–597.
- Dole, R. M. (1989), Life cycles of persistent anomalies. Part I: Evolution of 500 mb height fields, *Monthly Weather Review*, 117(1), 177–211.
- Draxler, R. R., and G. Hess (1998), An overview of the HYSPLIT_4 modelling system for trajectories, *Australian Meteorological Magazine*, 47(4).

- Draxler, R. R., and G. D. Rolph (2014), HYSPLIT (HYbrid Single-Particle Lagrangian Integrated Trajectory) Model access via NOAA ARL READY Website (<http://www.arl.noaa.gov/HYSPLIT.php>), NOAA Air Resources Laboratory, College Park, MD.
- Dumont, M., E. Brun, G. Picard, M. Michou, Q. Libois, J. Petit, M. Geyer, S. Morin, and B. Josse (2014), Contribution of light-absorbing impurities in snow to Greenland's darkening since 2009, *Nature Geoscience*.
- Fettweis, X. (2007), Reconstruction of the 1979–2006 Greenland ice sheet surface mass balance using the regional climate model MAR, *The Cryosphere Discussions*, 1, 123–168.
- Fettweis, X., E. Hanna, C. Lang, A. Belleflamme, M. Erpicum, and H. Gallée (2013), Important role of the mid-tropospheric atmospheric circulation in the recent surface melt increase over the Greenland ice sheet, *The Cryosphere*, 7(1), 241–248.
- Francis, J. A., and S. J. Vavrus (2012), Evidence linking Arctic amplification to extreme weather in mid-latitudes, *Geophysical Research Letters*, 39(6).
- Gómara, I., J. G. Pinto, T. Woollings, G. Masato, P. Zurita-Gotor, and B. Rodríguez-Fonseca (2014), Rossby wave-breaking analysis of explosive cyclones in the Euro-Atlantic sector, *Quarterly Journal of the Royal Meteorological Society*, 140, 738–753.
- Greene, C., J. Francis, and B. Monger (2013), Superstorm Sandy: A series of unfortunate events, *Oceanography*, 26(1), 8–9.
- Häkkinen, S., P. B. Rhines, and D. L. Worthen (2011), Atmospheric blocking and Atlantic multidecadal ocean variability, *Science*, 334(6056), 655–659.
- Hanna, E., J. M. Jones, J. Cappelen, S. H. Mernild, L. Wood, K. Steffen, and P. Huybrechts (2013a), The influence of North Atlantic atmospheric and oceanic forcing effects on

- 1900–2010 Greenland summer climate and ice melt/runoff, *International Journal of Climatology*, 33, 862–880.
- Hanna, E., X. Fettweis, S. H. Mernild, J. Cappelen, M. H. Ribergaard, C. A. Shuman, K. Steffen, L. Wood, and T. L. Mote (2013b), Atmospheric and oceanic climate forcing of the exceptional Greenland ice sheet surface melt in summer 2012, *International Journal of Climatology*.
- Kalnay, E., M. Kanamitsu, R. Kistler, W. Collins, D. Deaven, L. Gandin, M. Iredell, S. Saha, G. White, and J. Woollen (1996), The NCEP/NCAR 40-year reanalysis project, *Bulletin of the American Meteorological Society*, 77(3), 437–471.
- Keegan, K. M., M. R. Albert, J. R. McConnell, and I. Baker (2014), Climate change and forest fires synergistically drive widespread melt events of the Greenland Ice Sheet, *Proceedings of the National Academy of Sciences*, 111(22), 7964–7967.
- Konrad, C. E., and S. J. Colucci (1988), Synoptic climatology of 500 mb circulation changes during explosive cyclogenesis, *Monthly Weather Review*, 116(7), 1431–1443.
- Lackmann, G. (2011), *Midlatitude Synoptic Meteorology: Dynamics, Analysis, and Forecasting*, American Meteorological Society.
- Liu, J., Z. Chen, T. Mote, J. Francis, and M. Song (in review), The central role of decreasing Arctic sea ice in recent Greenland ice sheet surface melt.
- Lupo, A. R., and P. J. Smith (1995), Climatological features of blocking anticyclones in the Northern Hemisphere, *Tellus A*, 47(4), 439–456.
- Masato, G., B. J. Hoskins, and T. Woollings (2013), Winter and summer Northern Hemisphere blocking in CMIP5 models, *Journal of Climate*, 26(18), 7044–7059.

- Mattingly, K. S., J. T. McLeod, J. A. Knox, J. M. Shepherd, and T. L. Mote (2014), A climatological assessment of Greenland blocking conditions associated with the track of Hurricane Sandy and historical North Atlantic hurricanes, *International Journal of Climatology*.
- McCabe, G. J., M. P. Clark, and M. C. Serreze (2001), Trends in Northern Hemisphere surface cyclone frequency and intensity, *Journal of Climate*, 14(12), 2763–2768.
- McLeod, J. T., and T. L. Mote (in review), Linking seasonal changes in extreme Greenland blocking to the recent increase in summer melting across the Greenland ice sheet, *Journal of Geophysical Research: Atmospheres*.
- Mernild, S. H., T. L. Mote, and G. E. Liston (2011), Greenland ice sheet surface melt extent and trends: 1960–2010, *Journal of Glaciology*, 57(204), 621–628.
- Mote, T. L. (1998b), Mid-tropospheric circulation and surface melt on the Greenland ice sheet. Part II: Synoptic climatology, *International Journal of Climatology*, 18(2), 131–145.
- Mote, T. L. (2007), Greenland surface melt trends 1973–2007: Evidence of a large increase in 2007, *Geophysical Research Letters*, 34(22).
- Nakamura, H., and J. M. Wallace (1990), Observed changes in baroclinic wave activity during the life cycles of low-frequency circulation anomalies, *Journal of the Atmospheric Sciences*, 47(9), 1100–1116.
- Neff, W., G. P. Compo, F. M. Ralph, and M. D. Shupe (2014), Continental heat anomalies and the extreme melting of the Greenland ice surface in 2012 and 1889, *Journal of Geophysical Research: Atmospheres*, 119, 6520–6536.

- Nghiem, S., D. Hall, T. Mote, M. Tedesco, M. Albert, K. Keegan, C. Shuman, N. DiGirolamo, and G. Neumann (2012), The extreme melt across the Greenland ice sheet in 2012, *Geophysical Research Letters*, 39(20).
- Noel, B., X. Fettweis, W. van de Berg, M. van den Broeke, and M. Erpicum (2014), Small impact of surrounding oceanic conditions on 2007–2012 Greenland Ice Sheet surface mass balance, *The Cryosphere Discussions*, 8(2), 1453–1477.
- Rajewicz, J., and S. J. Marshall (2014), Variability and trends in anticyclonic circulation over the Greenland ice sheet, 1948–2013, *Geophysical Research Letters*.
- Screen, J. A., and I. Simmonds (2013), Exploring links between Arctic amplification and mid-latitude weather, *Geophysical Research Letters*, 40, 959–964.
- Serreze, M. C., and J. A. Francis (2006), The Arctic amplification debate, *Climatic Change*, 76(3–4), 241–264.
- Serreze, M. C., and A. P. Barrett (2008), The summer cyclone maximum over the central Arctic Ocean, *Journal of Climate*, 21(5), 1048–1065.
- Serreze, M. C. (2009), *Northern Hemisphere Cyclone Locations and Characteristics from NCEP/NCAR Reanalysis Data*, Boulder, Colorado USA: National Snow and Ice Data Center. Digital media.
- Shabbar, A., J. Huang, and K. Higuchi (2001), The relationship between the wintertime North Atlantic Oscillation and blocking episodes in the North Atlantic, *International Journal of Climatology*, 21(3), 355–369.
- Tedesco, M., X. Fettweis, T. Mote, J. Wahr, P. Alexander, J. Box, and B. Wouters (2013), Evidence and analysis of 2012 Greenland records from spaceborne observations, a regional climate model and reanalysis data, *The Cryosphere*, 7(2), 615–630.

- Tedesco, M., X. Fettweis, P. Alexander, G. Green, and T. Datta (2014), MAR Greenland Outputs 1979–2008 ver. 3.2, CCNY Digital Archive.
- Tsou, C. H., and P. J. Smith (1990), The role of synoptic/planetary-scale interactions during the development of a blocking anticyclone, *Tellus A*, 42(1), 174–193.
- Woollings, T., B. Hoskins, M. Blackburn, and P. Berrisford (2008), A new Rossby wave-breaking interpretation of the North Atlantic Oscillation, *Journal of the Atmospheric Sciences*, 65(2), 609–626.
- Yin, J. H. (2005), A consistent poleward shift of the storm tracks in simulations of 21st century climate, *Geophysical Research Letters*, 32(18).

3.6 Figures and Tables

Table 3.1. Geographic coordinates of the nine selected Greenland locations

Locations	Latitude (°N)	Longitude (°W)
(1) Southern Greenland	59.84	43.84
(2) Southwestern Greenland	65	52.32
(3) Western Greenland	70	53
(4) Northwestern Greenland	75	58
(5) Southeastern Greenland	65	40
(6) Eastern Greenland	70	22.32
(7) Northeastern Greenland	75	18.7
(8) South Dome	63.29	45
(9) Summit Station	73.13	36.59

Table 3.2. Comparison of precursor and non-precursor cyclone attributes by season (1979–2008)^a

<i>Average central pressure (hPa)</i>	Precursor cyclones	Non-precursor cyclones	<i>t</i> -test (p-value)	<i>Minimum central pressure (hPa)</i>	Precursor cyclones	Non-precursor cyclones	<i>t</i> -test (p-value)
Winter (DJF)	983.0	982.4	0.84	Winter (DJF)	974.9	974.3	0.86
Spring (MAM)	996.1	993.8	0.27	Spring (MAM)	991.5	987.9	0.18
Summer (JJA)	1,000.5	1,000.1	0.84	Summer (JJA)	995.9	996.0	0.97
Autumn (SON)	992.5	991.3	0.58	Autumn (SON)	986.6	984.5	0.43
<i>Maximum deepening rate (hPa)</i>	Precursor cyclones	Non-precursor cyclones	<i>t</i> -test (p-value)	<i>Average speed of movement (km / 6 hrs)</i>	Precursor cyclones	Non-precursor cyclones	<i>t</i> -test (p-value)
Winter (DJF)	-4.6	-5.9	0.15	Winter (DJF)	250.1	295.5	0.07
Spring (MAM)	-2.2	-3.7	0.008*	Spring (MAM)	208.4	250.4	0.04*
Summer (JJA)	-2.0	-2.7	0.14	Summer (JJA)	170.3	229.7	0.005*
Autumn (SON)	-3.8	-4.5	0.19	Autumn (SON)	201.5	266.7	<0.001*
<i>Duration (frequency of 6-hourly time)</i>	Precursor cyclones	Non-precursor cyclones	<i>t</i> -test (p-value)				
Winter (DJF)	10.7	8.4	0.03*				
Spring (MAM)	8.8	9.2	0.67				
Summer (JJA)	13.2	10.0	0.02*				
Autumn (SON)	10.7	9.0	0.07				

^aP-values that exceed the 95% confidence level are bolded.

Table 3.3. Seasonal distribution of extreme GBEs categorized by the number of precursor cyclones (1979–2008)

Seasons	0 cyclones	1 cyclone	2 cyclones	3–4 cyclones
Winter (DJF)	11.1%	22.2%	55.6%	11.1%
Spring (MAM)	10%	10%	40%	40%
Summer (JJA)	37.5%	0%	50%	12.5%
Autumn (SON)	7.7%	23.1%	61.5%	7.7%

Table 3.4. Comparison of HYSPLIT backward trajectories for extreme GBEs during the extended summer season^b

Potential temperature (K)			
Locations	Extreme GBEs with precursor cyclones	Extreme GBEs without precursor cyclones	<i>t</i> -test (p-value)
(1) Southern Greenland	298.2	297.8	0.21
(2) Southwestern Greenland	297.9	296.0	<0.001
(3) Western Greenland	297.0	295.0	<0.001
(4) Northwestern Greenland	293.8	292.1	0.001
(5) Southeastern Greenland	296.7	295.8	0.04
(6) Eastern Greenland	294.7	293.5	0.06
(7) Northeastern Greenland	292.6	292.3	0.66
(8) South Dome	296.2	295.4	0.01
(9) Summit Station	305.3	302.8	<0.001
Air temperature (K)			
Locations	Extreme GBEs with precursor cyclones	Extreme GBEs without precursor cyclones	<i>t</i> -test (p-value)
(1) Southern Greenland	268.4	266.9	<0.001
(2) Southwestern Greenland	267.9	267.4	0.25
(3) Western Greenland	267.4	266.6	0.08
(4) Northwestern Greenland	266.3	264.7	<0.001
(5) Southeastern Greenland	267.4	264.4	<0.001
(6) Eastern Greenland	263.7	263.8	0.83
(7) Northeastern Greenland	262.1	261.6	0.42
(8) South Dome	268.4	266.4	<0.001
(9) Summit Station	250.6	248.6	<0.001

^bFor each location, both the potential temperature and ambient air temperature during the final six hours of 5-day composite trajectories are compared. The backward trajectories are initialized at 700 hPa for all locations with the exception of Summit Station, which is initialized at 500 hPa due to its elevation. P-values that exceed the 95% confidence level are bolded.

Table 3.5. Comparison of surface energy budget fields for the nine selected Greenland locations^c

<i>Location #1: Northern Greenland</i>			<i>Location #2: Southwestern Greenland</i>			<i>Location #3: Western Greenland</i>		
Extreme blocking days	Non-extreme blocking days	<i>t</i> -test (p-value)	Extreme blocking days	Non-extreme blocking days	<i>t</i> -test (p-value)	Extreme blocking days	Non-extreme blocking days	<i>t</i> -test (p-value)
0.227	-0.003	0.04	0.198	-0.004	0.08	0.238	-0.004	0.03
0.525	-0.009	<0.001	0.297	-0.005	<0.01	0.405	-0.006	<0.001
-0.087	0.001	0.44	0.062	0.000	0.59	-0.030	0.001	0.78
-0.279	0.005	0.01	-0.608	0.010	<0.001	-0.416	0.008	<0.001
0.242	-0.004	0.03	-0.403	0.007	<0.001	-0.069	0.001	0.54
-0.826	0.013	<0.001	-0.488	0.009	<0.001	-0.595	0.011	<0.001
<i>Location #4: Northwestern Greenland</i>			<i>Location #5: Southeastern Greenland</i>			<i>Location #6: Eastern Greenland</i>		
Extreme blocking days	Non-extreme blocking days	<i>t</i> -test (p-value)	Extreme blocking days	Non-extreme blocking days	<i>t</i> -test (p-value)	Extreme blocking days	Non-extreme blocking days	<i>t</i> -test (p-value)
-0.004	0.000	0.97	0.242	-0.004	0.03	0.235	-0.003	0.04
0.508	-0.008	<0.001	0.301	-0.005	0.007	0.267	-0.004	0.02
0.367	-0.006	0.001	-0.063	0.001	0.58	-0.118	0.002	0.30
-0.515	0.009	<0.001	-0.148	0.003	0.19	-0.063	0.001	0.58
0.159	-0.003	0.16	-0.165	0.003	0.14	0.059	-0.001	0.60
-0.344	0.006	0.002	-0.480	0.007	<0.001	-0.587	0.010	<0.001
<i>Location #7: Northeastern Greenland</i>			<i>Location #8: South Dome</i>			<i>Location #9: Summit Station</i>		
Extreme blocking days	Non-extreme blocking days	<i>t</i> -test (p-value)	Extreme blocking days	Non-extreme blocking days	<i>t</i> -test (p-value)	Extreme blocking days	Non-extreme blocking days	<i>t</i> -test (p-value)
0.068	0.000	0.55	0.341	-0.005	0.002	0.026	0.000	0.82
0.000	0.000	0.99	0.257	-0.004	0.02	0.396	-0.006	<0.001
0.072	-0.001	0.52	-0.205	0.004	0.07	0.205	-0.003	0.07
-0.007	0.000	0.95	-0.613	0.010	<0.001	-0.180	0.003	0.11
-0.094	0.001	0.40	-0.245	0.004	0.03	-0.269	0.004	0.02
-0.297	0.005	0.008	-0.252	0.004	0.03	0.064	-0.001	0.57

^cOnly days during the extended summer season from May through September are included. Surface energy budget fields are based on simulated values from the MAR regional climate model [Tedesco et al., 2014]. P-values that exceed the 90% confidence level are bolded.



Figure 3.1. Geographic origin of all precursor cyclones associated with extreme GBEs from 1979–2008. The cyclones are grouped by meteorological season. The white symbols represent the geographic centroids for all cyclones within each season. Plot is generated using the Northern Hemisphere cyclone dataset provided by *Serreze* [2009].

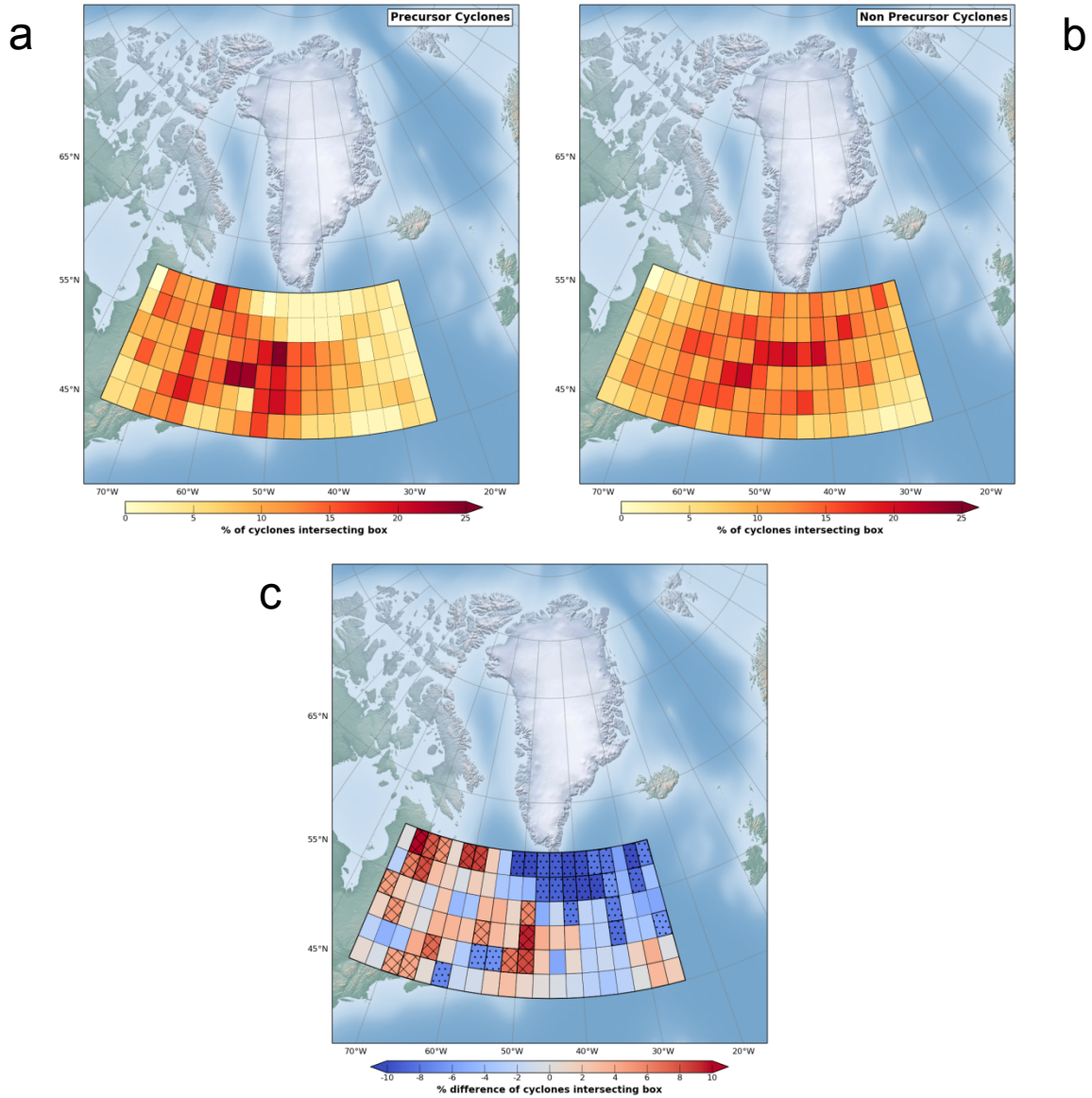


Figure 3.2. Geographic distribution of precursor (a) and non- precursor (b) cyclones from 1979–2008. The percentage difference in the frequency of precursor and non- precursor cyclones is presented in (c). The value in each $2.5^\circ \times 2.5^\circ$ grid box represents the percentage or percentage difference in the frequency of cyclones that intersect the box during the period of record. In plot (c), cross hatching (dot hatching) indicates percentage values that are at least 1 standard deviation greater (lower) than the sample mean. Plots are generated using the Northern Hemisphere cyclone dataset provided by *Serreze* [2009].

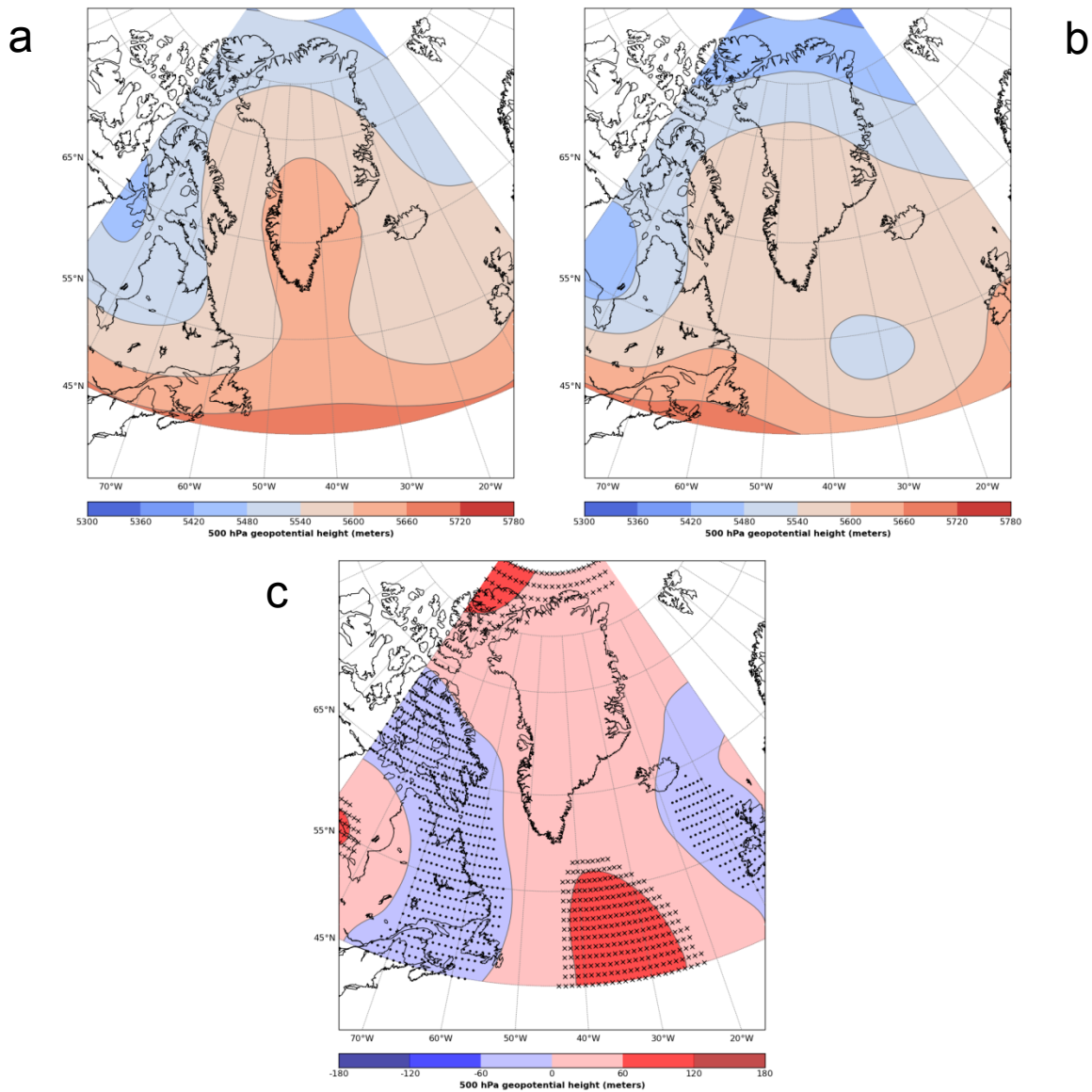


Figure 3.3. Composite maps of 500 hPa geopotential heights associated with extreme GBEs that were (a) and were not (b) accompanied by a precursor cyclone(s). Only extreme GBEs that occurred during the extended summer season from May through September are included. A composite difference map is also presented (c), with cross (dot) hatching representing 500 hPa height differences that are at least 1 standard deviation greater (lower) than the sample mean. Plots are generated using the ERA-Interim dataset [Dee *et al.*, 2011].

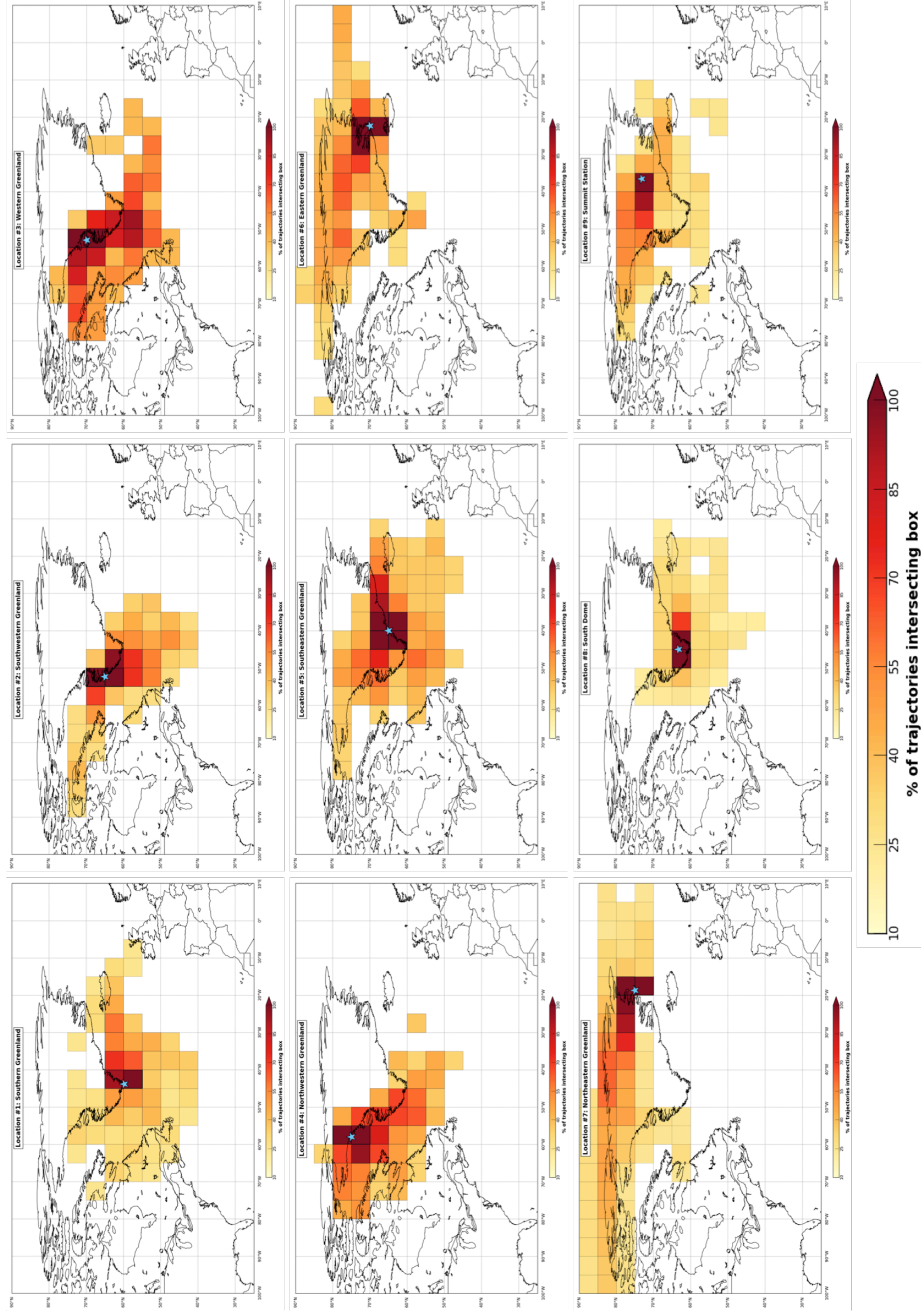


Figure 3.4. Geographic distribution of HYSPLIT backward trajectories for all extreme GBEs with a precursor cyclone(s) from 1979–2008. Only extreme GBEs that occurred during the extended summer season from May through September are included. Each geographic location is depicted by a blue star. The backward trajectories are initialized at 700 hPa over each location with the exception of Summit Station, which is initialized at 500 hPa due to its elevation. The value in each $5^\circ \times 5^\circ$ grid box represents the percentage in the frequency of backward trajectories that intersect the box during the period of record. Only values exceeding a 10% threshold are depicted for clarity. Plots are generated using the HYSPLIT trajectory model driven by NCEP/NCAR Reanalysis data [Draxler and Rolph, 2014].

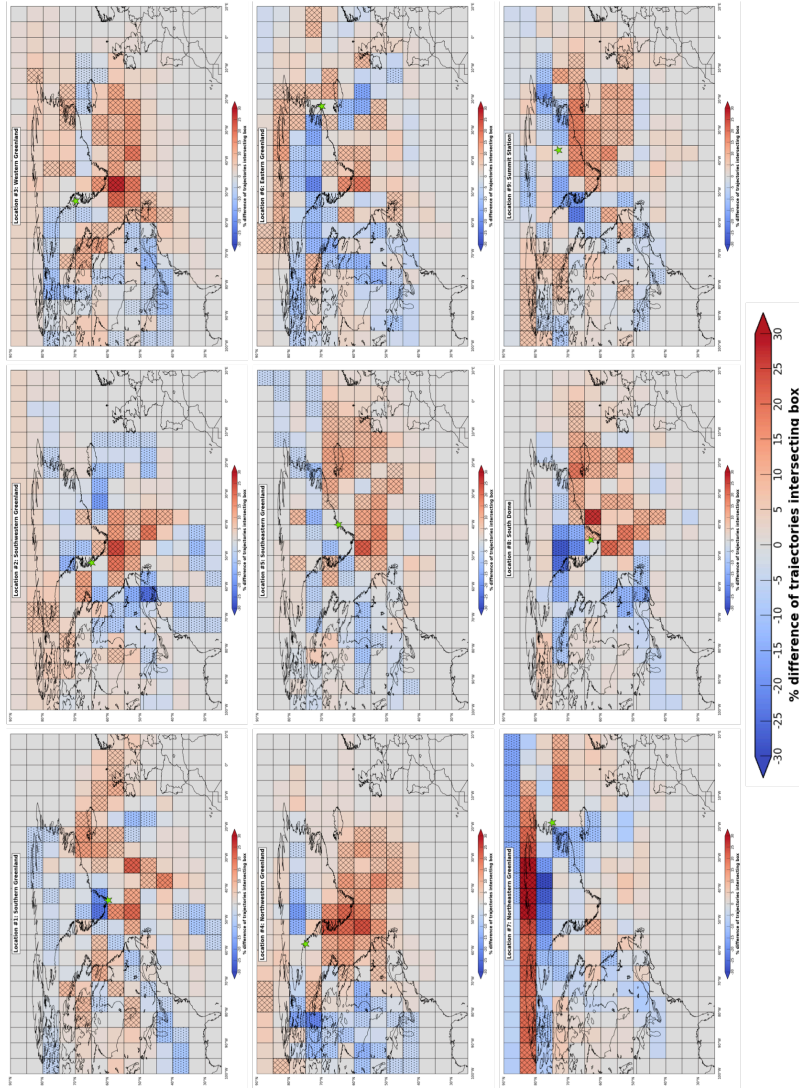


Figure 3.5. Geographic distribution of HYSPLIT backward trajectories for all extreme GBEs with a precursor cyclone(s) compared to all extreme GBEs without a precursor cyclone from 1979–2008. Only extreme GBEs that occurred during the extended summer season from May through September are included. Each geographic location is depicted by a green star. The backward trajectories are initialized at 700 hPa over each location with the exception of Summit Station, which is initialized at 500 hPa due to its elevation. The value in each $5^\circ \times 5^\circ$ grid box represents the percentage difference in the frequency of backward trajectories for the two extreme GBE samples that intersect the box during the period of record. Cross hatching (dot hatching) indicates percentage values that are at least 1 standard deviation greater (lower) than the sample mean. Plots are generated using the HYSPLIT trajectory model driven by NCEP/NCAR Reanalysis data [Draxler and Rolph, 2014].

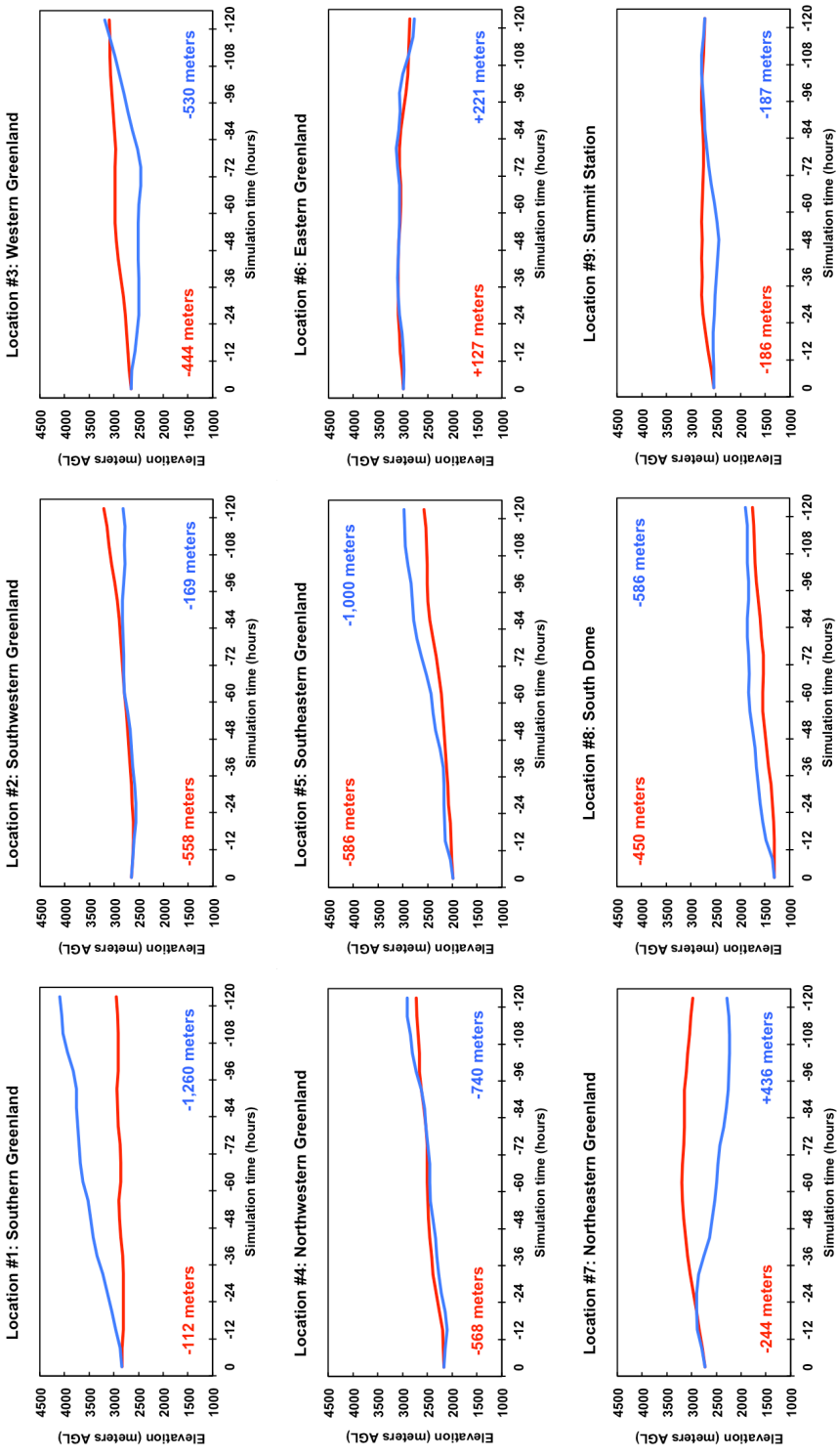


Figure 3.6. Composite time series of the air parcel elevation along backward trajectories during extreme GBEs with a precursor cyclone(s) (red lines) compared to extreme GBEs lacking a precursor cyclone (blue lines). The backward trajectories are initialized at 700 hPa for each location with the exception of Summit Station, which is initialized at 500 hPa due to its elevation. The total change in elevation along each 5-day composite trajectory is also provided. Plots are generated using the HYSPLIT trajectory model driven by NCEP/NCAR Reanalysis data [Draxler and Rolph, 2014].

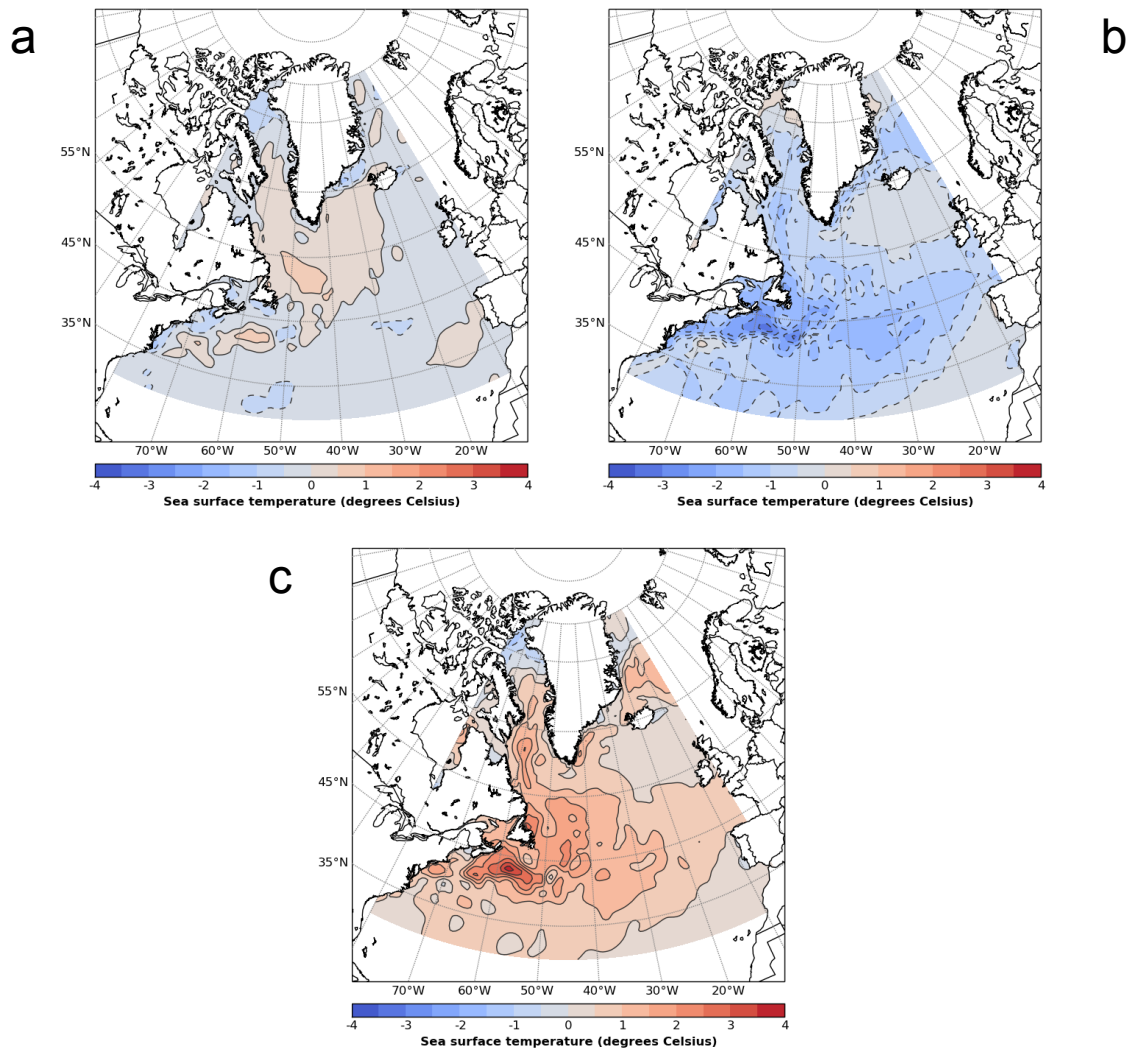


Figure 3.7. Composite maps of North Atlantic SST anomalies associated with extreme GBEs that were (a) and were not (b) accompanied by a precursor cyclone(s). A composite difference map is also presented (c). Only extreme GBEs that occurred during the extended summer season from May through September are included. Anomalies are based on the 1979–2008 climatological mean from May through September. Plots are generated using the ERA-Interim dataset [Dee *et al.*, 2011].

CHAPTER 4

CONCLUSION

In this thesis, the following research questions have been addressed. First, have the frequency, intensity, and duration of extreme GBEs significantly increased during 1958–2013, and does the interannual variability in Greenland blocking play a major role in the extent of GrIS surface melting since 1979? Second, can other atmospheric and oceanic features, such as North Atlantic cyclones and sea surface temperature variability, contribute to an enhancement of GrIS surface melting during the summer? Finally, can North Atlantic cyclones directly and indirectly influence melting conditions across the GrIS through the processes of warm air advection and Rossby wave amplification, respectively? These questions will be answered based on the findings within this thesis and previous studies, and possibilities for future research will also be discussed.

During the 56-year period of record from 1958–2013, the frequency and, to some extent, duration of extreme GBEs were unprecedentedly high from 2007–2013, with a majority of the increase occurring during the spring (MAM) and summer (JJA) months. Despite considerable interannual variability, the annual rate of extreme Greenland blocking days has doubled since 1958, reaching an average of approximately 20 days per year by 2013. About 24% of all extreme blocking days during 1958–2013 occurred during the 7-year period from 2007–2013, which is nearly twice the expected 7-year frequency (i.e. 12.5%) based on a 56-year period of record. The frequency (events or daily counts) of extreme GBEs was exceptionally high from 2007–2013, nearly two standard deviations greater than the long-term average. The mean duration of extreme GBEs was also considerably high during this recent 7-year period,

approaching two days greater than the long-term climatological mean. Thus, it is evident that extreme GBEs are developing more often and persisting somewhat longer during recent years, especially during the spring and summer seasons.

These results are very informative within the context of Arctic amplification and the potential linkage to atmospheric circulation variability over the North Atlantic region. The long-term increase in extreme GBEs since 1958 and the exceptional frequency of these blocking patterns during the last decade are consistent with the findings of numerous studies that have analyzed historical observations of the North Atlantic atmospheric circulation [Fettweis *et al.*, 2011; Overland *et al.*, 2012; Fettweis *et al.*, 2013; Bezeau *et al.*, 2014]. Employing an automatic Circulation Type Classification (CTC) scheme based on 500 hPa geopotential heights, Fettweis *et al.* [2011] reveal that warm synoptic patterns, particularly types 3 and 7 characterized by a strong ridge centered over Greenland, have become much more prevalent since 1998 relative to the climatological record spanning 1958–2009. In addition, the summer seasons during this 52-year period of record with the greatest number of days classified in the warm synoptic types occurred during 2007 and 2008 [Fettweis *et al.*, 2011]. In a subsequent study, Fettweis *et al.* [2013] found that the frequency of anticyclonic circulation days over the GrIS has increased significantly (from ~15% to ~40% of all days from June through August) over the past two decades, and this frequency increase was independent of the background signal corresponding to global warming. Based on self-organizing maps of 500 hPa height anomaly fields from the NCEP/NCAR Reanalysis, strong anticyclonic circulations over the Canadian Arctic Archipelago and western Greenland were 2.7 times more frequent between 2007 and 2012 than from 1948–2006 [Bezeau *et al.*, 2014]. The frequency of anticyclonic circulation patterns from 2007–2012 was significantly higher than any other period during the 65-year climatological period of record,

and none of the five CMIP5 models selected in this study were able to reproduce the magnitude of the anomalously high frequency of 500 hPa height anomalies from 2007–2012 [Bezeau *et al.*, 2014]. Moreover, the frequency of these strong positive anomalies in 500 hPa heights was greater than two standard deviations above the long-term (1951–2010) mean during four individual years from 2007–2012 [Bezeau *et al.*, 2014].

Despite the exceptionally high frequency of anticyclonic circulation patterns, including Greenland blocking, during the past decade, it is difficult to conclude whether this trend will persist into the future. Studies based on an assessment of historical observations have generally surmised that Rossby wave amplification will become more prevalent with an increasing thermal gradient between the polar and equatorial regions leading to higher-amplitude planetary wave patterns. In a seminal study, Francis and Vavrus [2012] detected a statistically significant northward stretching of 500 hPa ridge peaks and a weakened polar jet stream over the North American / North Atlantic region from 1979–2010, which suggests an increasingly favorable environment for block formation during more recent years. However, studies with a modeling approach are needed to provide a more definitive perspective on future projections of Greenland blocking. While most global circulation models (GCMs), even the most advanced versions such as the CMIP5 ensemble, have struggled to simulate atmospheric blocking reliably with respect to reanalysis-based verification, the model consensus generally indicates a future decrease in blocking frequency over the North Atlantic region, especially during the summer [Barnes *et al.*, 2012; Belleflamme *et al.*, 2013; Masato *et al.*, 2013]. Future changes in blocking frequency over the North Atlantic region remain highly uncertain.

The recent increase in extreme GBEs also has important ramifications for the magnitude and spatial extent of GrIS surface melting during the summer months. This relationship is

particularly significant given that the quantity of freshwater stored in the GrIS would correspond to 6–7 meters of global sea level rise if it were all to be released [Cuffey and Marshall, 2000; Nghiem *et al.*, 2012]. The multiple regression models developed for this thesis indicate that the interannual variability in average summer melting conditions across the GrIS can largely be attributed to Greenland blocking activity during the last 30 years. Quantified by the Greenland Blocking Index (GBI), the mean 500 hPa geopotential height over Greenland was the strongest predictor of daily surface meltwater production during the summer over both the eastern and western sectors of the GrIS. Likewise, Hanna *et al.* [2013a] detected a close relationship between unprecedented high pressure patterns over Greenland and highly anomalous surface melting and runoff across the ice sheet during the summers of 2007–2010. A noticeable shift toward strong melt anomalies associated with an increase in anticyclonic circulation over Greenland occurred in 2001, which partially explains the exceptional summer meltwater production in seven individual years from 1998–2012 [Fettweis *et al.*, 2013; Rajewicz and Marshall, 2014].

Future research should examine the climatological variability in Greenland blocking more thoroughly due to the potential for significant impacts within the Arctic region and the Northern Hemisphere mid-latitudes. While several previous studies [Fettweis *et al.*, 2011; Fettweis *et al.*, 2013; Bezeau *et al.*, 2014, Rajewicz and Marshall, 2014] have examined anticyclonic circulation patterns over Greenland and extreme GBEs have been analyzed in this thesis, a climatological investigation of non-extreme Greenland blocking remains unexplored. In addition, a sensitivity analysis of different blocking detection algorithms [Pelly and Hoskins, 2003; Barnes *et al.*, 2012; Dunn-Sigouin *et al.*, 2013; Masato *et al.*, 2013] would be useful in order to determine the robustness of historical trends in extreme Greenland blocking episodes

identified in this thesis. This is particularly important because Greenland blocks have been both directly and indirectly linked to two major climatic events in the North Atlantic within the past few years, namely the unusual landfall location of Hurricane Sandy in October 2012 and the record-breaking melt episode across the GrIS during July 2012 [Nghiem *et al.*, 2012; Mattingly *et al.*, 2014]. Moreover, Screen and Simmonds [2014] found that months characterized by extreme weather conditions (heat waves, cold outbreaks, droughts, floods) during 1979–2012 across the Northern Hemisphere mid-latitudes were often linked to significantly amplified quasi-stationary planetary waves, which would include Greenland blocks.

While enhanced GrIS melting is strongly associated with extreme GBEs during the summer, subtle differences in the magnitude and spatial extent of melting across the western and eastern sectors of the GrIS can be traced to secondary factors, including precursor cyclones, North Atlantic SSTs, and katabatic winds. According to the multiple regression models discussed in Chapter 2, North Atlantic cyclone activity is only a significant predictor of summer meltwater production over the eastern half of Greenland, with relatively weak but rapidly intensifying cyclones leading to high rates of meltwater production. This corroborates the finding in Chapter 3 that MAR-simulated meltwater production over eastern Greenland is more strongly modulated by variability in extreme blocks accompanied by precursor cyclones than meltwater generated over western Greenland. The extent of surface meltwater production across the GrIS is further influenced by variability in North Atlantic SSTs and katabatic winds originating over the elevated interior of Greenland. While Noel *et al.* [2014] suggested that the role of oceanic forcing on surface meltwater production may be restricted to the coastal regions of Greenland due to offshore katabatic wind flow, the regression models indicate that the AMO index is a statistically significant predictor of surface meltwater production over the entire western and

eastern sectors of the GrIS, not just the coastal regions. Moreover, katabatic winds were slightly weaker than climatological mean conditions across much of the eastern half of the ice sheet, particularly the southeastern and northeastern sectors, during high melt days over eastern Greenland.

Based on the analysis of precursor cyclones presented in Chapter 3, both direct and indirect effects of North Atlantic cyclones preceding Greenland blocks can contribute to a significant enhancement of surface melting across the GrIS. Precursor cyclones directly impact GrIS melting conditions by advecting warm, moist air masses situated over anomalously high North Atlantic SSTs poleward to Greenland, resulting in a more negative (downward) sensible and latent heat flux over portions of the ice sheet. The substantial influx of moisture over Greenland connected with precursor cyclones produces additional surface warming due to condensation. Similarly, *Neff et al.* [2014] identified several key features, including the poleward transport of warm, moist air by extratropical cyclone activity and the presence of unusually high North Atlantic SSTs, that contributed to the exceptional GrIS surface melting during July 2012. In addition to vigorous adiabatic warming and maximum clear-sky radiation associated with the blocking high, these diabatic sources of heating linked to precursor cyclones are also critical for enhancing GrIS surface melting.

Precursor cyclones can also indirectly affect GrIS melting conditions by contributing to downstream ridge-building over the North Atlantic region, eventually leading to the development of a full-fledged blocking pattern over Greenland. Indeed, extreme GBEs accompanied by precursor cyclones, resembling an omega blocking pattern, are significantly stronger than extreme GBEs lacking a precursor cyclone, which more closely reflect the split-flow Rex block. In contrast to the results from previous studies [*Konrad and Colucci, 1988; Lupo and Smith,*

1995; Gómará *et al.*, 2014], precursor cyclones do not necessarily have to undergo explosive development in order to cause upper-level wave amplification. Precursor cyclones across all seasons are not significantly stronger (based on either the average or minimum central pressure) and do not intensify more rapidly than non-precursor cyclones. Though not significant, with the exception of spring, the maximum deepening rates of precursor cyclones across all seasons are less than those of non-precursor cyclones, which suggests that explosive cyclogenesis may not be favorable for downstream block formation. Instead, the slow movement and persistent duration, rather than the strength and rate of intensification, of North Atlantic precursor cyclones, attributes possibly linked with enhanced air mass advection and upper-level wave enhancement, may be more important for the formation and maintenance of GBEs.

Based on the cumulative findings in this thesis, several questions remain unanswered in the context of future climate change. For example, what would it mean if the occurrence of Greenland blocking episodes increased but North Atlantic cyclone activity became less frequent or intense? Because these types of questions cannot be conclusively addressed using the results in this thesis, future research should focus on a more nuanced examination of the relationship between Greenland blocking and precursor cyclones. Though a linkage was confirmed between these two atmospheric features, it would be useful to diagnose blocking development with and without the presence of a precursor cyclone from a modeling approach. The role of precursor cyclogenesis on recent trends in extreme Greenland blocking, particularly during 2006–2012, could also be analyzed more directly by updating the Northern Hemisphere cyclone dataset provided by NSIDC to present.

A final question should also be considered for an improved understanding of atmospheric-cryospheric interactions near Greenland: To what extent has the recent acceleration

in GrIS surface melting contributed to the increasing tendency for anticyclonic circulation patterns, including Greenland blocks, over the North Atlantic? Is this a linkage that will likely persist into the future due to Arctic amplification? Numerous atmospheric and oceanic factors that have contributed to anomalous GrIS melting during recent years have been identified (e.g. black carbon and dust deposition, cyclonic activity, North Atlantic SST variability, thin liquid clouds, Arctic sea ice), but the relative impact of each factor remains unclear in the context of long-term melt acceleration and extreme melt events [*Bennartz et al.*, 2013; *Dumont et al.*, 2014; *Keegan et al.*, 2014; *Liu et al.*, in review]. Similarly to the analysis presented in Chapter 2, a multiple regression approach that incorporates a more comprehensive selection of variables that can potentially explain GrIS melting should be explored. In addition, an assessment of interactions between these identified factors, many of which can occur simultaneously at a given point in time, and the subsequent response in GrIS melting should be examined to determine cause-and-effect relationships, rather than associative linkages. Regardless of whether or not recent trends in the frequency of extreme GBEs persist into the future, GrIS melting will likely continue to accelerate as Arctic amplification reshapes the Earth's cryosphere.

REFERENCES

- Barnes, E. A., J. Slingo, and T. Woollings (2012), A methodology for the comparison of blocking climatologies across indices, models and climate scenarios, *Climate Dynamics*, 38(11–12), 2467–2481.
- Barnes, E. A. (2013), Revisiting the evidence linking Arctic amplification to extreme weather in midlatitudes, *Geophysical Research Letters*, 40(17), 4734–4739.
- Barnes, E. A., E. Dunn-Sigouin, G. Masato, and T. Woollings (2014), Exploring recent trends in Northern Hemisphere blocking, *Geophysical Research Letters*.
- Barriopedro, D., R. García-Herrera, A. R. Lupo, and E. Hernández (2006), A climatology of Northern Hemisphere blocking, *Journal of Climate*, 19(6), 1042–1063.
- Barry, R. G., and G. N. Kiladis (1982), Climatic characteristics of Greenland, *Climatic and Physical Characteristics of the Greenland Ice Sheet*, Cooperative Institute for Research in Environmental Science, University of Colorado, Boulder, CO, 7–34.
- Belleflamme, A., X. Fettweis, C. Lang, and M. Erpicum (2013), Current and future atmospheric circulation at 500 hPa over Greenland simulated by the CMIP3 and CMIP5 global models, *Climate Dynamics*, 41(7–8), 2061–2080.
- Benedict, J. J., S. Lee, and S. B. Feldstein (2004), Synoptic view of the North Atlantic Oscillation, *Journal of the Atmospheric Sciences*, 61(2), 121–144.
- Bennartz, R., M. Shupe, D. Turner, V. Walden, K. Steffen, C. Cox, M. Kulie, N. Miller, and C. Pettersen (2013), July 2012 Greenland melt extent enhanced by low-level liquid clouds, *Nature*, 496(7443), 83–86.

- Bezeau, P., M. Sharp, and G. Gascon (2014), Variability in summer anticyclonic circulation over the Canadian Arctic Archipelago and west Greenland in the late 20th/early 21st centuries and its effect on glacier mass balance, *International Journal of Climatology*.
- Blackmon, M. L. (1976), A climatological spectral study of the 500 mb geopotential height of the Northern Hemisphere, *Journal of the Atmospheric Sciences*, 33(8), 1607–1623.
- Box, J., X. Fettweis, J. Stroeve, M. Tedesco, D. Hall, and K. Steffen (2012), Greenland ice sheet albedo feedback: thermodynamics and atmospheric drivers, *The Cryosphere*, 6(4), 821–839.
- Brun, E., P. David, M. Sudul, and G. Brunot (1992), A numerical model to simulate snow-cover stratigraphy for operational avalanche forecasting, *Journal of Glaciology*, 38(1), 13–22.
- Clausen, H. B., N. S. Gundestrup, S. J. Johnsen, R. Bindshadler, and J. Zwally (1988), Glaciological investigations in the Crête area, central Greenland: A search for a new deep-drilling site, *Annals of Glaciology*, 10, 10–15.
- Colucci, S. J. (1985), Explosive cyclogenesis and large-scale circulation changes: Implications for atmospheric blocking, *Journal of the Atmospheric Sciences*, 42(24), 2701–2717.
- Colucci, S. J. (1987), Comparative diagnosis of blocking versus nonblocking planetary-scale circulation changes during synoptic-scale cyclogenesis, *Journal of the Atmospheric Sciences*, 44(1), 124–139.
- Colucci, S. J., and T. L. Alberta (1996), Planetary-scale climatology of explosive cyclogenesis and blocking, *Monthly Weather Review*, 124(11), 2509–2520.
- CPC (2014), Arctic Oscillation, *Climate Prediction Center WWW page*,
[ftp://ftp.cpc.ncep.noaa.gov/cwlinks/norm.daily.ao.index.b500101.current.ascii].

- Cuffey, K. M., and S. J. Marshall (2000), Substantial contribution to sea-level rise during the last interglacial from the Greenland ice sheet, *Nature*, 404(6778), 591–594.
- Davini, P., C. Cagnazzo, R. Neale, and J. Tribbia (2012), Coupling between Greenland blocking and the North Atlantic Oscillation pattern, *Geophysical Research Letters*, 39(14).
- Dee, D., S. Uppala, A. Simmons, P. Berrisford, P. Poli, S. Kobayashi, U. Andrae, M. Balmaseda, G. Balsamo, and P. Bauer (2011), The ERA-Interim reanalysis: Configuration and performance of the data assimilation system, *Quarterly Journal of the Royal Meteorological Society*, 137(656), 553–597.
- Dole, R. M. (1989), Life cycles of persistent anomalies. Part I: Evolution of 500 mb height fields, *Monthly Weather Review*, 117(1), 177–211.
- Draxler, R. R., and G. Hess (1998), An overview of the HYSPLIT_4 modelling system for trajectories, *Australian Meteorological Magazine*, 47(4).
- Draxler, R. R., and G. D. Rolph (2014), HYSPLIT (HYbrid Single-Particle Lagrangian Integrated Trajectory) Model access via NOAA ARL READY Website (<http://www.arl.noaa.gov/HYSPLIT.php>), NOAA Air Resources Laboratory, College Park, MD.
- Dumont, M., E. Brun, G. Picard, M. Michou, Q. Libois, J. Petit, M. Geyer, S. Morin, and B. Josse (2014), Contribution of light-absorbing impurities in snow to Greenland's darkening since 2009, *Nature Geoscience*.
- Dunn-Sigouin, E., S. W. Son, and H. Lin (2013), Evaluation of Northern Hemisphere blocking climatology in the global environment multiscale model, *Monthly Weather Review*, 141(2), 707–727.

- Fang, Z. (2004), Statistical relationship between the northern hemisphere sea ice and atmospheric circulation during wintertime, *Observation, Theory and Modeling of Atmospheric Variability*. Zhu X (ed.). *World Scientific Series on Meteorology of East Asia*. World Scientific Publishing Company: Singapore, 131–141.
- Fettweis, X. (2007), Reconstruction of the 1979–2006 Greenland ice sheet surface mass balance using the regional climate model MAR, *The Cryosphere Discussions*, 1, 123–168.
- Fettweis, X., G. Mabille, M. Erpicum, S. Nicolay, and M. Van den Broeke (2011), The 1958–2009 Greenland ice sheet surface melt and the mid-tropospheric atmospheric circulation, *Climate Dynamics*, 36(1–2), 139–159.
- Fettweis, X., E. Hanna, C. Lang, A. Belleflamme, M. Erpicum, and H. Gallée (2013), Important role of the mid-tropospheric atmospheric circulation in the recent surface melt increase over the Greenland ice sheet, *The Cryosphere*, 7(1), 241–248.
- Folland, C. K., J. Knight, H. W. Linderholm, D. Fereday, S. Ineson, and J. W. Hurrell (2009), The summer North Atlantic Oscillation: past, present, and future, *Journal of Climate*, 22(5), 1082–1103.
- Francis, J. A., and S. J. Vavrus (2012), Evidence linking Arctic amplification to extreme weather in mid-latitudes, *Geophysical Research Letters*, 39(6).
- Gómara, I., J. G. Pinto, T. Woollings, G. Masato, P. Zurita-Gotor, and B. Rodríguez-Fonseca (2014), Rossby wave-breaking analysis of explosive cyclones in the Euro-Atlantic sector, *Quarterly Journal of the Royal Meteorological Society*, 140, 738–753.
- Greene, C., J. Francis, and B. Monger (2013), Superstorm Sandy: A series of unfortunate events, *Oceanography*, 26(1), 8–9.

- Häkkinen, S., P. B. Rhines, and D. L. Worthen (2011), Atmospheric blocking and Atlantic multidecadal ocean variability, *Science*, 334(6056), 655–659.
- Häkkinen, S., D. K. Hall, C. A. Shuman, D. L. Worthen, and N. E. DiGirolamo (2014), Greenland ice sheet melt from MODIS and associated atmospheric variability, *Geophysical Research Letters*, 41(5), 1600–1607.
- Hanna, E., J. M. Jones, J. Cappelen, S. H. Mernild, L. Wood, K. Steffen, and P. Huybrechts (2013a), The influence of North Atlantic atmospheric and oceanic forcing effects on 1900–2010 Greenland summer climate and ice melt/runoff, *International Journal of Climatology*, 33, 862–880.
- Hanna, E., X. Fettweis, S. H. Mernild, J. Cappelen, M. H. Ribergaard, C. A. Shuman, K. Steffen, L. Wood, and T. L. Mote (2013b), Atmospheric and oceanic climate forcing of the exceptional Greenland ice sheet surface melt in summer 2012, *International Journal of Climatology*.
- Kalnay, E., M. Kanamitsu, R. Kistler, W. Collins, D. Deaven, L. Gandin, M. Iredell, S. Saha, G. White, and J. Woollen (1996), The NCEP/NCAR 40-year reanalysis project, *Bulletin of the American Meteorological Society*, 77(3), 437–471.
- Keegan, K. M., M. R. Albert, J. R. McConnell, and I. Baker (2014), Climate change and forest fires synergistically drive widespread melt events of the Greenland Ice Sheet, *Proceedings of the National Academy of Sciences*, 111(22), 7964–7967.
- KNMI (2014), Monthly climate indices, *KNMI Climate Explorer WWW page*, [<http://climexp.knmi.nl/selectindex.cgi>].
- Knox, J. L., and J. E. Hay (1985), Blocking signatures in the Northern Hemisphere: Frequency distribution and interpretation, *Journal of Climatology*, 5(1), 1–16.

- Konrad, C. E., and S. J. Colucci (1988), Synoptic climatology of 500 mb circulation changes during explosive cyclogenesis, *Monthly Weather Review*, 116(7), 1431–1443.
- Lackmann, G. (2011), *Midlatitude Synoptic Meteorology: Dynamics, Analysis, and Forecasting*, American Meteorological Society.
- Liu, J., Z. Chen, T. Mote, J. Francis, and M. Song (in review), The central role of decreasing Arctic sea ice in recent Greenland ice sheet surface melt.
- Lupo, A. R., and P. J. Smith (1995), Climatological features of blocking anticyclones in the Northern Hemisphere, *Tellus A*, 47(4), 439–456.
- Masato, G., B. J. Hoskins, and T. Woollings (2013), Winter and summer Northern Hemisphere blocking in CMIP5 models, *Journal of Climate*, 26(18), 7044–7059.
- Mattingly, K. S., J. T. McLeod, J. A. Knox, J. M. Shepherd, and T. L. Mote (2014), A climatological assessment of Greenland blocking conditions associated with the track of Hurricane Sandy and historical North Atlantic hurricanes, *International Journal of Climatology*.
- McCabe, G. J., M. P. Clark, and M. C. Serreze (2001), Trends in Northern Hemisphere surface cyclone frequency and intensity, *Journal of Climate*, 14(12), 2763–2768.
- McLeod, J. T., and T. L. Mote (in review), Linking seasonal changes in extreme Greenland blocking to the recent increase in summer melting across the Greenland ice sheet, *Journal of Geophysical Research: Atmospheres*.
- Mernild, S. H., T. L. Mote, and G. E. Liston (2011), Greenland ice sheet surface melt extent and trends: 1960–2010, *Journal of Glaciology*, 57(204), 621–628.

- Mote, T. L. (1998a), Mid-tropospheric circulation and surface melt on the Greenland ice sheet. Part I: Atmospheric teleconnections, *International Journal of Climatology*, 18(2), 111–129.
- Mote, T. L. (1998b), Mid-tropospheric circulation and surface melt on the Greenland ice sheet. Part II: Synoptic climatology, *International Journal of Climatology*, 18(2), 131–145.
- Mote, T. L. (2007), Greenland surface melt trends 1973–2007: Evidence of a large increase in 2007, *Geophysical Research Letters*, 34(22).
- Nakamura, H., and J. M. Wallace (1990), Observed changes in baroclinic wave activity during the life cycles of low-frequency circulation anomalies, *Journal of the Atmospheric Sciences*, 47(9), 1100–1116.
- Neff, W., G. P. Compo, F. M. Ralph, and M. D. Shupe (2014), Continental heat anomalies and the extreme melting of the Greenland ice surface in 2012 and 1889, *Journal of Geophysical Research: Atmospheres*, 119, 6520–6536.
- Nghiem, S., D. Hall, T. Mote, M. Tedesco, M. Albert, K. Keegan, C. Shuman, N. DiGirolamo, and G. Neumann (2012), The extreme melt across the Greenland ice sheet in 2012, *Geophysical Research Letters*, 39(20).
- Noel, B., X. Fettweis, W. van de Berg, M. van den Broeke, and M. Erpicum (2014), Small impact of surrounding oceanic conditions on 2007–2012 Greenland Ice Sheet surface mass balance, *The Cryosphere Discussions*, 8(2), 1453–1477.
- Overland, J. E., J. A. Francis, E. Hanna, and M. Wang (2012), The recent shift in early summer Arctic atmospheric circulation, *Geophysical Research Letters*, 39(19).
- Pelly, J., and B. Hoskins (2003), A new perspective on blocking, *Journal of the Atmospheric Sciences*, 60(5), 743–755.

- Petoukhov, V., S. Rahmstorf, S. Petri, and H. J. Schellnhuber (2013), Quasiresonant amplification of planetary waves and recent Northern Hemisphere weather extremes, *Proceedings of the National Academy of Sciences*, *110*(14), 5336–5341.
- Portis, D. H., J. E. Walsh, M. El Hamly, and P. J. Lamb (2001), Seasonality of the North Atlantic Oscillation, *Journal of Climate*, *14*(9), 2069–2078.
- Rajewicz, J., and S. J. Marshall (2014), Variability and trends in anticyclonic circulation over the Greenland ice sheet, 1948–2013, *Geophysical Research Letters*.
- Rex, D. F. (1950), Blocking action in the middle troposphere and its effect upon regional climate: The climatology of blocking action, *Tellus*, *2*(4), 275–301.
- Screen, J. A., and I. Simmonds (2013), Exploring links between Arctic amplification and mid-latitude weather, *Geophysical Research Letters*, *40*, 959–964.
- Screen, J. A., and I. Simmonds (2014), Amplified mid-latitude planetary waves favour particular regional weather extremes, *Nature Climate Change*.
- Serreze, M. C., and J. A. Francis (2006), The Arctic amplification debate, *Climatic Change*, *76*(3–4), 241–264.
- Serreze, M. C., and A. P. Barrett (2008), The summer cyclone maximum over the central Arctic Ocean, *Journal of Climate*, *21*(5), 1048–1065.
- Serreze, M. C. (2009), *Northern Hemisphere Cyclone Locations and Characteristics from NCEP/NCAR Reanalysis Data*, Boulder, Colorado USA: National Snow and Ice Data Center. Digital media.
- Shabbar, A., J. Huang, and K. Higuchi (2001), The relationship between the wintertime North Atlantic Oscillation and blocking episodes in the North Atlantic, *International Journal of Climatology*, *21*(3), 355–369.

- Sumner, E. J. (1954), A study of blocking in the Atlantic-European sector of the Northern Hemisphere, *Quarterly Journal of the Royal Meteorological Society*, 80(345), 402–416.
- Sumner, E. J. (1959), Blocking anticyclones in the Atlantic-European sector of the Northern Hemisphere, *Meteorological Magazine*, 88, 300–311.
- Tedesco, M., X. Fettweis, T. Mote, J. Wahr, P. Alexander, J. Box, and B. Wouters (2013), Evidence and analysis of 2012 Greenland records from spaceborne observations, a regional climate model and reanalysis data, *The Cryosphere*, 7(2), 615–630.
- Tedesco, M., X. Fettweis, P. Alexander, G. Green, and T. Datta (2014), MAR Greenland Outputs 1979–2008 ver. 3.2, CCNY Digital Archive.
- Thompson, D. W., and J. M. Wallace (1998), The Arctic Oscillation signature in the wintertime geopotential height and temperature fields, *Geophysical Research Letters*, 25(9), 1297–1300.
- Treidl, R., E. Birch, and P. Sajecki (1981), Blocking action in the Northern Hemisphere: A climatological study, *Atmosphere-Ocean*, 19(1), 1–23.
- Tsou, C. H., and P. J. Smith (1990), The role of synoptic/planetary-scale interactions during the development of a blocking anticyclone, *Tellus A*, 42(1), 174–193.
- Tyrlis, E., and B. Hoskins (2008), Aspects of a Northern Hemisphere atmospheric blocking climatology, *Journal of the Atmospheric Sciences*, 65(5), 1638–1652.
- Uppala, S. M., P. Kållberg, A. Simmons, U. Andrae, V. Bechtold, M. Fiorino, J. Gibson, J. Haseler, A. Hernandez, and G. Kelly (2005), The ERA-40 re-analysis, *Quarterly Journal of the Royal Meteorological Society*, 131(612), 2961–3012.

van Oldenborgh, G., L. Te Raa, H. Dijkstra, and S. Philip (2009), Frequency-or amplitude-dependent effects of the Atlantic meridional overturning on the tropical Pacific Ocean, *Ocean Science Discussions*, 6(3).

Woollings, T., B. Hoskins, M. Blackburn, and P. Berrisford (2008), A new Rossby wave-breaking interpretation of the North Atlantic Oscillation, *Journal of the Atmospheric Sciences*, 65(2), 609–626.

Yin, J. H. (2005), A consistent poleward shift of the storm tracks in simulations of 21st century climate, *Geophysical Research Letters*, 32(18).